

SHIP MANOEUVRABILITY PREDICTION
USING NEURAL NETWORKS

CENTRE FOR NEWFOUNDLAND STUDIES

**TOTAL OF 10 PAGES ONLY
MAY BE XEROXED**

(Without Author's Permission)

YIE WANG



SHIP MANOEUVRABILITY PREDICTION USING NEURAL NETWORKS

BY

© YIE WANG, B. Eng.

A Thesis Submitted To the School of Graduate Studies
in Partial Fulfillment of the Requirements for
the Degree of Master of Engineering

Faculty of Engineering and Applied Science

Memorial University of Newfoundland

August, 1996

St. John's

Newfoundland

Canada



National Library
of Canada

Acquisitions and
Bibliographic Services Branch

395 Wellington Street
Ottawa, Ontario
K1A 0N4

Bibliothèque nationale
du Canada

Direction des acquisitions et
des services bibliographiques

395, rue Wellington
Ottawa (Ontario)
K1A 0N4

Your file *Votre référence*

Our file *Notre référence*

The author has granted an irrevocable non-exclusive licence allowing the National Library of Canada to reproduce, loan, distribute or sell copies of his/her thesis by any means and in any form or format, making this thesis available to interested persons.

L'auteur a accordé une licence irrévocable et non exclusive permettant à la Bibliothèque nationale du Canada de reproduire, prêter, distribuer ou vendre des copies de sa thèse de quelque manière et sous quelque forme que ce soit pour mettre des exemplaires de cette thèse à la disposition des personnes intéressées.

The author retains ownership of the copyright in his/her thesis. Neither the thesis nor substantial extracts from it may be printed or otherwise reproduced without his/her permission.

L'auteur conserve la propriété du droit d'auteur qui protège sa thèse. Ni la thèse ni des extraits substantiels de celle-ci ne doivent être imprimés ou autrement reproduits sans son autorisation.

ISBN 0-612-17661-4

Canada



Memorial

University of Newfoundland

This is to authorize the Dean of Graduate Studies to deposit two copies of my thesis/report entitled

Ship Manoeuvrability Prediction Using Neural Networks

in the University Library, on the following conditions. I understand that I may choose only ONE of the Options here listed, and may not afterwards apply for any additional restriction. I further understand that the University will not grant any restriction on the publication of thesis/report abstracts.

(After reading the explanatory notes at the foot of this form, delete TWO of (a), (b) and (c), whichever are inapplicable.)

The conditions of deposit are:

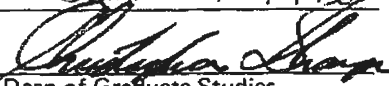
(a) that two copies are to be made available to users at the discretion of their custodians,

OR

(b) that access to, and quotation from, this thesis/report is to be granted only with my written permission for a period of one year from the date on which the thesis/report, after the approval of the award of a degree, is entrusted to the care of the University, namely, _____ 19 ____, after which time the two copies are to be made available to users at the discretion of their custodians,

OR

(c) that access to, and quotation from, this thesis/report is to be granted only with my written permission for a period of _____ years from the date on which the thesis/report, after approval for the award of a degree, is entrusted to the care of the University; namely, _____, 19 ____; after which time two copies are to be made available to users at the discretion of their custodians.

Date June 6, 1996

 Dean of Graduate Studies

Signed Yie Wang
 Witnessed by K. Flute

NOTES

- Restriction (b) will be granted on application, without reason given.
 However, applications for restriction (c) must be accompanied with a detailed explanation, indicating why the restriction is thought to be necessary, and justifying the length of time requested. Restrictions required on the grounds that the thesis is being prepared for publication, or that patents are awaited, will not be permitted to exceed three years.
 Restriction (c) can be permitted only by a Committee entrusted by the University with the task of examining such applications, and will be granted only in exceptional circumstances.
- Thesis writers are reminded that, if they have been engaged in contractual research, they may have already agreed to restrict access to their thesis until the terms of the contract have been fulfilled.

Abstract

This thesis is divided into three parts. The first two parts deal with two different methods for predicting the manoeuvring characteristics of ships using a neural network technique. The third part deals with the application of the random decrement concept to the coupled sway-yaw motions.

In the first part of this thesis, a new predictive method is presented for the estimation of the hydrodynamic characteristics of a ship performing certain standard manoeuvres. This method uses the static neural network technique to predict the nonlinear hydrodynamic forces of the ship during its motion in the horizontal plane. The neural network model uses a steepest descent search to find the neural network weights. In this thesis, a back propagation algorithm is used to calculate the slope of the sum-of-squared-error curve as a function of the different weights. Data for training the neural network consists of the data from a 35-35 degree zigzag manoeuvre. Surge, sway, yaw velocities and rudder angles are used as input to the predictive model. The target output data are the lumped nonlinear hydrodynamic functions.

The generalization of the trained neural network model is checked by simulating the manoeuvres of the ship in a situation different from the one used in the training of neural network. A moderate 20-20 degree zigzag manoeuvre, a 25 degree turning (starboard) and a 20 degree Dieudonne spiral manoeuvre are selected to check the

validity of the neural network model.

In the second part of this thesis, another approach to predict ship turning manoeuvres is proposed. This model maps the relationship between sway velocities and yaw rates during the circular manoeuvre using a neural network technique. This method reduces the number of equations to be used in the prediction to a single yaw equation. This new yaw equation can then be used for predicting turning manoeuvres.

In the last part of the thesis work, the extension of the random decrement approach to the nonlinear sway-yaw motions is presented. The random waves are simulated based on the ITTC spectrum formula. The linear system and the nonlinear system of sway and yaw motion equations are discussed. The autocorrelation functions of the response of sway and yaw velocities in random waves are obtained. A method for using these functions to identify the hydrodynamic characteristics of the coupled sway-yaw motions is suggested.

Acknowledgements

I would like to express my special appreciation to Dr. M. R. Haddara for his guidance, support, patience and encouragement.

Also, thanks are most gratefully extended to the following: to Dr. M. Hinchey for his course of Wave and Tides; to Dr. G. Sabin for his help in enhancing my mathematical analytic ability in the course of Engineering Analysis; and to Dr. J. J. Sharp for his course and his financial support during my program.

The author also wishes to acknowledge the assistance from my fellow graduate students, Mr. Z. Wang and Mr. J. Xu.

Contents

Abstract	ii
Acknowledgements	iv
List of Figures	ix
List of Tables	xiv
List of Symbols	xvi
1 Introduction and Literature Survey	1
1.1 Introduction	1
1.2 Theoretical Methods	2
1.3 Semi-empirical Methods	3
1.4 Experimental Methods	4
1.5 Parametric Identification Methods	4
1.6 The Scope of This Study	8
2 Neural Network Model	10
2.1 Static Neural Networks	10
2.2 Nonlinear Function Approximation	12

2.3	Steepest Descent Search	13
2.4	Back-propagation Algorithm	15
2.5	Empirical Rules to Improve Network Training	17
3	Numerical Simulation of Ship Motions	20
3.1	Ship Motion Equations	20
3.2	Zigzag Manoeuvre Simulation Procedures	24
3.3	Results of Zigzag Simulation	25
3.4	Ship Turning Simulation	31
3.5	Ship Spiral Manoeuvre Simulation	33
4	Parametric Identification Using Neural Networks	36
4.1	Mathematical Model	36
4.2	Estimation of the Linear Part	38
4.3	Approximation of Lumped Nonlinear Functions Using Neural Networks	41
4.4	Training Static Neural Networks	42
4.4.1	Choosing Training Samples and Setting Up Network	42
4.4.2	Nondimensionalization of the Input and Output	46
4.4.3	Training Process	47
4.5	Prediction of Ship Motion Using Trained g_1 , g_2 and g_3	54
5	Generalization of the Neural Network Model	60
5.1	Choosing Test Manoeuvres	60
5.2	Results of the Generalization Check	62
5.3	Regression Analysis	67

6	Ship Turning Manoeuvre Prediction	79
6.1	Mathematical Formulation	79
6.2	Mapping $v = v(r)$ using Neural Networks	81
6.3	Results and Discussion	82
7	Study of Sway and Yaw Motions in Random Waves	93
7.1	Exciting Wave Forces	93
7.1.1	Random Waves	93
7.1.2	Wave Exciting Forces and Moments	95
7.2	Simplest Case of Sway-Yaw Motions	102
7.2.1	Analytic and Numerical Solutions	102
7.2.2	Autocorrelation Functions	103
7.3	The Linear System	107
7.4	The Nonlinear System	112
7.5	Discussion	114
8	Conclusions	116
	References	119
	Appendices	123
A	Results Using a Great Lake Bulk Carrier	124
A.1	Ship Principal Particulars and Hydrodynamic Coefficients	124
A.2	Neural Network Training Results	126
A.3	Prediction of Ship Manoeuvres (1)	130
A.4	Prediciton of Ship Manoeuvres (2)	133

List of Figures

2.1	Structure of Neural Networks	11
2.2	One Input/Output, One Middle-layer Node Mapping	13
3.1	Coordinate Systems	21
3.2	Surge Velocity of 20-20 and 35-35 degree Zigzag Manoeuvres	28
3.3	Sway Velocity of 20-20 and 35-35 degree Zigzag Manoeuvres	28
3.4	Yaw Rate of 20-20 and 35-35 degree Zigzag Manoeuvres	29
3.5	Trajectory of 20-20 and 35-35 degree Zigzag Manoeuvres	29
3.6	Ship Heading and Rudder Command of 35-35 Zigzag Manoeuvre	30
3.7	Ship Heading and Rudder Command of 20-20 Zigzag Manoeuvre	30
3.8	Surge Velocity of 25 degree Turning (Starboard)	31
3.9	Sway Velocity of 25 degree Turning (Starboard)	32
3.10	Yaw Rate of 25 degree Turning (Starboard)	32
3.11	Trajectory of 25 degree Turning (Starboard)	33
3.12	Yaw Rates and Rudder Angles in 20 degree Spiral Manoeuvre	35
4.1	Comparison of Nonlinear Part in Surge Function	44
4.2	Comparison of Nonlinear Part in Sway Function	45
4.3	Comparison of Nonlinear Part in Yaw Function	45

4.4	Surge Accelerations of 35-35 deg Zigzag	48
4.5	Sway Accelerations of 35-35 deg Zigzag	48
4.6	Yaw Accelerations of 35-35 deg Zigzag	49
4.7	Trained Network Force g_1 and Simulation Values	50
4.8	Trained Network Force g_2 and Simulation Values	53
4.9	Trained Network Moment g_3 and Simulation Values	53
4.10	Predicted Surge Velocity of 35-35 deg Zigzag Manoeuvre	56
4.11	Predicted Sway Velocity of 35-35 deg Zigzag Manoeuvre	56
4.12	Predicted Yaw Rate of 35-35 deg Zigzag Manoeuvre	57
4.13	Predicted Heading Angle of 35-35 deg Zigzag Manoeuvre	57
4.14	Predicted Trajectory of 35-35 deg Zigzag Manoeuvre	58
4.15	Comparison of Surge Accelerations in 35-35 deg Zigzag	58
4.16	Comparison of Sway Accelerations in 35-35 deg Zigzag	59
4.17	Comparison of Yaw Accelerations in 35-35 deg Zigzag	59
5.1	Velocity Space of 35-35 deg Zigzag and 20-20 deg Zigzag	61
5.2	Velocity Space of 35-35 deg Zigzag and 25 deg Turning	61
5.3	Predicted Surge Velocity of 20-20 deg Zigzag Manoeuvre	62
5.4	Predicted Sway Velocity of 20-20 deg Zigzag Manoeuvre	63
5.5	Predicted Yaw Rate of 20-20 deg Zigzag Manoeuvre	63
5.6	Predicted Heading Angle of 20-20 deg Zigzag Manoeuvre	64
5.7	Predicted Trajectory of 20-20 deg Zigzag Manoeuvre	64
5.8	Predicted Surge Velocity of 25 deg Turning, Starboard	65
5.9	Predicted Sway Velocity of 25 deg Turning, Starboard	65
5.10	Predicted Yaw Rate of 25 deg Turning, Starboard	66

5.11	Predicted Trajectory of 25 deg Turing, Starboard	66
5.12	20 deg Dieudonne Spiral Manoeuvre	67
5.13	Lumped Nonlinear Functions g_1 to g_3 in 35 deg Zigzag Prediction	68
5.14	Velocities and Rudder Angles in 35-35 deg Zigzag Prediction	69
5.15	Predicted Surge Velocity of 15-15 deg Zigzag Manoeuvre	76
5.16	Predicted Sway Velocity of 15-15 deg Zigzag Manoeuvre	76
5.17	Predicted Yaw Rate of 15-15 deg Zigzag Manoeuvre	77
5.18	Predicted Heading Angle of 15-15 deg Zigzag Manoeuvre	77
5.19	Predicted Trajectory of 15-15 deg Zigzag Manoeuvre	78
6.1	Relationships between v and r in Turning Manoeuvres	80
6.2	Sway Velocities in 10 degree Turning, Starboard	85
6.3	Yaw Rates in 10 degree Turning, Starboard	85
6.4	Trajectory in 10 degree Turning, Starboard	86
6.5	Sway Accelerations in 10 degree Turning, Starboard	86
6.6	Yaw Accelerations in 10 degree Turning, Starboard	87
6.7	Sway Velocities in 20 degree Turning, Starboard	87
6.8	Yaw Rates in 20 degree Turning, Starboard	88
6.9	Trajectory in 20 degree Turning, Starboard	88
6.10	Sway Accelerations in 20 degree Turning, Starboard	89
6.11	Yaw Accelerations in 20 degree Turning, Starboard	89
6.12	Sway Velocities in 30 degree Turning, Starboard	90
6.13	Yaw Rates in 30 degree Turning, Starboard	90
6.14	Trajectory in 30 degree Turning, Starboard	91
6.15	Sway Accelerations in 30 degree Turning, Starboard	91

6.16	Yaw Accelerations in 30 degree Turning, Starboard	92
7.1	ITTC Spectrum	94
7.2	Coordinate Axes	96
7.3	Wave Exciting Force of Sway	100
7.4	Wave Exciting Moment of Yaw	100
7.5	Amplitude of Wave Exciting Forces of Sway	101
7.6	Amplitude of Wave Exciting Moments of Yaw	101
7.7	Responses of Sway Velocity in Simplest System	103
7.8	Responses of Yaw Rate in Simplest System	104
7.9	Autocorr. Functions of $v(t)$ in Simplest System	105
7.10	Autocorr. Functions of $r(t)$ in Simplest System	106
7.11	Logarithm of the Functions in Simplest System	107
7.12	Responses of Sway Velocity in Linear System	109
7.13	Responses of Yaw Rate in Linear System	109
7.14	Autocorr. Functions of $v(t)$ in Linear System	111
7.15	Autocorr. Functions of $r(t)$ in Linear System	111
7.16	Responses of Sway Velocity in Nonlinear System	113
7.17	Responses of Yaw Rate in Nonlinear System	113
7.18	Autocorr. Functions of $v(t)$ in Nonlinear System	114
7.19	Autocorr. Functions of $r(t)$ in Nonlinear System	115
A.1	Trained Network Force g_1 and Simulation Values	129
A.2	Trained Network Force g_2 and Simulation Values	129
A.3	Trained Network Moment g_3 and Simulation Values	130

A.4	Predicted Surge Velocity of 35-35 deg Zigzag Manoeuvre	131
A.5	Predicted Sway Velocity of 35-35 deg Zigzag Manoeuvre	131
A.6	Predicted Yaw Rate of 35-35 deg Zigzag Manoeuvre	132
A.7	Predicted Heading Angle of 35-35 deg Zigzag Manoeuvre	132
A.8	Predicted Trajectory of 35-35 deg Zigzag Manoeuvre	133
A.9	Predicted Surge Velocity of 20-20 deg Zigzag Manoeuvre	134
A.10	Predicted Sway Velocity of 20-20 deg Zigzag Manoeuvre	134
A.11	Predicted Yaw Rate of 20-20 deg Zigzag Manoeuvre	135
A.12	Predicted Heading Angle of 20-20 deg Zigzag Manoeuvre	135
A.13	Predicted Trajectory of 20-20 deg Zigzag Manoeuvre	136
A.14	Predicted Surge Velocity of 25 deg Turning, Starboard	136
A.15	Predicted Sway Velocity of 25 deg Turning, Starboard	137
A.16	Predicted Yaw Rate of 25 deg Turning, Starboard	137
A.17	Predicted Trajectory of 25 deg Turing, Starboard	138

List of Tables

3.1	Ship Principal Dimensions	25
3.2	Hydrodynamic Coefficients of a Mariner Class Ship	26
4.1	Estimated Nondimensional Linear Coefficients	41
4.2	Trained Weights	51
4.3	Trained Weights (continued)	52
5.1	Regression and Original Coefficients (SURGE)	73
5.2	Regression and Original Coefficients (SWAY)	74
5.3	Regression and Original Coefficients (YAW)	75
6.1	Sum of Squared Error in Training	82
6.2	Trained Weights	83
7.1	Table of Offsets (Half-breadths, m)	98
7.2	Table of Offsets Continued (Half-breadths, m)	99
A.1	Ship Principal Particulars	124
A.2	Hydrodynamic Coefficients of 730-ft Great Lake Bulk Carrier	125
A.3	Estimated Nondimensional Linear Coefficients of Surge	126
A.4	Estimated Nondimensional Linear Coefficients of Sway	126

A.5	Estimated Nondimensional Linear Coefficients of Yaw	126
A.6	Trained Weights	127
A.7	Trained Weights (continued)	128

List of Symbols

A	ship rudder area
A_i	wave amplitude of the i th component
B	ship beam
B_{ik}	weight connecting the k th output node with the i th node in middle-layer
$B_{(net+1)k}$	bias weight connecting middle-layer unity with the k th output node
C_b	ship block coefficient
c_1, c_2, d_1, d_2	constants in the solution of the linear system
E	sum of squared error
E_k	error of the k th output node
$f(M_i)$	squashing function of the i th node in middle-layer
f_1	hydrodynamic force of surge
f_2	hydrodynamic force of sway
f_3	hydrodynamic moment of yaw
g_1	lumped nonlinear force of surge
g_2	lumped nonlinear force of sway
g_3	lumped nonlinear moment of yaw
g'_1	nondimensional form of g_1
g'_2	nondimensional form of g_2
g'_3	nondimensional form of g_3
$H_{1/3}$	significant wave height
I_j	input to the j th input node
I_z	mass moment of inertia of ship about z_0 -axis
k	wave number
k_i	wave number of the i th component
kin	number of input nodes
kon	number of output nodes
k_1, k_2, l_1, l_2	constants in the autocorrelation function for the linear system
L	ship length
M_i	sum of weighted input nodes for the i th node in middle-layer
N	yaw moment
N_f	wave exciting moment of yaw

N_f^*	linear combination of wave exciting moment of yaw
n	number of data points
net	number of middle-layer nodes
O_k	output of the kth output node
oxyz	coordinate system fixed to the center of gravity of the ship
$ox_0y_0z_0$	coordinate system fixed to the earth
p	pressure distribution around ship hull
$R_\phi(\tau)$	autocorrelation function of data $\phi(t)$
$R_{vv}(\tau)$	autocorrelation function of $v(t)$
$R_{rr}(\tau)$	autocorrelation function of $r(t)$
r	yaw rate
r_0	initial yaw rate
r'	nondimensional form of r
\dot{r}	derivative of r with respect to time
\dot{r}_0	initial yaw acceleration
rate	rudder turning rate
S	wave spectral density
S_i	wave spectral density of the i th component
T	ship draft
T^*	length of the observation time
T_1	time period corresponding to average wave frequency
T_k	target data for the kth output node
t	time
u	surge velocity
u_0	ship approach velocity
u'	nondimensional form of u
\dot{u}	derivative of u with respect to time
v	sway velocity
v_0	initial sway velocity
v'	nondimensional form of v
\dot{v}	derivative of v with respect to time
\dot{v}_0	initial sway acceleration
W_{ij}	weight connecting the j th input node with the i th node in middle-layer
$W_{i(kin+1)}$	bias weight connecting input unity with the i th node in middle-layer
X	surge force
x_{0G}	x-coordinate of the center of gravity of ship

	in the $0x_0y_0z_0$ system
Y	sway force
Y_f	wave exciting force of sway
Y_f^*	linear combination of wave exciting force of sway
y_{0G}	y-coordinate of the center of gravity of ship in the $0x_0y_0z_0$ system
z_0	vertical distance between the center of gravity of ship and water line
Δ	mass of ship
δ	angle between ship heading and wave propagation direction
δ_R	rudder angle
η	training rate
γ	uniform random number
λ	wave length
λ_1, λ_2	characteristic roots of characteristic function
ω	wave frequency
ω_i	wave frequency of the i th component
ω_b	left end of the frequency band
ω_f	right end of the frequency band
$\phi(t)$	record of data
ψ	heading angle of ship
τ	time lag
θ_i	wave phase angle of the i th component

Note: X, Y and N with subscripts u, v, r, δ_R , \dot{u} , \dot{v} and \dot{r} are hydrodynamic coefficients with respect to their subscripts.

Chapter 1

Introduction and Literature Survey

1.1 Introduction

With the great progress in the area of Naval Architecture, more and more different types of ships have been developed in the maritime transportation. Due to the growth in ship sizes and the diversity in ship types, a great deal of attention has been paid to the manoeuvrability of a ship for the safe navigation in ports and waterways. For a ship designer, careful examination of the ship manoeuvrability is needed at the preliminary design stage. Moreover, at the time of ship completion, manoeuvring information such as the manoeuvring booklet and the wheelhouse poster should be provided for each ship. This is required by Panama Canal Regulations (1977).

To meet the above requirements, it is necessary to provide reliable data for predicting ship manoeuvring motion during a ship's trip. Prediction of ship manoeuvring motions is best performed through the use of mathematical models (Haddara

and Sabin, 1995). The three manoeuvring motions, surge, sway and yaw, can be described by a set of three coupled first order nonlinear differential equations. For special cases, the roll equation is needed. These equations are all based on the second Newtonian law. The hydrodynamic surge and sway forces and yaw moment are usually expressed in their Taylor series expansions. The derivatives in the Taylor series are known as ship hydrodynamic coefficients. The more accurate these hydrodynamic coefficients, the more reliable the results of the prediction of the ship manoeuvring motions.

Currently, four principal approaches are used for the prediction of the hydrodynamic forces and moments acting on a ship during its manoeuvring motion. These approaches are: theoretical methods, semi-empirical methods, experimental methods and parametric identification methods. The last one of the four is quite new and powerful compared with the other three. In this thesis, a new method for parametric identification will be presented to predict ship manoeuvring motions in a more efficient and more economical way.

1.2 Theoretical Methods

Several theoretical methods for the evaluation of the hydrodynamic coefficients for a ship's manoeuvring motions can be found in the literature. Mikelis and Price (1980) used a three-dimensional potential flow analysis of the fluid and a finite element method to calculate hydrodynamic coefficients. Accurate acceleration coefficients can be developed taking into account the ship's form. An assumption of a double layer singularity distribution over the hull with a hydrodynamic vortex sheet was

employed by Remez (1989) for the estimation of hydrodynamic derivatives in the case of small Strouhal number. Clarke et al. (1982) used the assumption that the hull is a low aspect ratio wing turning on its side. By considering the horizontal added mass coefficients for sections along the hull, Clarke extended the slender body strip method to yield expressions for the hydrodynamic derivatives dependent on hull shape through the longitudinal added mass distribution. Wu and Liu (1990) presented a boundary element method for estimating the lateral hydrodynamic forces and yaw moment acting on a ship during its manoeuvring motion. The effect of free surface and separate vorticity was taken into consideration in their method.

1.3 Semi-empirical Methods

Several semi-empirical methods can be used to derive empirical expressions for the hydrodynamic derivatives based on measured values from the planar motion mechanism and rotation arm experiment. Clarke et al. (1982) used multiple linear regression analysis to find empirical formulas to explain the variation in the available data for the velocity and acceleration derivatives. Inoue et al. (1981b) presented a practical calculation method for the ship manoeuvring motion using the principal particulars of a ship hull, propeller and rudder as basic input data. The effect of the loading condition on the ship manoeuvrability was investigated by taking three factors into consideration: the draft, the trim and the immersed rudder area. Inoue et al. (1981a) proposed a method for estimating the linear derivatives of the force acting on the bare hull using the nonlinear lifting surface theory and the measured results. The linear and nonlinear derivatives in the mathematical

models for manoeuvring were examined semi-empirically by both using the model tests of various kinds of ships and applying a theoretical approach. Kijima et al. (1993) applied the prediction method of ship manoeuvring characteristics for zig-zag manoeuvre and free running model test. Compared with the model test results, the predicted ship manoeuvrability has a very good agreement with experimental results.

1.4 Experimental Methods

Captive model tests in tanks are now carried out using a planar motion mechanism (PMM) or a rotating arm. The model is tested over a suitable range of important variables such as drift angle, yaw rate, sway acceleration, yaw acceleration, propeller RPM and rudder angle, and the results are analyzed to obtain the hydrodynamic coefficients required in the equations of motion; see Crane et al. (1989). Yang et al. (1992) presented a formula for calculating the hydrodynamic coefficients for ships by analyzing a database using multi-variate regression techniques. The difficulties in the use of the experimental methods lie in both the high expense of model tests and the unavoidable viscous scale effects.

1.5 Parametric Identification Methods

Parametric identification determines an estimate of the parameters in the mathematical model which are related to the observed data from a given input/output data record of experiments or simulations. The unknown parameters of the model are determined by choosing them to optimize the performance index that measures

how well the mathematical model represents the observed data. The values of the parameters are continuously updated by an algorithm that minimizes the error functions.

Gill (1975) suggested a method of predicting the coefficients in the equations of motion from standard full-scale ship manoeuvring trials. The equations of motion used were applicable over a wide range of forward speeds. The coefficients in the equations may be obtained either from model tests (constrained or free-sailing) or from full-scale ship trials. The technique used in Gill (1975) was based on standard full-scale manoeuvring trials, namely, spiral manoeuvres. The procedure for identifying the coefficients was a mixture of output error and equation error methods. The spiral test results were used to establish certain relationships among some of the coefficients. By varying these unknown coefficients, different solutions of the equations were obtained, and these were compared with the measured output from the trials results of the spiral test. The solution closest to the measured output (i.e. minimum output error) indicated the best coefficient values.

Before the process of the identification in Gill (1975) was started, some pre-coefficients could be estimated fairly accurately, others could be estimated to within certain limits, and furthermore, relationships between some coefficients were established. This process reduced the range and number of variables from 12 to 4 or 5, which immediately simplified the actual matching problem. All the pre-coefficients could be estimated from standard resistance and propulsion model experiments, from the principal dimensions of the ship, or by using empirical formulae estab-

lished from constrained model tests by rotating arm and oblique tow tests, or planar motion mechanism experiments.

The final equations were verified by other trials, and for this purpose some transient manoeuvres should be performed. Kempf manoeuvre was an obvious choice and it was desirable to perform a number of manoeuvres using different rudder angles and heading angle changes. The set of equations described the manoeuvring properties of the directionally unstable VLCC fairly accurately and would be eminently suitable for programming into a real-time ship handling simulator.

Abkowitz (1980) and Abkowitz and Liu (1988) applied the system identification analysis technique to specified ship trial maneuvers and provided a way of "measuring" the hydrodynamic coefficients of the ship and helped to verify proper form of the equations of motion used in simulation. The system identification programs using the extended Kalman filter technique were developed for direct application to realistic ship maneuvers wherein the ship may suffer large speed loss and significant currents may exist. The identification process compared the measured output with the given input. The input to the system identification process was both the rudder deflection and the resulting motion responses, while the output was the identified parameters of the simulation model. The motion variables in case of u , v , r , and Ψ as functions of time were compared with the measured variables and the difference was the error in the estimation. In the extended Kalman filter (EKF) approach of Abkowitz (1980), the hydrodynamic coefficients were treated as additional state variables, but must be constant in time.

Full-scale trials of ship maneuvers were carried out and the results were analyzed using the identification programs. Those maneuvers performed specifically for system identification purposes were mild zigzag maneuvers (10-degree rudder/ 10-degree heading), moderate zigzag maneuvers (20-degree/ 20-degree), offset zigzag (5 to 25 to 5-degree rudder), and tight turning circles of 35-degree rudder. This system identification procedure has been successfully applied to the maneuvering trials in deep and shallow water. When the identified values of the coefficients were used to simulate the trial maneuvers, very good agreement was obtained between the simulated motion responses and those measured during the ship trials.

Trankle (1989) used Marine Coefficient Identification System (MARCIS) to estimate the coefficients for the nonlinear hydrodynamic model in the manoeuvring motions. The complete system identification method used to process raw sensor data to determine hydrodynamic coefficient estimates had two steps: filtering and parameter estimation. Filtering used an extended Kalman filter to compute estimates of vessel velocity and acceleration. These values were used as input to the process of hydrodynamic parameter estimation. The unknown parameter values were adjusted using a nonlinear optimization procedure to minimize mean square error between actual measurements and simulated measurements.

The MARCIS package functioned effectively throughout the trials, recording all of the desired data channels with no data dropouts. All of the desired system identification results including estimation of both linear and nonlinear aspects of

the hydrodynamic model were produced using MARCIS processor alone.

The methods described above are time consuming and do not provide accurate estimates for the individual coefficients. The main difficulty arises from the large number of the parameters to be estimated. It is well known that in system identification procedures, the more parameters that need to be identified from the same pieces of data, the less likely that successful identification will be achieved. Abkowitz and Liu (1988). Another problem that these techniques suffer from is the cancellation effect. Compensating errors in two or more of the coefficients may result in a reasonable prediction of the motion response for a certain manoeuvre, Abkowitz (1980). The method suggested in this thesis tries to avoid these difficulties.

1.6 The Scope of This Study

A new parametric identification approach is presented in this thesis. It is assumed that the hydrodynamic forces or moments are composed of two components: a linear part and a lumped nonlinear part. The former is the linear terms in the previous Taylor series expansions and the latter is made up of all the nonlinear terms in the remaining Taylor series expansion. The linear part can be estimated using semi-empirical methods as in Clarke et al. (1982) and the lumped non-linear component can be obtained using a neural network technique based on full scale ship trial data. Finally, the relationship between the lumped non-linear functions and the variables of surge velocity, sway velocity, yaw rate and rudder angle are identified. The approach enables us to obtain the values of the hydrodynamic forces.

Velocities can then be determined in real time. Therefore, the on-line prediction of ship trajectory can be available for the purpose of ship navigation.

The present approach shares the common advantages of the parametric identification methods (Haddara and Sabin, 1995). These are: 1) elimination of the scale effects. 2) The accuracy of coefficient can be checked based on the measured ship response. 3) The cost is low because the input data to the identification process are from measuring instruments usually found on board ships. 4) If the identification process is obtained on-line (real time), the trajectory can then be predicted to help the captain in steering his ship. Moreover, the new approach can effectively avoid the cancellation effects of coefficients by employing only two parts (linear and nonlinear) in the expression of the hydrodynamic forces. This is because a fewer number of hydrodynamic coefficients are being predicted. With respect to the required data, this new approach needs only one set of surge, sway and yaw velocities from one 35 degree zigzag manoeuvre and the time lag for measuring data is about 2 to 5 seconds. This makes the required full scale trials much simpler than that in Abkowitz (1980) and Gill (1975). More details can be found in chapter 4.

Chapter 2

Neural Network Model

2.1 Static Neural Networks

The technique of neural networks has a wide applications in performing a variety of computational tasks including sequence recognition, trajectory following, nonlinear prediction, and system modeling. The network models are partitioned into two basic categories: static networks and dynamic networks. In this thesis, the static neural network model is used to predict nonlinear functions.

Static networks, of which the multi-layer perceptron (MLP) is the most widely used, are characterized by node equations that are memoryless. That is, their outputs are functions only of the current input, not of past or future inputs or outputs.

Static networks implement nonlinear transformations of the form $O = G(I)$, where I and O represent the input vector with k_{in} dimensions and the output vector with k_{on} dimensions, respectively. The network structure used in this thesis consists of an input layer, a middle layer and an output layer of neurons or nodes. This is usually referred to as a two-layer network. Figure 2.1 shows the details of

the neural network structure.

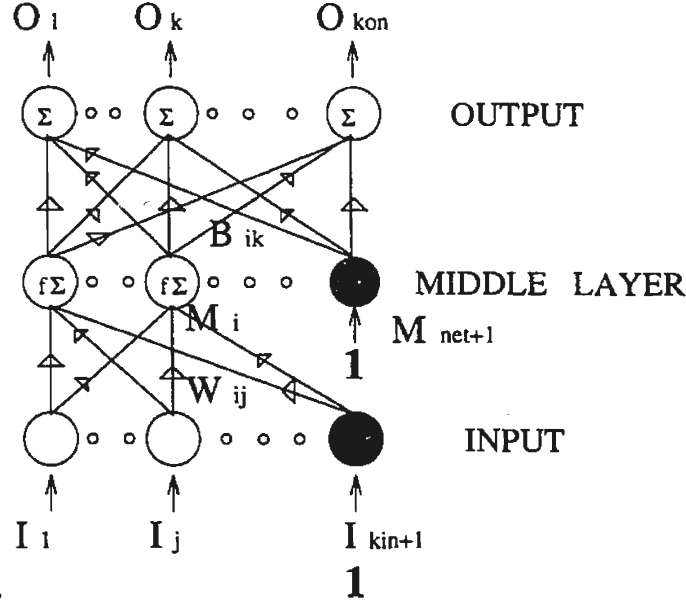


Figure 2.1: Structure of Neural Networks

The neural network will be modeled as the sum of weighted sigmoidal functions (Hornik et al., 1989). The input to the i th node in the middle layer consists of a weighted sum of the $kin + 1$ components in the input vector. This can be expressed as

$$M_i = \sum_{j=1}^{kin+1} W_{ij} * I_j \quad (2.1)$$

where $I_{kin+1} = 1$.

The input to the i th node in the middle layer is applied upon by a nonlinear

transformation, also called a squashing function. We will use the following transformation:

$$f(M_i) = \frac{1}{1 + e^{-M_i}} \quad (2.2)$$

The reasons for the choice of this form for the squashing function are that it is differentiable and it can be easily differentiated; thus, it makes the back-propagation algorithm easier to implement. The derivative of the squashing function is given as

$$\frac{df(y)}{dy} = f(y)(1 - f(y)) \quad (2.3)$$

No squashing function is applied at the output layer. It is common practice to use linear output nodes since this tends to make the learning easier. The output of the k th node in the output layer is given as

$$O_k = \sum_{i=1}^{net+1} B_{ik} * f(M_i) \quad (2.4)$$

2.2 Nonlinear Function Approximation

The nonlinear function approximation can be carried out using a neural network (Hornik et al., 1989). The function is approximated by a combination of net squashing functions from each of the net nodes in the middle layer. Let's consider a network which has one node in its input, output and middle layers. Equation 2.4 is then reduced to

$$O_1 = B_{21} + B_{11}f(W_{11}I_1 + W_{21}) \quad (2.5)$$

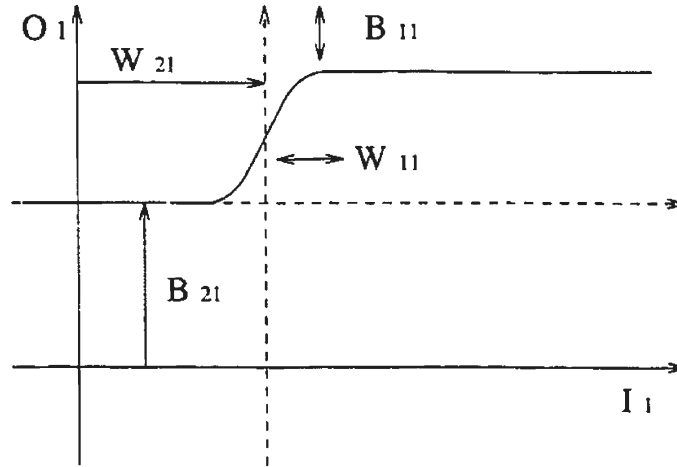


Figure 2.2: One Input/Output, One Middle-layer Node Mapping

Figure 2.2 shows the relationship between the input and output of this simple network. The bias weights W_{21} and B_{21} change the position of the sigmoid in the horizontal and vertical directions while W_{11} and B_{11} change the scale of the sigmoid in the horizontal and vertical directions. Hinchey (1994) stated that in the general case, a map of nonlinearity is formed by patching together in a hyperspace many scaled and shifted squashing functions. Because of the continuity of the sigmoid function, the approximation is smooth and continuous. The numerous alternatives to the sigmoid include $\tanh(\alpha)$, $\text{erf}(\alpha)$, $\alpha/(1 + |\alpha|)$ etc. It was shown in Cybenko (1989) that a 2-layer network which contains one middle layer can form an arbitrarily close approximation to any continuous nonlinear mapping.

2.3 Steepest Descent Search

In order to carry out the transformation of $O = G(I)$, the most common learning algorithm for MLP neural networks uses a gradient search technique to find the network weights that minimize a criterion function. The criterion function to be

minimized is the sum-of-squared-error function given by

$$E = \sum_{k=1}^{kon} (O_k - T_k)^2 \quad (2.6)$$

where T_k is the k th target data corresponding to the k th output node. Substituting equation 2.1 into equation 2.6 gives

$$E = \sum_{k=1}^{kon} \left(\sum_{i=1}^{net+1} B_{ik} f(M_i) - T_k \right)^2 \quad (2.7)$$

where T_k is considered to be constant. So, the sum of the squared errors, E , depends on B_{ik} and $f(M_i)$. Consider a small variation in a specific B_{ik} and a specific $f(M_i)$, the variation in the sum of squared errors, E , is given as

$$\delta E = \frac{\partial E}{\partial B_{ik}} \delta B_{ik} + \frac{\partial E}{\partial [f(M_i)]} \delta [f(M_i)] \quad (2.8)$$

Using equations 2.1, 2.4 and 2.6, one gets the following form

$$\begin{aligned} \delta [f(M_i)] &= \delta \left[f \left(\sum_{j=1}^{kin+1} W_{ij} * I_j \right) \right] \\ &= \frac{\partial f}{\partial W_{ij}} \delta W_{ij} \end{aligned} \quad (2.9)$$

where in equation 2.9, the I_j 's are considered constants. Then equation 2.8 can be rewritten as

$$\delta E = \frac{\partial E}{\partial B_{ik}} \delta B_{ik} + \frac{\partial E}{\partial [f(M_i)]} \frac{\partial f}{\partial W_{ij}} \delta W_{ij} \quad (2.10)$$

According to the principle of steepest descent, the weights of the $(n+1)$ th iteration in training are obtained from the weights of the n th iteration in the following fashion:

$$B_{ik}(n+1) = B_{ik}(n) - \eta \frac{\partial E}{\partial B_{ik}} \quad (2.11)$$

$$W_{ij}(n+1) = W_{ij}(n) - \eta \frac{\partial E}{\partial f} \frac{\partial f}{\partial W_{ij}} \quad (2.12)$$

where η is the training rate.

2.4 Back-propagation Algorithm

The derivatives in equation 2.11 and 2.12 can be easily obtained through a number of manipulations. The final forms of the derivatives will be directly related to the error of a single node in the output layer, $E_k = O_k - T_k$. This algorithm is known as the back-propagation algorithm. For the derivatives with respect to B_{ik} , one gets

$$\begin{aligned} \frac{\partial E}{\partial B_{ik}} &= \frac{\partial [\sum_{k=1}^{kon} (O_k - T_k)^2]}{\partial B_{ik}} \\ &= 2(O_k - T_k) \frac{\partial O_k}{\partial B_{ik}} \end{aligned} \quad (2.13)$$

where the target data T_k is considered to be constant. Substituting equation 2.4 into equation 2.13 gives

$$\begin{aligned}
\frac{\partial O_k}{\partial B_{ik}} &= \frac{\partial \{\sum_{i=1}^{net+1} B_{ik} * f(M_i)\}}{\partial B_{ik}} \\
&= f(M_i)
\end{aligned} \tag{2.14}$$

Combining equations 2.13 and 2.14 gives the form for the derivatives, $\frac{\partial E}{\partial B_{ik}}$, as

$$\frac{\partial E}{\partial B_{ik}} = 2(O_k - T_k)f(M_i) \tag{2.15}$$

For the derivatives with respect to W_{ij} in equation 2.12, it can be worked out as follows

$$\begin{aligned}
\frac{\partial E}{\partial f} \frac{\partial f}{\partial W_{ij}} &= \frac{\partial \{\sum_{k=1}^{kon} (O_k - T_k)^2\}}{\partial f} \frac{\partial f}{\partial W_{ij}} \\
&= 2(O_k - T_k) \frac{\partial O_k}{\partial f} \frac{\partial f}{\partial W_{ij}}
\end{aligned} \tag{2.16}$$

where T_k is a constant and

$$\begin{aligned}
\frac{\partial O_k}{\partial f} &= \frac{\partial \{\sum_{i=1}^{net+1} B_{ik} * f(M_i)\}}{\partial f(M_i)} \\
&= B_{ik}
\end{aligned} \tag{2.17}$$

Using equations 2.1, 2.3 and 2.16, one gets

$$\begin{aligned}
\frac{\partial f}{\partial W_{ij}} &= \frac{\partial f(M_i)}{\partial M_i} \frac{\partial M_i}{\partial W_{ij}} \\
&= M_i(1 - M_i) \frac{\partial \{\sum_{j=1}^{kin+1} W_{ij} * I_j\}}{\partial W_{ij}} \\
&= M_i(1 - M_i)I_j
\end{aligned} \tag{2.18}$$

where I_j 's are constants. Finally, an expression for the derivatives of E with respect to W_{ij} can be obtained as

$$\frac{\partial E}{\partial f} \frac{\partial f}{\partial W_{ij}} = 2(O_k - T_k)B_{ik}M_i(1 - M_i) * I_j \quad (2.19)$$

Equations 2.15 and 2.19 enable us to compute the derivatives of the sum-of-squared error, E, with respect to each weight in the neural network from the output layer backwards.

2.5 Empirical Rules to Improve Network Training

The learning rate in equations 2.11 and 2.12 can be chosen in different ways. It can be the same for all weights in the network, the same for all weights in the same layer, or it can be different for each weight in the network. In general, it is difficult to determine the best learning rate, but a useful empirical rule is to make the rate for each node inversely proportional to the average magnitude of vectors feeding into the node. If the magnitude of the rate is chosen too large, the iteration of steepest descent search cannot converge towards the global minimum of the error, E.

A simple approach that works quite well in practice is to add a momentum term of the form $\alpha(W(n) - W(n - 1))$ to modify the updated weights, where $0 < \alpha < 1$ and n is the nth iteration. The weight updating equations can thus be rewritten as follows:

$$B_{ik}(n+1) = B_{ik}(n) - \eta \frac{\partial E}{\partial B_{ik}} + \alpha(B_{ik}(n) - B_{ik}(n-1)) \quad (2.20)$$

$$W_{ij}(n+1) = W_{ij}(n) - \eta \frac{\partial E}{\partial f} \frac{\partial f}{\partial W_{ij}} + \alpha(W_{ij}(n) - W_{ij}(n-1)) \quad (2.21)$$

The momentum term modifies the current search direction by a weighted average of the previous direction, and helps in keeping the weights moving across the flat portions of the performance surface after they have descended from the steep portions (Hush and Horne, 1993).

With regards to the stopping rule of the search algorithm, the process of computing derivatives and adjusting weights is repeated until a minimum is found. But, it may be difficult to terminate the algorithm automatically. There are several stopping criteria that may be considered. The first is to use the magnitudes of the derivatives as a criterion. One can terminate the search when the magnitudes of the derivatives are sufficiently small. Another criterion for terminating the search is to set a fixed threshold for the error. Thus, the search is terminated when the error reaches a magnitude less than the preset threshold value. However, this requires some knowledge of the acceptable minimal values of the error. A third method would be to terminate the search when a fixed number of iterations have been performed. There is little guarantee that it will stop the algorithm at the exact minimum point. Still a fourth method is to use the method of cross-validation to monitor the generalization performance during learning. Typically, two sets of data are prepared. One is a training set used for training the network, the other is

a test set for measuring the generalization performance of the trained network.

In this thesis, the last three methods are combined together and the results show that this combination is helpful and robust. Before the network is trained, a set of training data and a set of test data are prepared. During the process of data training, an estimated number of iterations is set. After the iteration is finished, the error is checked to determine if the next iteration is necessary. If the error is small enough, the training task will be completed and the trained network will be used to simulate a nonlinear function. Based on these functions, a set of data, say, surge velocity, sway velocity and yaw rate will be calculated using numerical integration. These data will be compared with a set of test data to check how well they fit with the test data. If they fit well, it indicates a good generalization performance of the network and a successful prediction of nonlinear function using neural network. This is a trial and error process and it requires one's wits and patience. Details are in chapter 4.

Chapter 3

Numerical Simulation of Ship Motions

The application of numerical simulation will provide a controlled test for checking the validity of the proposed method by comparing the results with the ones obtained from simulation. The set of surge velocity, sway velocity and yaw rate from different simulations of zigzag manoeuvres are used for training and validating the neural network model in this thesis. The simulations of the ship turning and spiral manoeuvres are used to check the generalization of the proposed model trained from a zigzag manoeuvre. The hydrodynamic coefficients used in simulation are also employed to check the estimated coefficients as identified by a multi-variate regression using the neural network results.

3.1 Ship Motion Equations

Numerical simulation of ship manoeuvring motion is based on ship motion equations. The equations of ship motion describing ship manoeuvres in the horizontal plane can be written with respect to a system of coordinate axes fixed in the ship. This system will be denoted xyz , where the origin of the coordinates will be at-

tached to the center of gravity of the ship. The ship trajectory should be referred to a global coordinate system which is fixed relative to the earth. This system is denoted $ox_0y_0z_0$. The relationships between the two axes are given by

$$x_0 = x \cos \psi - y \sin \psi \quad (3.1)$$

$$y_0 = x \sin \psi + y \cos \psi \quad (3.2)$$

Figure 3.1 shows the two coordinates systems. The most frequently used ship

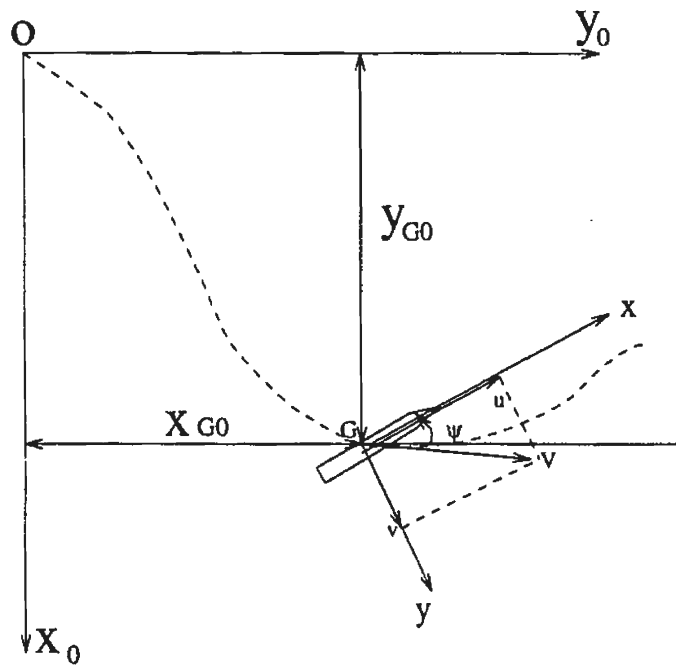


Figure 3.1: Coordinate Systems

motion equations in horizontal plane are a set of three coupled first order nonlinear differential equations that describe the surge, sway and yaw motions of the ship. In Crane et al. (1989), these equations are expressed as

$$\text{Surge : } (\Delta - X_{\dot{u}})\dot{u} = f_1(u, v, r, \delta_R) \quad (3.3)$$

$$\text{Sway : } (\Delta - Y_{\dot{v}})\dot{v} - Y_{\dot{r}}\dot{r} = f_2(u, v, r, \delta_R) \quad (3.4)$$

$$\text{Yaw : } -N_{\dot{v}}\dot{v} + (I_z - N_{\dot{r}})\dot{r} = f_3(u, v, r, \delta_R) \quad (3.5)$$

where u , v , r and δ_R are surge velocity, sway velocity, yaw rate and rudder angle, respectively. A dot over the variable denotes differentiation with respect to time. Δ is the mass of ship and I_z is the mass moment of inertia of ship about the z_0 -axis. f_1 , f_2 and f_3 are the hydrodynamic forces and moments acting on the ship in the surge, sway and yaw modes, respectively. X , Y and N are the surge force in x-direction, the sway force in y-direction and the yaw moment about z -axis. A subscripted variable designates the derivative of the variable with respect to the subscript.

The hydrodynamic forces f_1 , f_2 and f_3 are functions of u , v , r , δ_R and their time derivatives, the propeller thrust and its velocity. These forces can be expressed in their Taylor series expansions as follows:

$$\begin{aligned} f_1(u, v, r, \delta_R) = & X^0 + X_u\delta u + 1/2X_{uu}\delta u^2 + 1/6X_{uuu}\delta u^3 \\ & + 1/2X_{vv}v^2 + 1/2X_{rr}r^2 + 1/2X_{\delta\delta}\delta_R^2 + 1/2X_{vvu}v^2\delta u \\ & + 1/2X_{rru}r^2\delta u + 1/2X_{\delta\delta u}\delta_R^2\delta u + (X_{vr} + \Delta)vr \\ & + X_{v\delta}v\delta_R + X_{r\delta}r\delta_R + X_{vru}vr\delta u + X_{v\delta u}v\delta_R\delta u \\ & + X_{r\delta u}r\delta_R\delta u \end{aligned} \quad (3.6)$$

$$\begin{aligned}
f_2(u, v, r, \delta_R) &= Y_0 + Y_u^0 \delta u + Y_{uu}^0 \delta u^2 + Y_v v \\
&+ 1/6 Y_{vvv} v^3 + 1/2 Y_{vrr} v r^2 + 1/2 Y_{v\delta\delta} v \delta_R^2 + Y_{vu} v \delta u \\
&+ 1/2 Y_{vuu} v \delta u^2 + (Y_r - \Delta u_0) r + 1/6 Y_{rrr} r^3 + 1/2 Y_{rvv} r v^2 \\
&+ 1/2 Y_{r\delta\delta} r \delta_R^2 + Y_{ru} r \delta u + 1/2 Y_{ruu} r \delta u^2 + Y_\delta \delta_R \\
&+ 1/6 Y_{\delta\delta\delta} \delta_R^3 + 1/2 Y_{\delta vv} \delta_R v^2 + 1/2 Y_{\delta rr} \delta_R r^2 + Y_{\delta u} \delta_R \delta u \\
&+ 1/2 Y_{\delta uu} \delta_R \delta u^2 + Y_{vr\delta} v r \delta_R
\end{aligned} \tag{3.7}$$

$$\begin{aligned}
f_3(u, v, r, \delta_R) &= N^0 + N_u^0 \delta u^2 + N_{uu}^0 \delta u^2 + N_v v \\
&+ 1/6 N_{vvv} v^3 + 1/2 N_{vrr} v r^2 + 1/2 N_{v\delta\delta} v \delta_R^2 + N_{vu} v \delta u \\
&+ 1/2 N_{vuu} v \delta u^2 + N_r r + 1/6 N_{rrr} r^3 + 1/2 N_{rvv} r v^2 \\
&+ 1/2 N_{r\delta\delta} r \delta_R^2 + N_{ru} r \delta u + 1/2 N_{ruu} r \delta u^2 + N_\delta \delta_R \\
&+ 1/6 N_{\delta\delta\delta} \delta_R^3 + 1/2 N_{\delta vv} \delta_R v^2 + 1/2 N_{\delta rr} \delta_R r^2 + N_{\delta u} \delta_R \delta u \\
&+ 1/2 N_{\delta uu} \delta_R \delta u^2 + N_{vr\delta} v r \delta_R
\end{aligned} \tag{3.8}$$

where u_0 is the ship approach velocity and $\delta u = u - u_0$.

Substituting equations 3.6 to 3.8 into equations 3.3 to 3.5 and decoupling them gives

$$\dot{u} = \frac{f_1(u, v, r, \delta_R)}{(\Delta - X_{\dot{u}})} \tag{3.9}$$

$$\dot{v} = \frac{(I_z - N_{\dot{r}})f_2(u, v, r, \delta_R) + Y_{\dot{r}}f_3(u, v, r, \delta_R)}{(\Delta - Y_{\dot{v}})(I_z - N_{\dot{r}}) - N_{\dot{v}}Y_{\dot{r}}} \quad (3.10)$$

$$\dot{r} = \frac{(\Delta - Y_{\dot{v}})f_3(u, v, r, \delta_R) + N_{\dot{v}}f_2(u, v, r, \delta_R)}{(\Delta - Y_{\dot{v}})(I_z - N_{\dot{r}}) - N_{\dot{v}}Y_{\dot{r}}} \quad (3.11)$$

3.2 Zigzag Manoeuvre Simulation Procedures

The zigzag manoeuvre is also known as the Kempf overshoot or "Z" manoeuvre. The results of this manoeuvre are indicative of the ability of a ship's rudder to control the ship. Moreover, the results depend somewhat on the stability characteristics of the ship as well as on the effectiveness of the rudder motion. The typical procedure for conducting the zigzag manoeuvre is given as follows (Gertler, 1959):

- (a) Steady the ship on a straight course at a preselected approach speed, u_0 .
- (b) Deflect the rudder at maximum rate to a preselected angle, say 20 degrees, starboard, and hold until a preselected heading angle, say 20 degrees, is reached.
- (c) At this point, deflect the rudder at maximum rate to an angle of 20 degrees, port, and hold until the heading angle reaches 20 degrees at the side of port. This completes one cycle of zigzag manoeuvre.
- (d) If a zigzag test is continued, deflect the rudder again at maximum rate to the same angle as that in step (b). This procedure can be repeated through the

third, the fourth cycle and so on.

3.3 Results of Zigzag Simulation

The data for a Mariner Class ship given in Crane et al. (1989) are used to generate the simulations. The particulars of the ship used to obtain the simulations are shown in Table 3.1.

Table 3.1: Ship Principal Dimensions

Length	Beam	Draft	Block Coef.	Velocity	Rudder Rate
152.4 m	21.763 m	8.138 m	0.600	7.614 m/sec	2.5 deg/sec

The hydrodynamic coefficients needed to calculate the hydrodynamic forces f_1 , f_2 and f_3 in equations 3.6 to 3.8 are given in Table 3.2, taken from Crane et al. (1989). The velocities, u , v and r are calculated by applying a fourth order Runge-Kutta integration method to equations 3.9 to 3.11. Performing the integration over a selected time period will give a set of simulation data for u , v and r . The velocities are integrated once more to obtain a trajectory of the ship. The trajectories are calculated using the following equations:

$$\psi(t) = \psi(0) + \sum_{\tau=0}^{t-\delta t} r(\tau)\delta t \quad (3.12)$$

$$x_{0G}(t) = x_{0G}(0) + \sum_{\tau=0}^{t-\delta t} \{u(\tau)\cos\psi(\tau) - v(\tau)\sin\psi(\tau)\}\delta t \quad (3.13)$$

$$y_{0G}(t) = y_{0G}(0) + \sum_{\tau=0}^{t-\delta t} \{v(\tau)\cos\psi(\tau) + u(\tau)\sin\psi(\tau)\}\delta t \quad (3.14)$$

Table 3.2: Hydrodynamic Coefficients of a Mariner Class Ship

Coefficients (X-equation)	Values	Coefficients (Y-equation)	Values	Coefficients (N-equation)	Values
$\Delta - X_{\dot{u}}$	0.17700	$\Delta - Y_{\dot{v}}$	0.32700	$N_{\dot{v}}$	0.00221
X_u	-0.02530	$Y_{\dot{r}}$	-0.00077	$I_z - N_{\dot{r}}$	0.01750
X_{uu}	0.01896	Y_v	-0.24400	N_v	-0.05550
X_{uuu}	-0.01302	Y_{vvv}	-10.2120	N_{vvv}	2.07000
X_{vv}	-0.37800	Y_{vrr}	0	N_{vrr}	0
X_{rr}	0.01272	$Y_{v\delta\delta}$	-0.00160	$N_{v\delta\delta}$	0.00528
$X_{\delta\delta}$	-0.04000	Y_{vu}	0	N_{vu}	0
X_{vvu}	0	Y_{vuu}	0	N_{vuu}	0
X_{rru}	0	$Y_r - \Delta$	-0.10500	N_r	-0.03747
$X_{\delta\delta u}$	0	Y_{rrr}	0	N_{rrr}	0
$X_{vr} + \Delta$	0.16800	Y_{rvv}	6.46000	N_{rvv}	-2.31600
$X_{v\delta}$	0.01960	$Y_{r\delta\delta}$	0	$N_{r\delta\delta}$	0
$X_{r\delta}$	0	Y_{ru}	0	N_{ru}	0
X_{vru}	0	Y_{ruu}	0	N_{ruu}	0
$X_{v\delta u}$	0	Y_{δ}	0.05860	N_{δ}	-0.02930
$X_{r\delta u}$	0	$Y_{\delta\delta\delta}$	-0.05850	$N_{\delta\delta\delta}$	0.02892
X_{λ^0}	0	$Y_{\delta vv}$	0.50000	$N_{\delta vv}$	0.20640
		$Y_{\delta rr}$	0	$N_{\delta rr}$	0
		$Y_{\delta u}$	0	$N_{\delta u}$	0
		$Y_{\delta uu}$	0	$N_{\delta uu}$	0
		$Y_{vr\delta}$	0	$N_{vr\delta}$	0
		Y^0	-0.00080	N^0	0.00059
		Y_u^0	0	N_u^0	0
		Y_{uu}^0	0	N_{uu}^0	0

where $x_{0G}(t)$, $y_{0G}(t)$ are the instantaneous coordinates of the path of the center of gravity of the ship relative to the fixed set of earth axes. $\psi(t)$ is the instantaneous orientation of the ship.

It should be mentioned here that the process of rudder's deflection can be simulated in real time as follows

$$\delta_R(t) = \delta_R(t_0) \quad \text{until } t > t_0 \quad (3.15)$$

$$\delta_R(t) = \delta_R(t_0) + rate(t - t_0) \quad \text{until } \delta_R(t) = \delta_{Rconst} \quad (3.16)$$

$$\text{then } \delta_R(t) = \delta_{Rconst} \quad (3.17)$$

where δ_R is rudder angle, $rate$ is rudder turning rate and t_0 is the time point from which rudder starts to turn. δ_{Rconst} is the selected rudder angle.

The results of simulation of 20-20 and 35-35 degree zigzag manoeuvres are shown in Figures 3.2 to 3.7. The velocities from the 35-35 degree zigzag manoeuvre will be used to train neural network models for predicting other different ship motions. The results from the 20-20 degree zigzag manoeuvre will be compared with the outcome of neural networks to check the generalization of this model. In addition to using a 20-20 zigzag manoeuvre, a 25 degree turning circle (starboard) will be simulated in a similar way. The velocity and the trajectory of the 25 degree circle will provide an alternative test to check the validity of the generalization of this model.

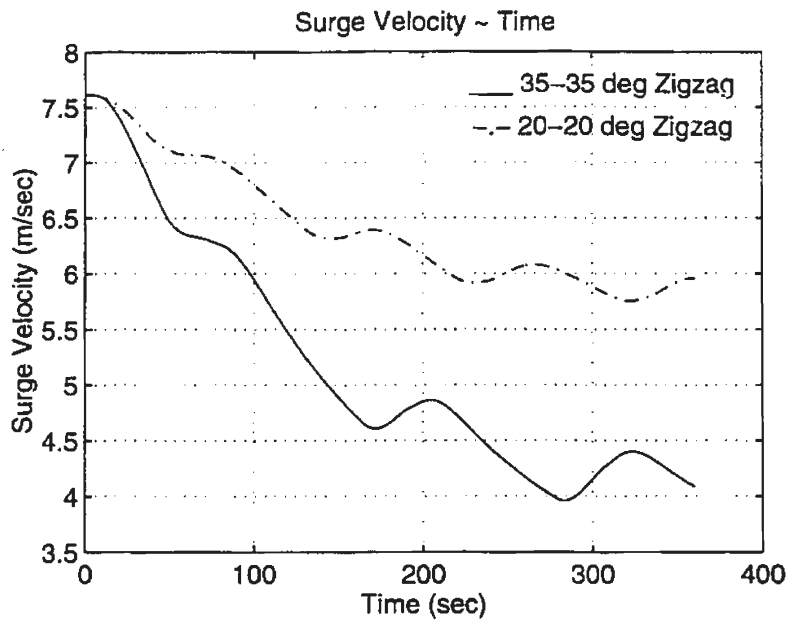


Figure 3.2: Surge Velocity of 20-20 and 35-35 degree Zigzag Manoeuvres

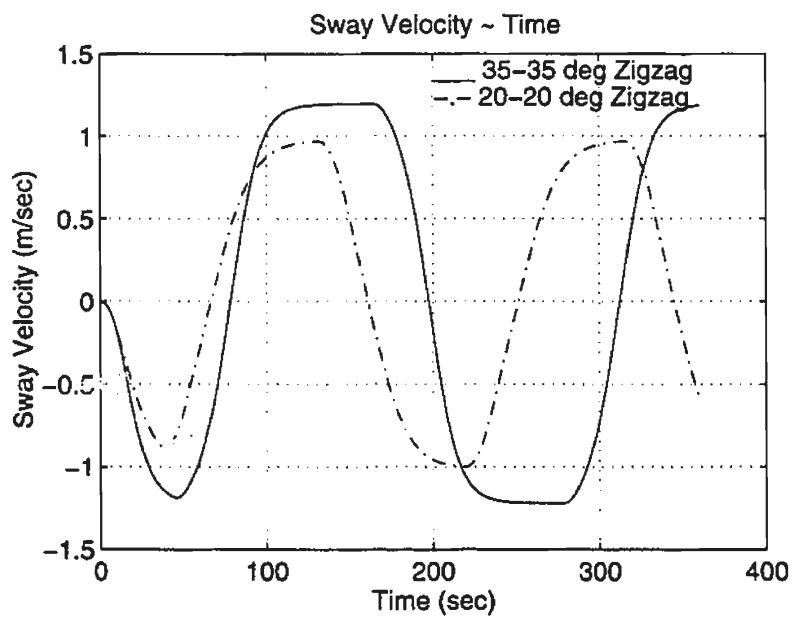


Figure 3.3: Sway Velocity of 20-20 and 35-35 degree Zigzag Manoeuvres

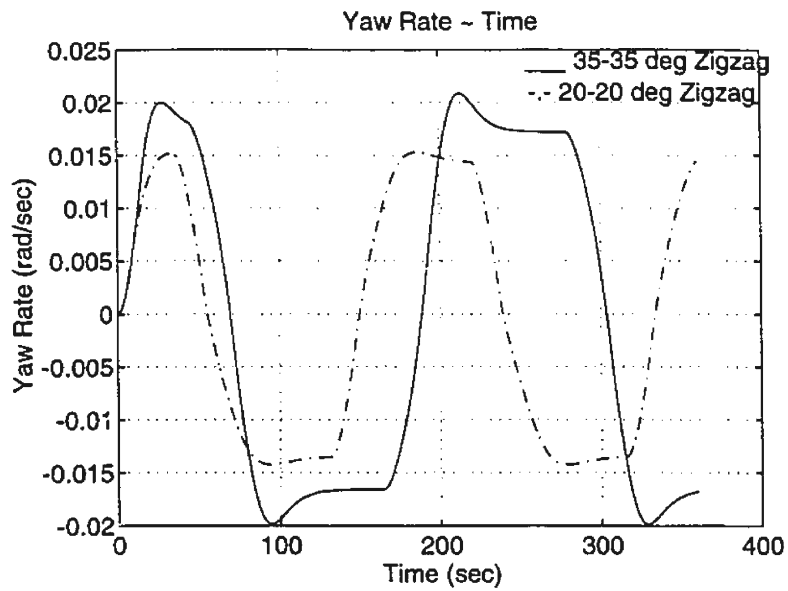


Figure 3.4: Yaw Rate of 20-20 and 35-35 degree Zigzag Manoeuvres

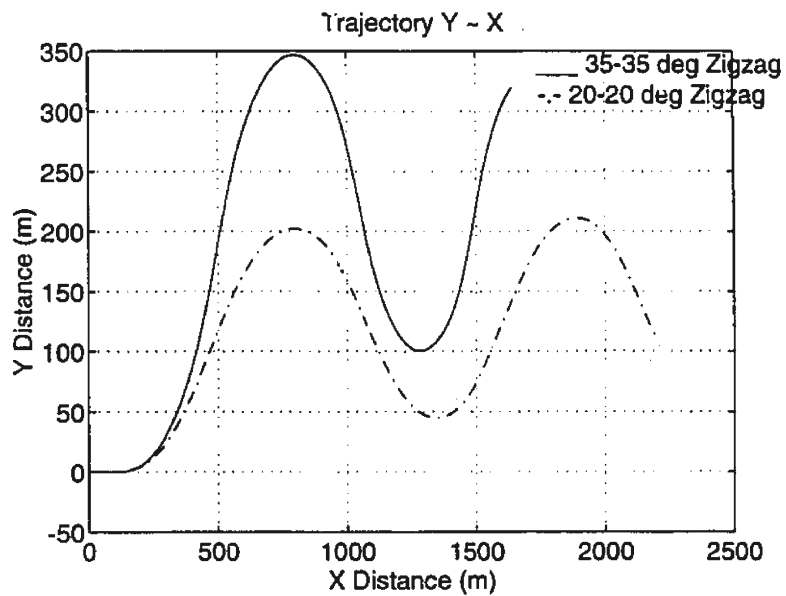


Figure 3.5: Trajectory of 20-20 and 35-35 degree Zigzag Manoeuvres

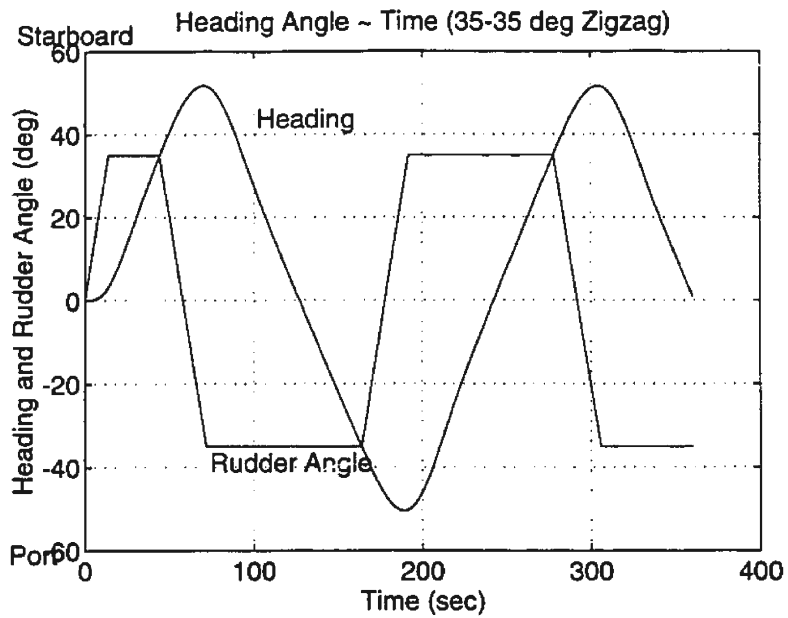


Figure 3.6: Ship Heading and Rudder Command of 35-35 Zigzag Manoeuvre

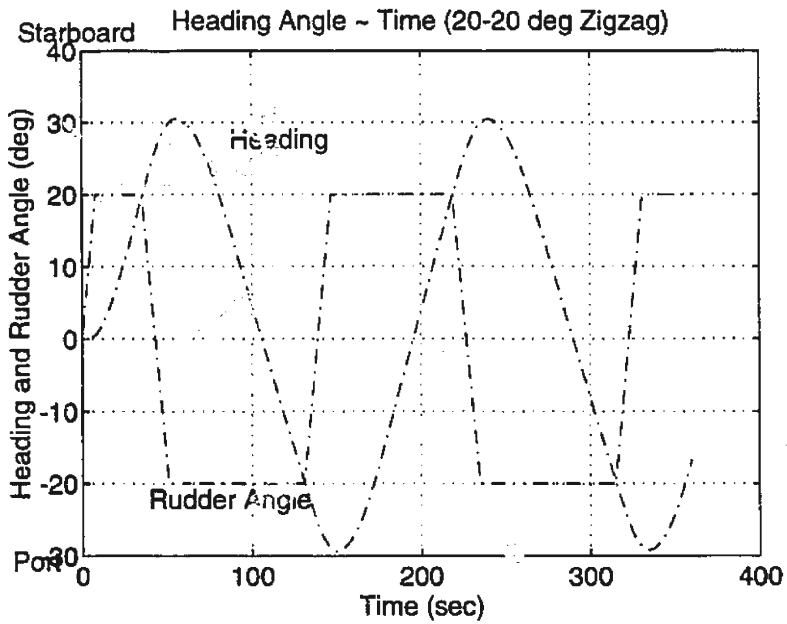


Figure 3.7: Ship Heading and Rudder Command of 20-20 Zigzag Manoeuvre

3.4 Ship Turning Simulation

All ship manoeuvres involve turning. The forces and moments produced by the rudder and the response of the ship to these forces involve a transient and a steady turning phases. The motions in these two phases are governed by the ship motion equations 3.3 to 3.5. The same ship where the hydrodynamic coefficients are shown in Table 3.2 is used to simulate the turning circle manoeuvre. Figures 3.8 to 3.11 show the velocities and trajectory during the ship turning manoeuvre with a rudder angle of 25 degrees, starboard.

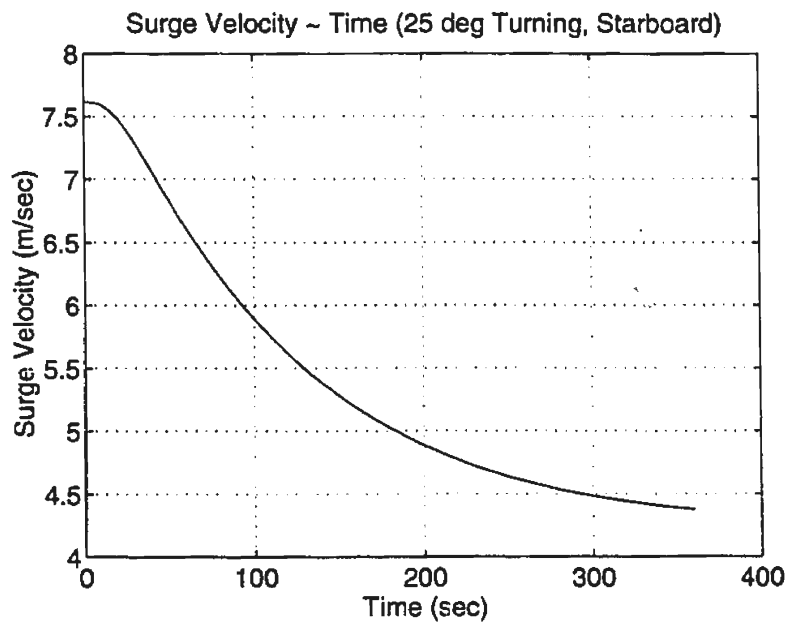


Figure 3.8: Surge Velocity of 25 degree Turning (Starboard)

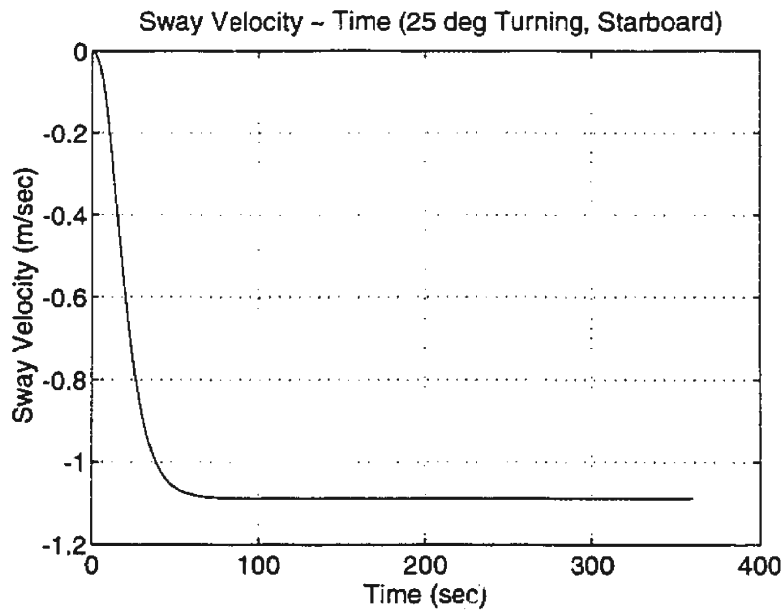


Figure 3.9: Sway Velocity of 25 degree Turning (Starboard)

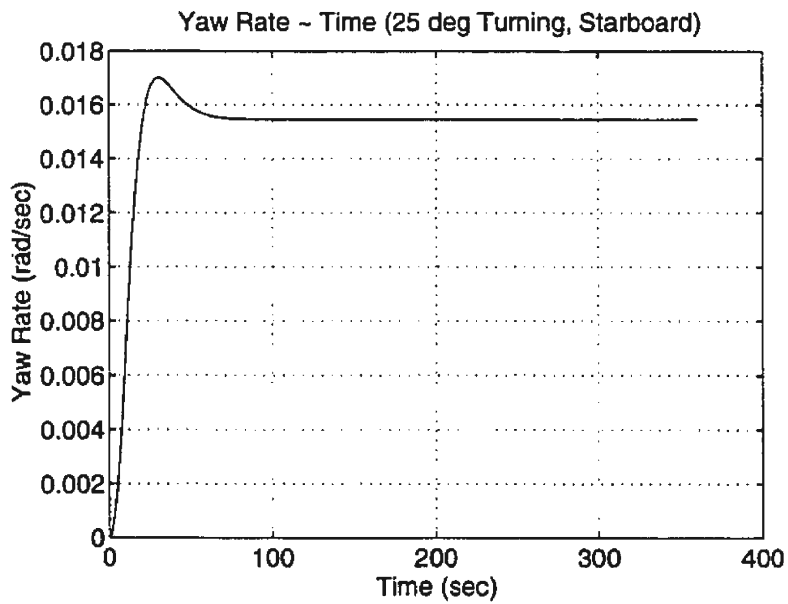


Figure 3.10: Yaw Rate of 25 degree Turning (Starboard)

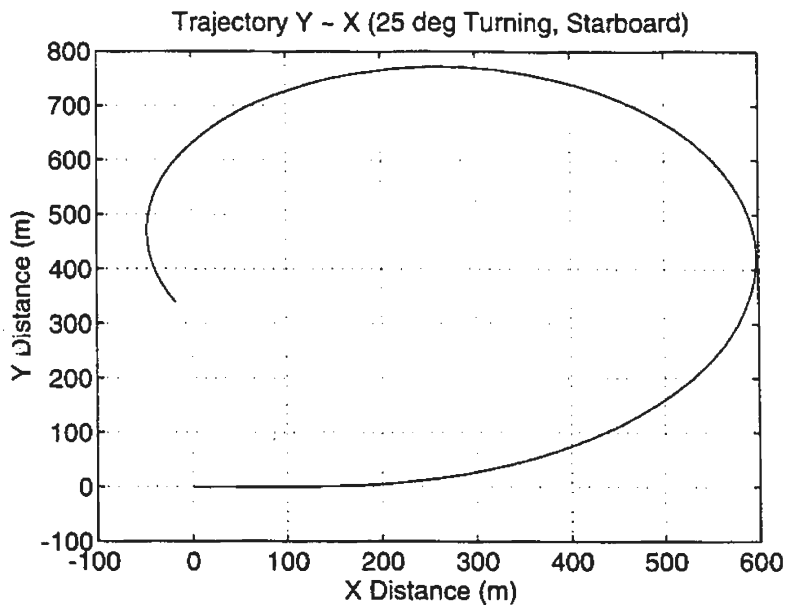


Figure 3.11: Trajectory of 25 degree Turning (Starboard)

3.5 Ship Spiral Manoeuvre Simulation

The direct or Dieudonne spiral manoeuvre is a definitive ship trial (Dieudonne, 1953) which identifies the directional stability characteristics of the vessel. The manoeuvre consists the procedures as follows:

(a) Initially, the ship is kept on a straight course at a constant speed. After about 1 minute, the rudder is turned to an angle of, say, 20 degrees, starboard. The rudder is held until the rate of change of yaw angle maintains a constant value for about 1 minute.

(b) The rudder angle is then decreased by a small amount, say, 5 degrees and held fixed again until a new yaw rate is achieved and is constant for 1 minute.

(c) The foregoing procedure is repeated for different rudder angles changed by small increments from large starboard values to large port values and back again to large starboard values.

The numerical measure obtained from the above spiral manoeuvre is the steady yaw rate as a function of the rudder angle. The spiral manoeuvre simulation is obtained using the ship and its hydrodynamic coefficients as shown in Table 3.2. The maximum rudder angle of this spiral manoeuvre is 20 degrees, starboard and port. The small increment of the rudder in this manoeuvre is 5 degrees. The time interval between consecutive rudder deflections are 60 seconds. Figure 3.12 shows the relationships between steady yaw rates and rudder angles in the 20-degree spiral manoeuvre. The simulation gives a sloped loop in Figure 3.12 indicating a slight directional instability of the ship.

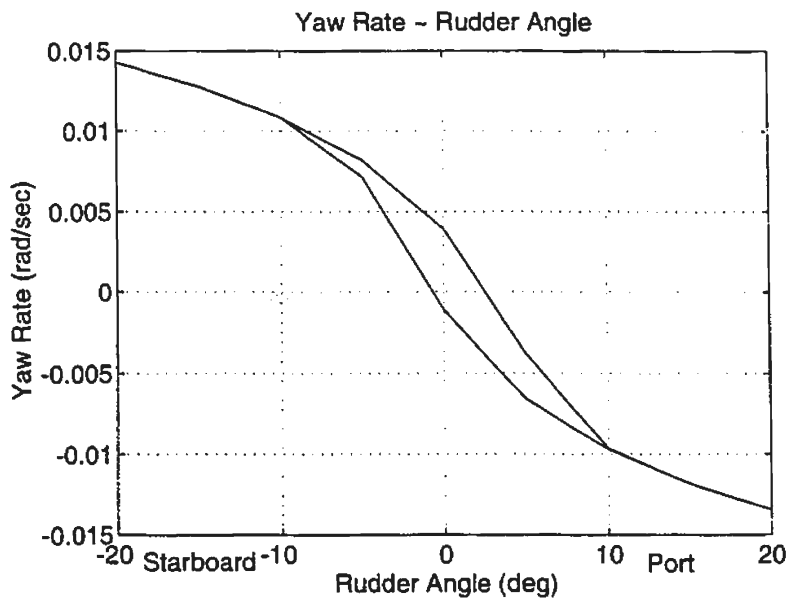


Figure 3.12: Yaw Rates and Rudder Angles in 20 degree Spiral Manoeuvre

Chapter 4

Parametric Identification Using Neural Networks

4.1 Mathematical Model

Equations 3.6 to 3.8 are usually used to calculate hydrodynamic forces acting on the ship during ship manoeuvres under the condition that the hydrodynamic coefficients are known. The coefficients in these equations can be obtained by different approaches as mentioned in chapter 1. Identification of the individual coefficients in these equations is difficult, Abkowitz (1980). Instead of identifying individual hydrodynamic coefficients in equations 3.6 to 3.8, the new method that we will develop in this thesis is to identify the hydrodynamic forces f_1 , f_2 and f_3 in equations 3.6 to 3.8 using experimental results obtained from full scale trials. To test this method, the results of numerical simulation of ship motions will temporarily take the place of the experimental data required in this method. For the purpose of this work, we are going to express the hydrodynamic forces and moments as the sum of a linear part and a nonlinear part. The linear part of forces will retain their Taylor series expansions while the nonlinear part will be lumped together in one

term, known as lumped nonlinear function. The surge force f_1 , the sway force f_2 and the yaw moment f_3 will be written as follows

$$f_1(u, v, r, \delta_R) = X_u \delta u + 1/2 X_{\delta\delta} \delta_R^2 + g_1(u, v, r, \delta_R) \quad (4.1)$$

$$f_2(u, v, r, \delta_R) = Y_v v + (Y_r - \Delta u_0) r + Y_\delta \delta_R + g_2(u, v, r, \delta_R) \quad (4.2)$$

$$f_3(u, v, r, \delta_R) = N_v v + N_r r + N_\delta \delta_R + g_3(u, v, r, \delta_R) \quad (4.3)$$

where g_1 , g_2 and g_3 are lumped nonlinear functions in surge, sway and yaw modes and they are dependent on the surge velocity u , the sway velocity v , the yaw rate r and the rudder angle δ_R .

Compared with equations 3.6 to 3.8, g_1 , g_2 and g_3 correspond to the nonlinear terms in the forms as

$$\begin{aligned} g_1(u, v, r, \delta_R) = & X^0 + 1/2 X_{uu} \delta u^2 + 1/6 X_{uuu} \delta u^3 \\ & + 1/2 X_{vv} v^2 + 1/2 X_{rr} r^2 + 1/2 X_{vvu} v^2 \delta u \\ & + 1/2 X_{rru} r^2 \delta u + 1/2 X_{\delta\delta u} \delta_R^2 \delta u + (X_{vr} + \Delta) v r \\ & + X_{v\delta} v \delta_R + X_{r\delta} r \delta_R + X_{vru} v r \delta u + X_{v\delta u} v \delta_R \delta u \\ & + X_{r\delta u} r \delta_R \delta u \end{aligned} \quad (4.4)$$

$$\begin{aligned} g_2(u, v, r, \delta_R) = & Y_0 + Y_u^0 \delta u + Y_{uu}^0 \delta u^2 \\ & + 1/6 Y_{vvv} v^3 + 1/2 Y_{vrr} v r^2 + 1/2 Y_{v\delta\delta} v \delta_R^2 + Y_{vu} v \delta u \\ & + 1/2 Y_{vuu} v \delta u^2 + 1/6 Y_{rrr} r^3 + 1/2 Y_{rvv} r v^2 \\ & + 1/2 Y_{r\delta\delta} r \delta_R^2 + Y_{ru} r \delta u + 1/2 Y_{ruu} r \delta u^2 \\ & + 1/6 Y_{\delta\delta\delta} \delta_R^3 + 1/2 Y_{\delta vv} \delta_R v^2 + 1/2 Y_{\delta rr} \delta_R r^2 + Y_{\delta u} \delta_R \delta u \\ & + 1/2 Y_{\delta uu} \delta_R \delta u^2 + Y_{v\delta} v r \delta_R \end{aligned} \quad (4.5)$$

$$\begin{aligned}
g_3(u, v, r, \delta_R) &= N^0 + N_u^0 \delta u^2 + N_{uu}^0 \delta u^2 \\
&+ 1/6 N_{vvv} v^3 + 1/2 N_{vrr} v r^2 + 1/2 N_{v\delta\delta} v \delta_R^2 + N_{vu} v \delta u \\
&+ 1/2 N_{vuu} \delta u^2 + 1/6 N_{rrr} r^3 + 1/2 N_{rvv} r v^2 \\
&+ 1/2 N_{r\delta\delta} r \delta^2 + N_{ru} r \delta u + 1/2 N_{ruu} r \delta u^2 \\
&+ 1/6 N_{\delta\delta\delta} \delta_R^3 + 1/2 N_{\delta vv} \delta_R v^2 + 1/2 N_{\delta rr} \delta_R r^2 + N_{\delta u} \delta_R \delta u \\
&+ 1/2 N_{\delta uu} \delta_R \delta u^2 + N_{vr\delta} v r \delta_R
\end{aligned} \tag{4.6}$$

It should be mentioned that the second order term $1/2 X_{\delta\delta} \delta_R^2$ in the surge equation 4.1 was separated from the nonlinear function g_1 . This second order term is quite significant because there is no first order term $X_{\delta} \delta_R$ in the surge equation. In equations 4.1 to 4.3, the linear part gives a qualitative description of ship manoeuvres while the nonlinear part plays the role of the refinement of the quantitative description of these manoeuvres.

The linear coefficients in equations 4.1 to 4.3 will be estimated using Clarke's formula, Clarke et al. (1982). The lumped nonlinear functions g_1 , g_2 and g_3 will be identified through a neural network approach.

4.2 Estimation of the Linear Part

To identify the hydrodynamic forces f_1 , f_2 and f_3 , we need to estimate the linear derivatives of hydrodynamic forces in equations 4.1 to 4.3. These can be obtained by doing planar motion mechanism or rotation arm ship model tests. In this thesis, we use Clarke's Formula, Clarke et al. (1982), to obtain estimates for these

derivatives as follows

$$Y_{\dot{v}} = -\pi(T/L)^2(1 + 0.16C_B B/T - 5.1(B/L)^2) \quad (4.7)$$

$$Y_{\dot{r}} = -\pi(T/L)^2(0.67B/L - 0.0033(B/T)^2) \quad (4.8)$$

$$Y_v = -\pi(T/L)^2(1 + 0.40C_B B/T) \quad (4.9)$$

$$Y_r = -\pi(T/L)^2(-1/2 + 2.2B/L - 0.080B/T) \quad (4.10)$$

$$Y_{\delta} = (A/L/T)(T/L)const \quad (\text{Note : } const = 3.0) \quad (4.11)$$

$$N_{\dot{v}} = -\pi(T/L)^2(1.1B/L - 0.041B/T) \quad (4.12)$$

$$N_{\dot{r}} = -\pi(T/L)^2(1/12 + 0.017C_B B/T - 0.33B/L) \quad (4.13)$$

$$N_v = -\pi(T/L)^2(1/2 + 2.4T/L) \quad (4.14)$$

$$N_r = -\pi(T/L)^2(1/4 + 0.039B/T - 0.56B/L) \quad (4.15)$$

$$N_{\delta} = -1/2Y_{\delta} \quad (4.16)$$

where L, B, T and C_B are ship length, breadth, draft and block coefficient. A is the rudder area. In this work, we take the ratio of A to LT to be 0.02. All of the above derivatives are nondimensionalized using the system of density ρ , length L and velocity u_0 . In this work, we use ρ , L, T and u_0 system and transform the nondimensional coefficients into ρ , L, T and u_0 system by multiplying the above formulae with L/T. The derivative $X_{\dot{u}}$ is estimated by 5% of the displacement of the ship. X_u is chosen in the range of -0.02 to -0.05. It is very difficult to get the exact estimation of X_u because it depends on so many factors as the propeller properties, the interaction effects of ship and propeller and the rotation speed of propeller etc. But, the errors of the estimation will not affect the accuracy of the neural network model. According to equations 4.1 to 4.3, the left hand sides of equations are hydrodynamic forces and the right hand sides are composed of two

parts: the linear part and the lumped nonlinear functions. If some errors occur in the estimation of the linear part, the lumped nonlinear part will offset these errors to keep the left hand side forces still correct. Therefore, the errors in estimating the linear coefficients will be absorbed in the nonlinear components of the forces.

As to $X_{\delta\delta}$, we have the relationship

$$X = -Y \tan \delta_R \quad (4.17)$$

where X is the x-component of the rudder force. Y is the component of the rudder force normal to the ship center plane when the rudder is turned at an angle of δ_R degrees. Equation 4.17 can be rewritten as follows

$$\begin{aligned} X &= -Y \tan \delta_R \\ &= -Y_\delta \delta_R \tan \delta_R \\ &= -Y_\delta \delta_R (\delta_R - 1/6 \delta_R^3 + \dots) \\ &= -Y_\delta \delta_R^2 + 1/6 Y_\delta \delta_R^4 - \dots \end{aligned} \quad (4.18)$$

where Y_δ is the derivative of Y with respect to δ . From equation 4.18, it is easy to find that $X_{\delta\delta}$ is equal to $-2Y_\delta$ where the nondimensional Y_δ in Clarke et al. (1982) is as follows

$$Y_\delta = \frac{A}{LT} \frac{T}{L} * 3.0 \quad (4.19)$$

where A is the rudder area.

So $X_{\delta\delta}$ will end up in the following form:

$$X_{\delta\delta} = -2Y_\delta$$

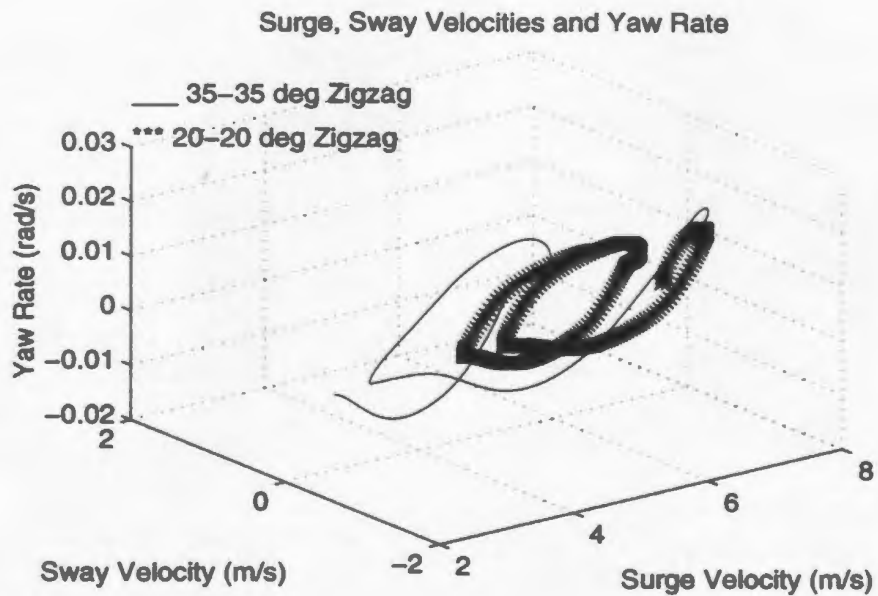


Figure 5.1: Velocity Space of 35-35 deg Zigzag and 20-20 deg Zigzag

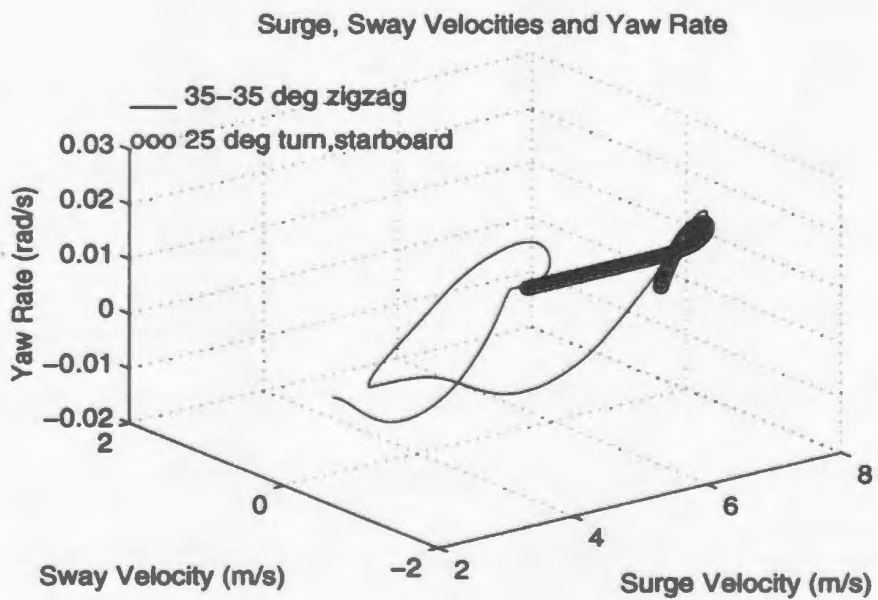


Figure 5.2: Velocity Space of 35-35 deg Zigzag and 25 deg Turning

entiation algorithm was used to obtain the accelerations. Figures 4.4 to 4.6 show the numerical results of the surge, sway and yaw accelerations of the 35-35 degree zigzag manoeuvre. With the coefficients in equations 4.21 to 4.23 estimated using Clarke's Formula (Clarke et al., 1982), the three lumped nonlinear functions g_1 , g_2 and g_3 in equations 4.21 to 4.23 corresponding to the set data of u , v , r and δ_R can be obtained. This will make it possible to employ a neural network to approximate the relationship between u , v , r , δ_R and g_1 , g_2 , g_3 . In this neural network model, u , v , r and δ are used as input data to the network, while g_1 , g_2 and g_3 are used as target data for the output of the network. After training the network using different data samples, we will finally have a functional mapping between u , v , r , δ_R and g_1 , g_2 , g_3 , which can be used to predict ship manoeuvring motions.

4.4 Training Static Neural Networks

4.4.1 Choosing Training Samples and Setting Up Network

Generalization in neural networks is a measure of how well the network performs on the actual problem once training is complete. It is influenced by three parameters: the number of data samples (how well they represent the problem at hand), the complexity of the underlying problem, and the network size and structure.

The second factor is fixed because the complexity of the problem is to approximate high order multi-variate functions as shown in equations 4.4 to 4.6. As to the structure of the network, the four input nodes are input of u , v , r and δ_R . The only one output node is one of the three lumped nonlinear equations. So, three different

networks are employed for training three nonlinear equations. As far as the number of the middle layer nodes is concerned, it is suggested in theory (IEEE Press, 1992a and b) that $2n+1$ would be sufficient where n is the number of inputs. Here, $n=4$, so $2n+1$ is 9. The larger the number of the middle layer nodes, the more squashing functions the network can form and the more likely the true function mapping is achieved. But, too many middle layer nodes would result in a network that is not good at generalization. We set the number of the middle layer nodes to 11. However, according to Hinchey's opinion (1994), common sense would suggest that a mapping for even a single input / single output system could require thousands of hidden neurons. The number depends only on the complexity of system. For the work of this thesis, we set the number of middle-layer nodes to 11 and have found that the neural network training results are pretty good. (See Figures 4.7 to 4.9)

After the size of the network is set, the issue becomes how many training samples are required in this network. It is known that all ship manoeuvres involve turning motions. For one specific turning, only one steady sway velocity, yaw rate and their corresponding rudder angle are available. For generalization, many different rudder-angle turning manoeuvres are required in the training samples. One simple and reliable approach is to take the zigzag manoeuvre. Consider a typical zigzag manoeuvre, see Figures 3.2 to 3.4. During zigzag manoeuvre, the rudder is turned to a selected rudder angle, say, 35 degrees, at the rudder rate of 2.5 degree/second. After the heading angle is reached, a selected heading angle, say, 35 degrees, the rudder will deflect to the opposite side until 35 degrees rudder angle is reached and so on. If the data measuring frequency is 1 per second. the data of surge, sway

and yaw velocities at the rudder angles of $0, \pm 2.5, \pm 5.0, \pm 7.5, \pm 10.0, \dots, \pm 35$ degrees can be obtained. These data will provide sufficient information of different rudder angle turning motions. Therefore, one zigzag manoeuvre is sufficient to provide the training sample. The reasons for choosing 35-35 degree zigzag manoeuvre are: 1) the maximum rudder angle is usually 35 degrees and the 35-35 degree zigzag can cover the range of rudder angles from 0 to ± 35.0 degrees with an interval of 2.5 degrees. 2) The nonlinear components in the hydrodynamic terms in equations at large rudder angle zigzag manoeuvres are more significant than those at small rudder angle manoeuvres. For training the lumped nonlinear functions, we should consider using a large rudder angle zigzag manoeuvre to get a sufficiently large magnitude in the nonlinear terms. Figures 4.1 to 4.3 show the difference between 35-35 degree zigzag and 15-15 degree zigzag manoeuvre.

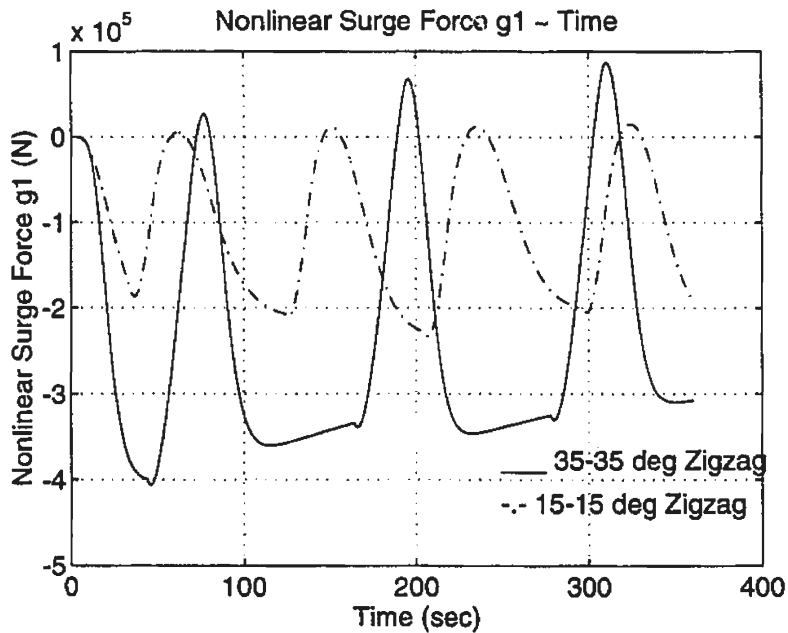


Figure 4.1: Comparison of Nonlinear Part in Surge Function

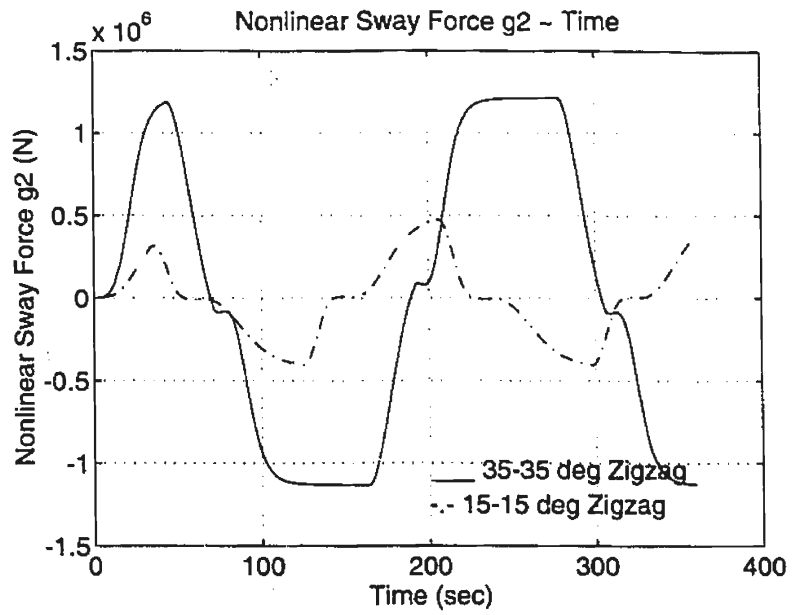


Figure 4.2: Comparison of Nonlinear Part in Sway Function

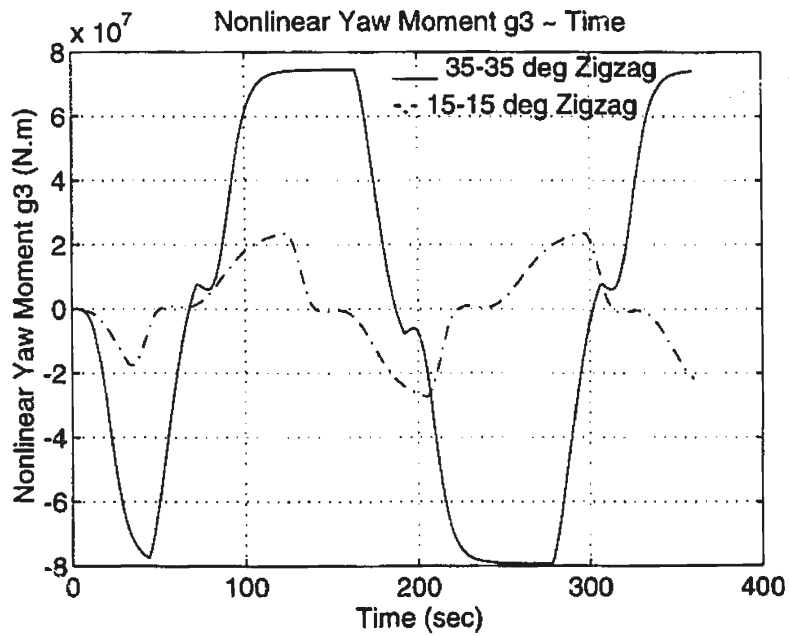


Figure 4.3: Comparison of Nonlinear Part in Yaw Function

A reasonable length of measured data, u , v , r and δ_R is sufficient to formulate the model with good generalization. The measuring length of data of u , v , r and δ_R is 6 minutes, about two cycles of zigzag motions. The data measuring frequency is 1 per second. An alternative way to do this is to use the Dieudonne spiral manoeuvre with maximum rudder angle of 35 degrees. This is not done in this thesis.

4.4.2 Nondimensionalization of the Input and Output

To facilitate the training, we will use the dimensionless forms of input data and target data. Their nondimensional forms are given as follows

$$u' = u/u_0 \quad (4.24)$$

$$v' = v/u_0 \quad (4.25)$$

$$r' = rL/u_0 \quad (4.26)$$

$$g'_1 = g_1/(0.5\rho LTu_0^2) \quad (4.27)$$

$$g'_2 = g_2/(0.5\rho LTu_0^2) \quad (4.28)$$

$$g'_3 = g_3/(0.5\rho L^2Tu_0^2) \quad (4.29)$$

where u' , v' , r' , g'_1 , g'_2 and g'_3 are dimensionless forms of surge velocity, sway velocity, yaw rate and the lumped nonlinear functions.

This helps, for example, if r is adopted as input of the neural network, the magnitude of r is very small, say, 0.01 rad/sec, and the nondimensional r' will enlarge their values by L/u_0 times, i.e., 152.4/7.614 times. The magnitude of r' will be in the range of 10^{-1} to 10^0 . This makes it easier to train enlarged data in

neural network. In another way, the huge ship surge, sway force and yaw moment will be changed into small magnitude in nondimensional forms. These nonlinear forces will thus be decreased from the magnitude of around 10^6 to that of around 10^{-1} . See Figures 4.1 to 4.3 and 4.7 to 4.9. The nondimensionalization will greatly improve the accuracy and the efficiency of the neural work model.

4.4.3 Training Process

Three similar neural networks are used for training g_1 , g_2 and g_3 . Each of the three has four input nodes, u , v , r and δ_R . The data of u , v , r and δ_R are from the 35-35 degree zigzag manoeuvre. Eleven middle-layer nodes are employed. One output node is used for each of the three networks. Target data for each of the three networks are calculated according to equations 4.21 to 4.23, where the accelerations in them can be obtained either by differentiating velocities with respect to time or by measuring them on board the ship. Figures 4.4 to 4.6 give the surge, sway and yaw accelerations of the 35-35 degree zigzag manoeuvre.

The initial weights in these three networks are taken at random. The initial training rate η is set 10^{-2} and the number of the iteration is fixed to 6000. For each iteration, the weights are updated by those from the previous iteration according to equations 2.20 and 2.21. The derivatives of sum-of-squared-error with respect to every weight are given in equations 2.15 and 2.19, which is a back-propagation algorithm. After a fixed number of iterations, we check the errors between the target data and the network output. After the first 6000 times' training, the errors are still pretty large. Then, we set the number of iteration to 10,000 and the

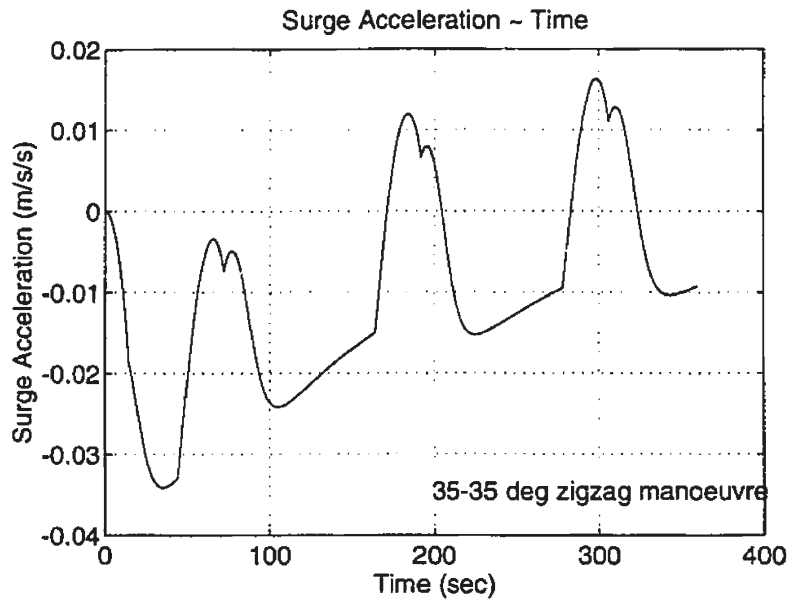


Figure 4.4: Surge Accelerations of 35-35 deg Zigzag

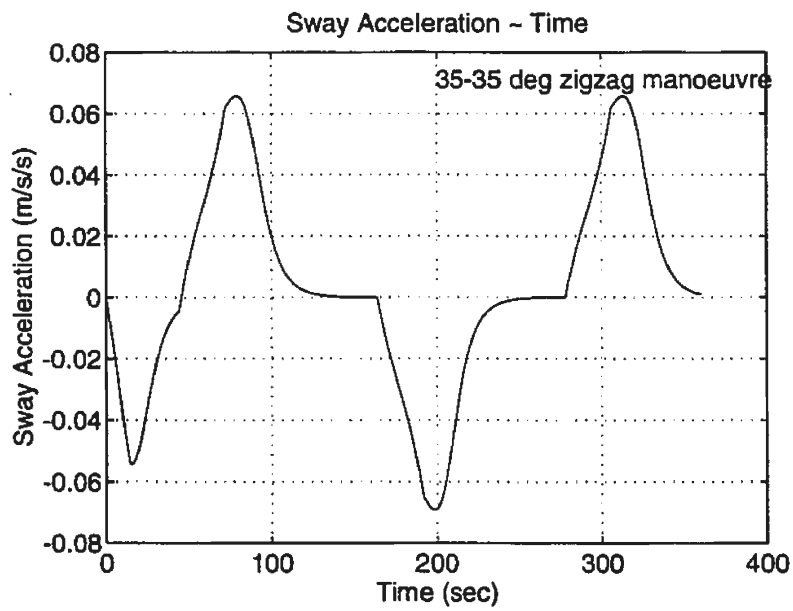


Figure 4.5: Sway Accelerations of 35-35 deg Zigzag

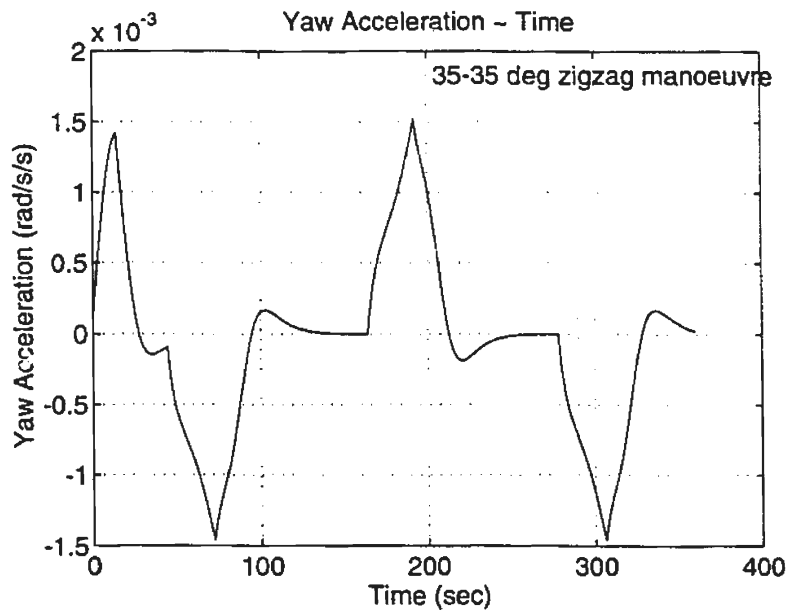


Figure 4.6: Yaw Accelerations of 35-35 deg Zigzag

training rate to 10^{-3} . After finishing that training, we find that the errors become smaller, but they haven't converged to the global minimum. So, the training rate is decreased to 10^{-6} and the training is repeated 60,000 times. At that time, the training results become quite satisfactory. (see Figures 4.7 to 4.9)

Hinchey (1994) postulated that for large $W * I + B$ in the squashing function of $f(W * I + B)$, the value of the squashing function changes slowly and the slopes are very small; thus, steepest descent training is often very slow. After training several thousands of times, the errors decrease significantly, but they still remain at a certain level that may probably be a local minimum. Noise is added to the weights to shake up the iteration by increasing the training rate from 10^{-6} to 10^{-3} . After shaking up the network, we restore the training rate to 10^{-6} . The noise is

used periodically to avoid converging to local minima.

Tables 4.2 and 4.3 give the weights of each of the three neural networks after a total 6 million iterations of training. Figures 4.7 to 4.9 show the training results after 6 million iterations.

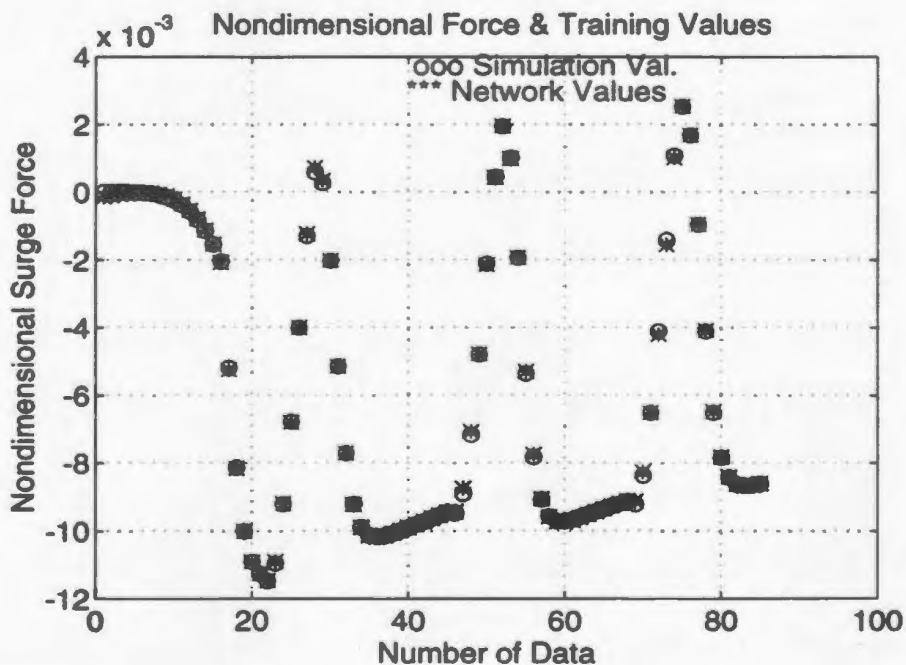


Figure 4.7: Trained Network Force g_1 and Simulation Values

The trained g_1 , g_2 and g_3 are then used to calculate a set of data, u , v and r through numerical integration, see the next section. These results from networks will be compared with the training data of the 35-35 degree zigzag. In addition to this, the trained g_1 , g_2 and g_3 are also used to generate different modes of ship manoeuvres, say, 20-20 degree zigzag manoeuvre or 25 degree turning to check the validity of this trained neural network model. See chapter 5 for details. Only if

Table 4.2: Trained Weights

Notation	Weights of g_1	Weights of g_2	Weights of g_3
$W_{1,1}$	6.881667e-01	1.124596e-01	1.445560e-01
$W_{1,2}$	-3.944832e-01	-7.153550e-01	-2.026504e-01
$W_{1,3}$	-3.527213e-02	-3.141433e-01	-2.895210e-01
$W_{1,4}$	1.328625e-01	-1.211525e+00	1.018099e-01
$W_{1,5}$	-5.807726e-02	3.582274e-01	-1.470738e-02
$W_{2,1}$	-2.488225e-01	-9.658595e-02	-2.212969e-02
$W_{2,2}$	3.612388e-01	1.236665e-01	-1.891460e-03
$W_{2,3}$	2.930168e-01	2.227684e-01	4.450960e-01
$W_{2,4}$	3.809817e-01	7.343950e-01	1.628508e-01
$W_{2,5}$	-5.631810e-01	3.268214e-02	-3.284865e-01
$W_{3,1}$	6.661150e-01	-1.964452e-02	8.668510e-02
$W_{3,2}$	1.378698e-02	-2.574852e-02	-3.123397e-01
$W_{3,3}$	2.381621e-01	-2.938214e+00	-4.291038e-01
$W_{3,4}$	-4.724814e-01	-1.301846e-03	4.851505e+00
$W_{3,5}$	1.035585e+00	1.931175e+00	5.937653e-01
$W_{4,1}$	2.416924e-01	-3.331723e-01	-2.162823e-01
$W_{4,2}$	-8.350883e-01	-5.640769e+00	7.046855e-01
$W_{4,3}$	8.619278e-02	-3.519750e-01	-3.534379e-02
$W_{4,4}$	3.073842e-01	9.035505e+00	-1.547367e+00
$W_{4,5}$	2.183856e-01	5.283974e+00	9.438439e-01
$W_{5,1}$	6.596430e-02	3.748139e-01	5.365179e-01
$W_{5,2}$	2.319937e+00	-4.943792e+00	-3.471369e+00
$W_{5,3}$	5.187373e-01	-2.324225e+00	1.004732e-01
$W_{5,4}$	8.867126e-01	1.210262e+00	-5.075208e-01
$W_{5,5}$	9.101403e-01	7.052080e-01	1.920630e+00
$W_{6,1}$	3.826588e-01	2.684716e+00	1.233939e+00
$W_{6,2}$	7.144276e-01	-3.650819e+00	-3.840159e+00
$W_{6,3}$	9.013611e-01	6.843653e-02	8.110864e-01
$W_{6,4}$	1.115638e+00	9.748793e+00	2.627589e+00
$W_{6,5}$	5.981893e-01	-2.510483e+00	-2.661712e-01
$W_{7,1}$	1.048308e-01	-6.160183e-01	-7.446582e-02
$W_{7,2}$	4.564520e-01	-5.237246e+00	-1.769820e-01
$W_{7,3}$	4.807633e-01	-1.897283e-01	-8.972702e-01

Table 4.3: Trained Weights (continued)

Notation	Weights of g_1	Weights of g_2	Weights of g_3
$W_{7,4}$	4.643421e-01	8.722503e-01	2.205615e-01
$W_{7,5}$	3.196577e-01	-7.771210e-01	4.379680e-01
$W_{8,1}$	1.245919e-01	-2.064622e-01	-5.369309e-02
$W_{8,2}$	1.681337e-01	-4.559899e-01	-2.104892e+00
$W_{8,3}$	2.966626e-01	2.110949e-01	-1.580829e+00
$W_{8,4}$	1.904150e+00	9.413087e-01	7.669541e-01
$W_{8,5}$	1.492542e+00	-1.514163e+00	8.674012e-01
$W_{9,1}$	1.395203e-01	5.816624e-01	-2.474599e-01
$W_{9,2}$	1.715687e+00	2.860595e+00	-2.268058e+00
$W_{9,3}$	-5.235515e-01	-3.586910e+00	-9.999372e-01
$W_{9,4}$	5.407330e-01	3.418939e-02	5.782262e-01
$W_{9,5}$	1.070580e+00	1.895018e+00	7.882830e-01
$W_{10,1}$	1.190725e-01	-6.458673e-01	4.028050e-01
$W_{10,2}$	-1.572068e+00	-5.328222e+00	-1.200331e+00
$W_{10,3}$	-6.974020e-01	-3.754626e+00	-1.791450e-01
$W_{10,4}$	-1.500409e+00	-4.340130e-01	1.934278e+00
$W_{10,5}$	-7.620439e-01	1.397392e+00	-3.149415e+00
$W_{11,1}$	8.695507e-03	-1.026031e-01	-4.551900e-01
$W_{11,2}$	-1.817876e+00	-5.718252e+00	2.809314e-01
$W_{11,3}$	-7.909079e-01	4.083211e-01	-3.350986e-02
$W_{11,4}$	3.808360e-01	-1.006815e+01	-6.576354e-01
$W_{11,5}$	7.625293e-01	2.389434e+00	3.685727e+00
$B_{1,1}$	1.642322e-01	3.261543e-01	1.806269e+00
$B_{2,1}$	-2.390909e+00	-5.411926e+00	-2.776546e-01
$B_{3,1}$	-6.168362e-02	-2.400292e+00	-1.465113e-01
$B_{4,1}$	1.042998e+00	4.345065e-01	5.826147e+00
$B_{5,1}$	1.271263e-01	4.989832e-02	-2.857234e+00
$B_{6,1}$	1.347139e-01	-5.240397e-01	-1.536862e-01
$B_{7,1}$	2.764921e-01	-3.369925e+00	2.142906e-01
$B_{8,1}$	-7.323281e-03	-2.489338e+00	1.552479e-01
$B_{9,1}$	2.374341e+00	9.109346e-01	3.129434e+00
$B_{10,1}$	-1.182426e+00	2.402799e-01	-1.006095e+00
$B_{11,1}$	-1.643149e-01	-3.054061e-01	-7.080138e-01
$B_{12,1}$	1.259074e+00	-2.960220e+00	-3.138889e-02

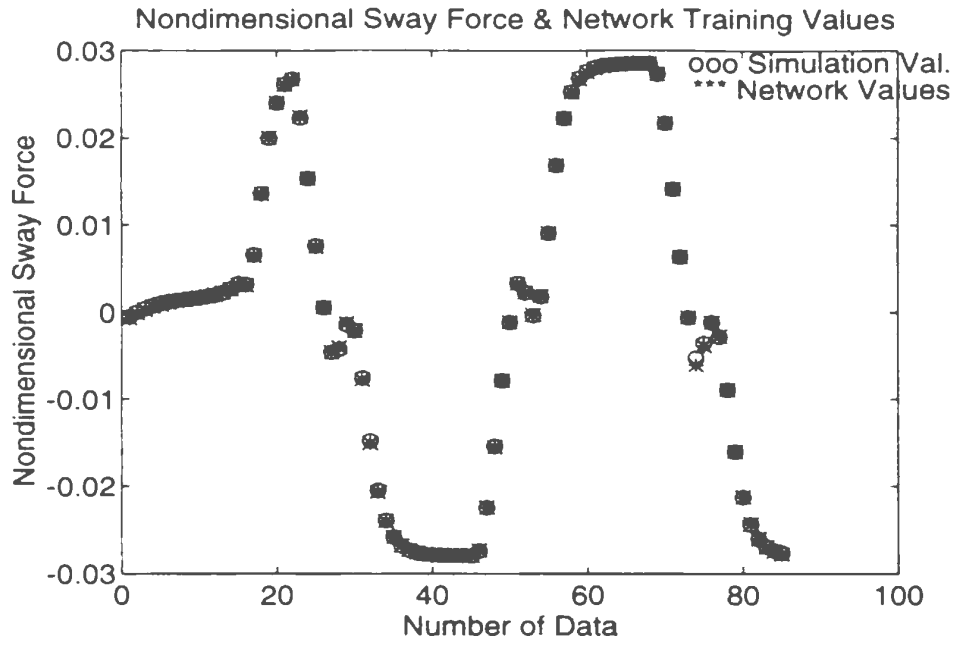


Figure 4.8: Trained Network Force g_2 and Simulation Values

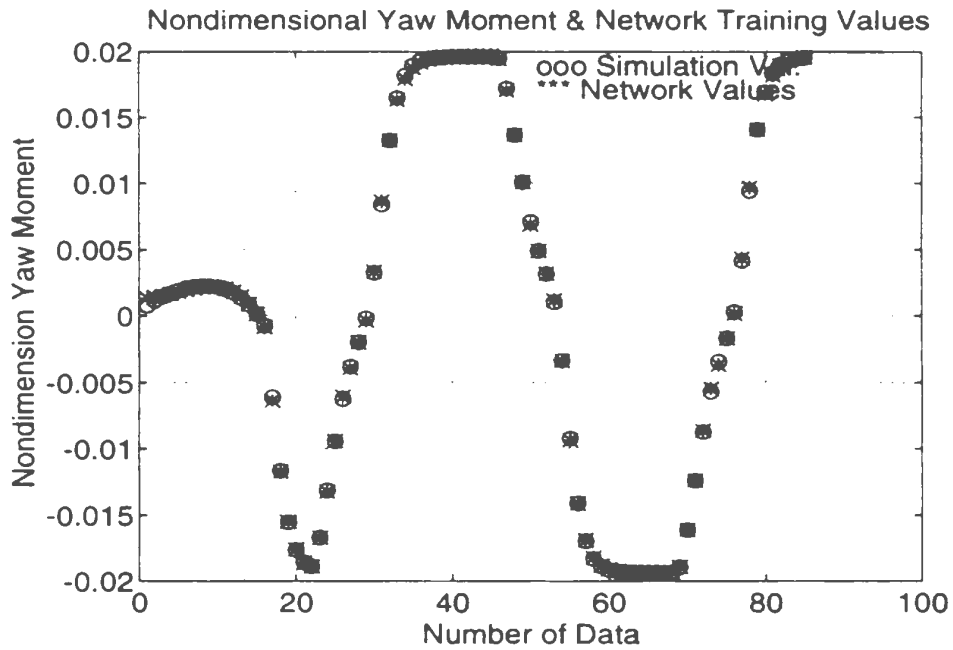


Figure 4.9: Trained Network Moment g_3 and Simulation Values

the results from the networks fit well with the test data can the training process be considered complete.

In the process of training the data, we find that the lumped surge function g_1 converges so slowly that it takes three times as long as the sway function g_2 and the yaw function g_3 . This is caused by the dependence of surge force on $(u - u_0)$.

Since there are many different order nonlinear terms in these three lumped nonlinear functions, the speed for training the neural network to map the relationship between g_1, g_2, g_3 and u, v, r, δ_R is slow. For example, it takes 6 million iterations and 10 hours of computation time to complete training the network for the function g_2 . However, this is still cheaper than using the experimental methods to determine these hydrodynamic force functions.

4.5 Prediction of Ship Motion Using Trained g_1, g_2 and g_3

If an initial condition of u, v, r and δ_R is known, the hydrodynamic forces acting on the ship can be calculated using equations 4.1 to 4.3. Substituting equations 4.1 to 4.3 into equations 3.3 to 3.5 gives the following forms:

$$(\Delta - X_{\dot{u}})\dot{u} = X_u \delta u + 1/2 X_{\delta\delta} \delta_R^2 + g_1(u, v, r, \delta_R) \quad (4.30)$$

$$(\Delta - Y_{\dot{v}})\dot{v} - Y_r \dot{r} = Y_v v + (Y_r - \Delta u_0)r + Y_\delta \delta_R + g_2(u, v, r, \delta_R) \quad (4.31)$$

$$-N_{\dot{v}}\dot{v} + (I_z - N_r)\dot{r} = N_v v + N_r r + N_\delta \delta_R + g_3(u, v, r, \delta_R) \quad (4.32)$$

The above equations are coupled by accelerations of \dot{u} , \dot{v} and \dot{r} . Decoupling the three equations gives

$$\dot{u} = \frac{X_u \delta u + 1/2 X_{\delta\delta} \delta_R^2 + g_1(u, v, r, \delta_R)}{(\Delta - X_{\dot{u}})} \quad (4.33)$$

$$\begin{aligned} \dot{v} = & \frac{1}{(\Delta - Y_{\dot{v}})(I_z - N_{\dot{r}}) - N_{\dot{v}} Y_{\dot{r}}} \\ & * \{(I_z - N_{\dot{r}})[Y_v v + (Y_r - \Delta u_0)r + Y_{\delta} \delta_R + g_2(u, v, r, \delta_R)] \\ & + Y_{\dot{r}}[N_v v + N_r r + N_{\delta} \delta_R + g_3(u, v, r, \delta_R)]\} \end{aligned} \quad (4.34)$$

$$\begin{aligned} \dot{r} = & \frac{1}{(\Delta - Y_{\dot{v}})(I_z - N_{\dot{r}}) - N_{\dot{v}} Y_{\dot{r}}} \\ & * \{(\Delta - Y_{\dot{v}})[N_v v + N_r r + N_{\delta} \delta_R + g_3(u, v, r, \delta_R)] \\ & + N_{\dot{v}}[Y_v v + (Y_r - \Delta u_0)r + Y_{\delta} \delta_R + g_2(u, v, r, \delta_R)]\} \end{aligned} \quad (4.35)$$

The linear terms in the above equations are estimated using Clarke et al. (1982) formula in chapter 4. The lumped nonlinear functions g_1 to g_3 are obtained from the three trained neural networks. The velocities, u , v and r are calculated by applying a fourth order Runge-Kutta integration method to equations 4.33 to 4.35. Performing the integration over a time period of 300 seconds, will give a set of data for u , v and r , which are designated the neural network values in the figures. According to equations 3.12 to 3.14, the velocities are integrated once more to obtain a ship trajectory. Figures 4.10 to 4.17 show the velocities, trajectories and accelerations calculated from the neural network model.

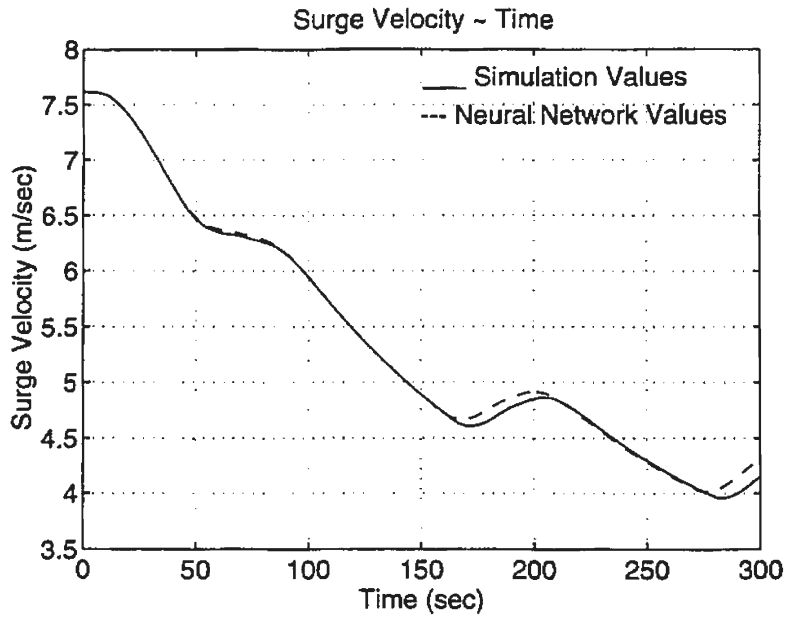


Figure 4.10: Predicted Surge Velocity of 35-35 deg Zigzag Manoeuvre

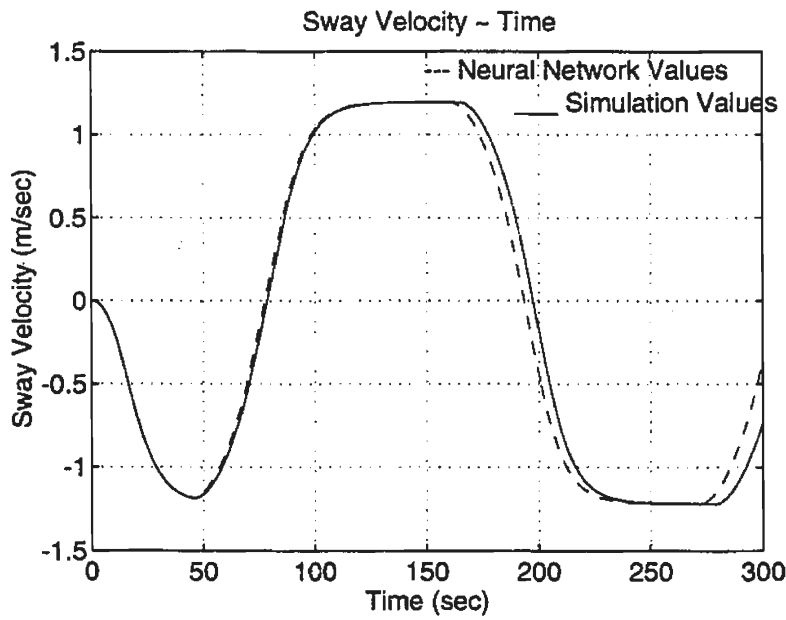


Figure 4.11: Predicted Sway Velocity of 35-35 deg Zigzag Manoeuvre

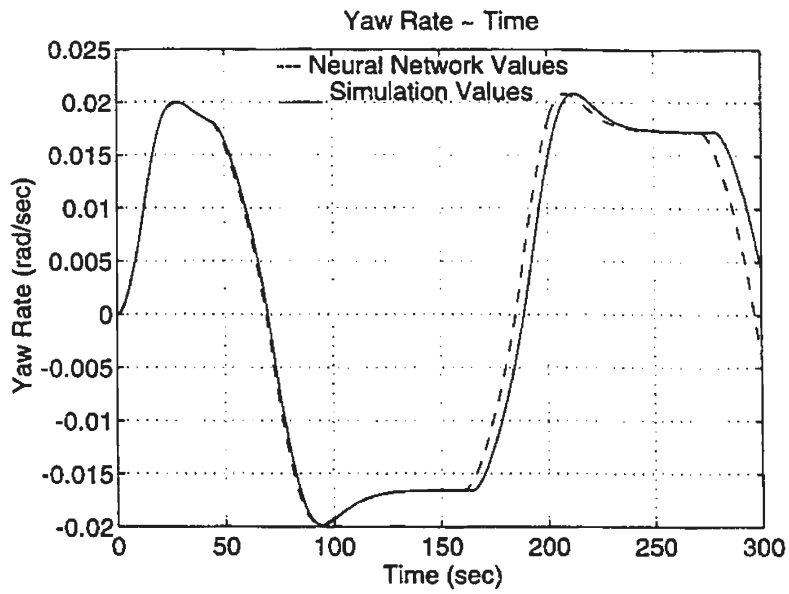


Figure 4.12: Predicted Yaw Rate of 35-35 deg Zigzag Manoeuvr

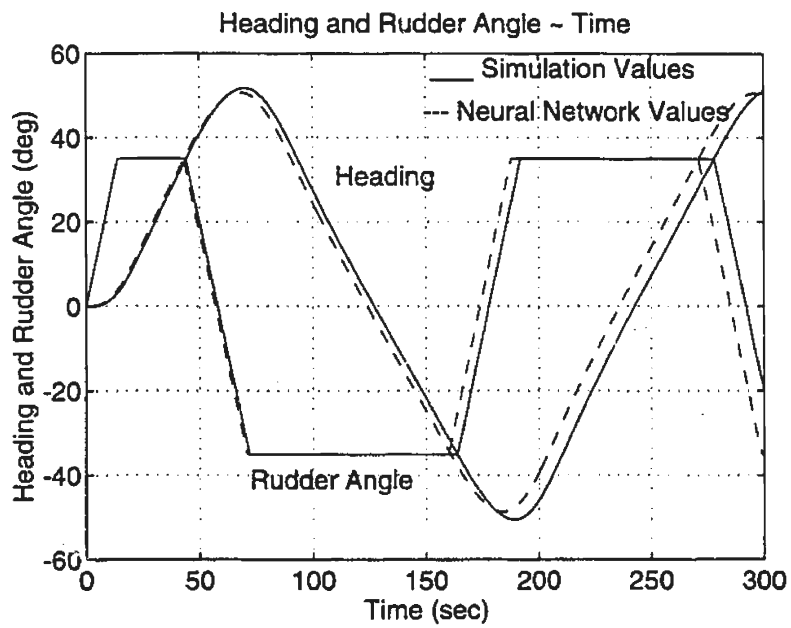


Figure 4.13: Predicted Heading Angle of 35-35 deg Zigzag Manoeuvr

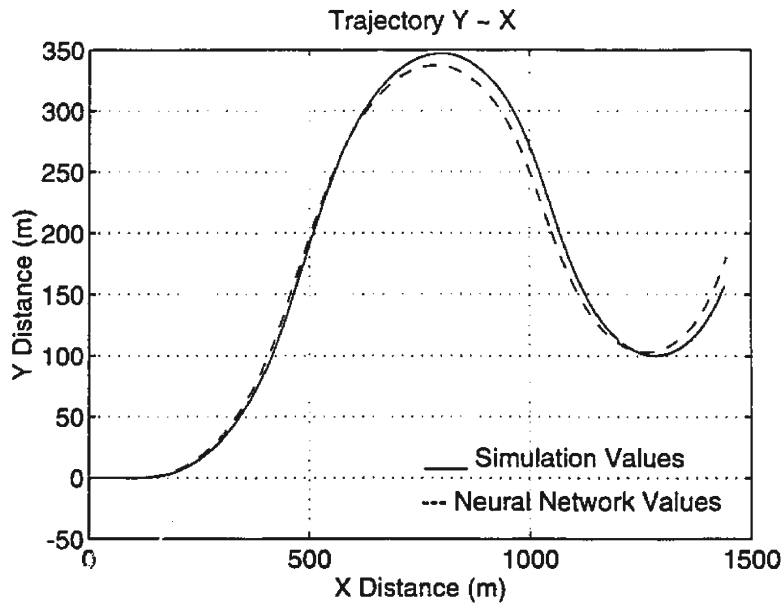


Figure 4.14: Predicted Trajectory of 35-35 deg Zigzag Manoeuvre

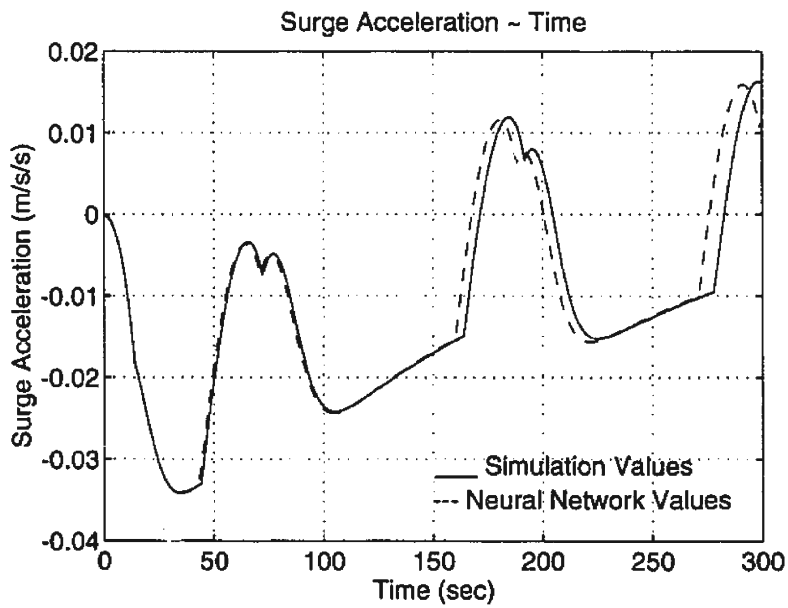


Figure 4.15: Comparison of Surge Accelerations in 35-35 deg Zigzag

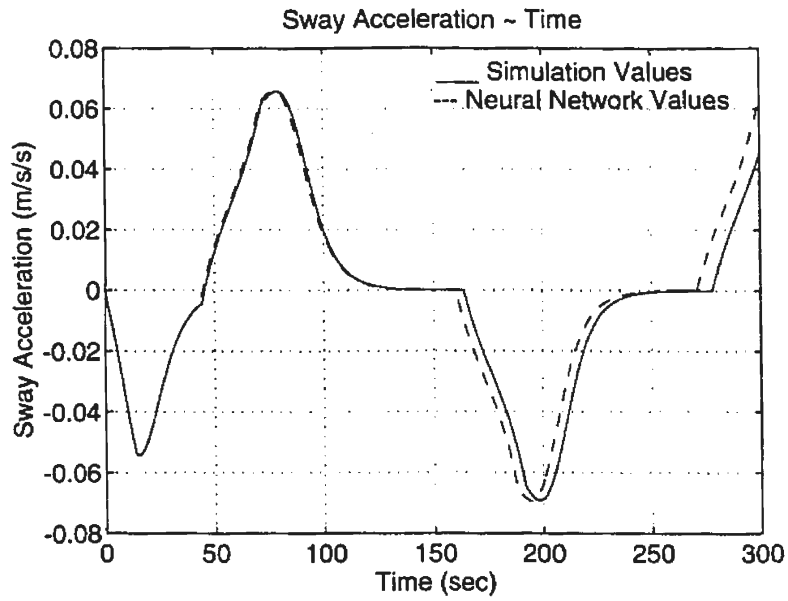


Figure 4.16: Comparison of Sway Accelerations in 35-35 deg Zigzag

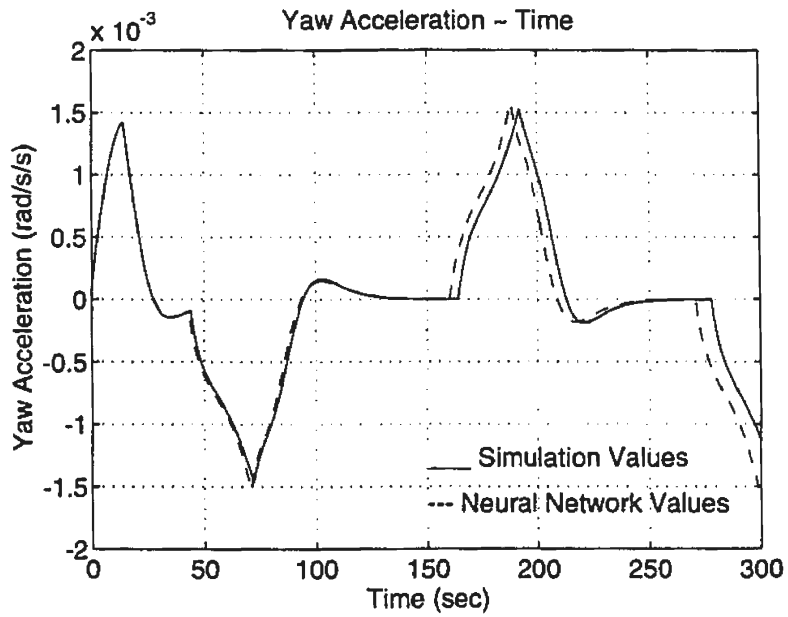


Figure 4.17: Comparison of Yaw Accelerations in 35-35 deg Zigzag

Chapter 5

Generalization of the Neural Network Model

5.1 Choosing Test Manoeuvres

The method developed in this thesis can only be useful if the predicted model simulates the manoeuvrability of the ship in a situation different from the one used to train the neural network. This is usually tested by evaluating the performance of the network on a new set of data different from the training set. A moderate zigzag manoeuvre (20-20 degree zigzag manoeuvre), a 25 degree turning (starboard), and a 20 degree Dieudonne spiral manoeuvre have been selected to check the validity of the trained network model. In addition to the fact that the rudder angle commands in each of the above test manoeuvres are unique, the surge, sway velocities and yaw rates form a totally different path with time in the space of u , v and r , as shown in Figures 5.1 and 5.2.

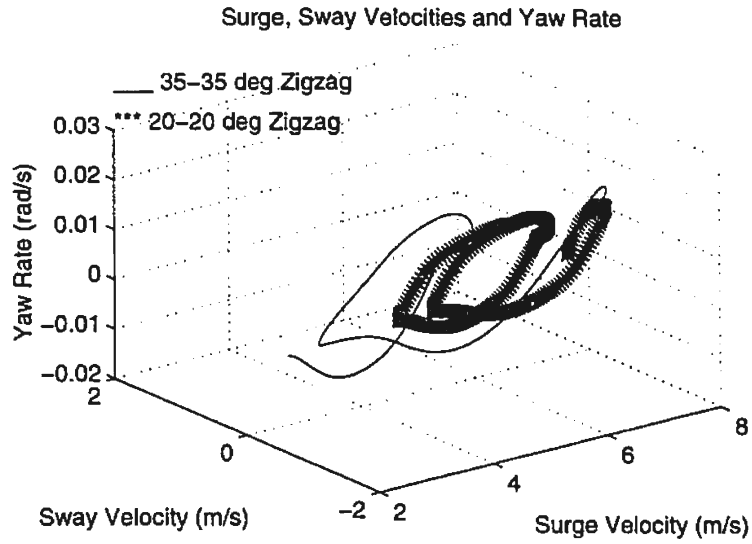


Figure 5.1: Velocity Space of 35-35 deg Zigzag and 20-20 deg Zigzag

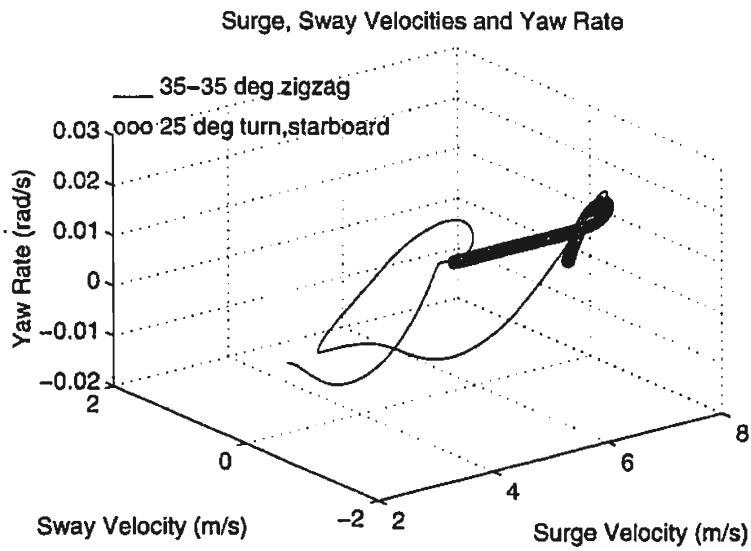


Figure 5.2: Velocity Space of 35-35 deg Zigzag and 25 deg Turning

5.2 Results of the Generalization Check

The 20-20 degree zigzag manoeuvre predicted by the neural network model in Figures 5.3 to 5.7 fits well with the 20-20 degree zigzag manoeuvre from simulations. When the results of the 25 degree turning (starboard) using the neural network are compared with the simulation, a good agreement is reached indicating a good generalization of this model. See Figures 5.8 to 5.11. Figure 5.12 gives the relationship between the steady yaw rate and the rudder angle in a 20 degree Dieudonne spiral manoeuvre. From the results predicted by the neural network in this figure, we can judge that the ship has a slight directional instability as can be deduced from the existence of a hysteresis loop.

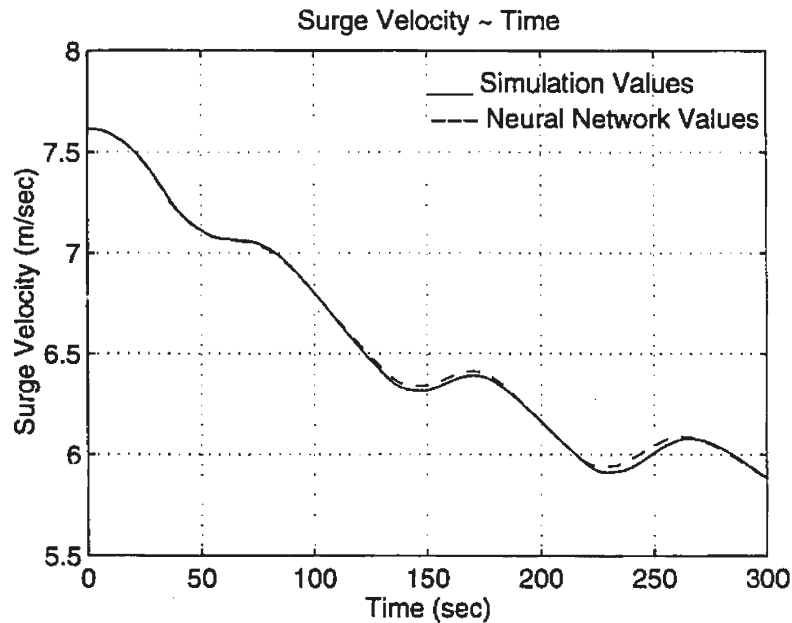


Figure 5.3: Predicted Surge Velocity of 20-20 deg Zigzag Manoeuvre

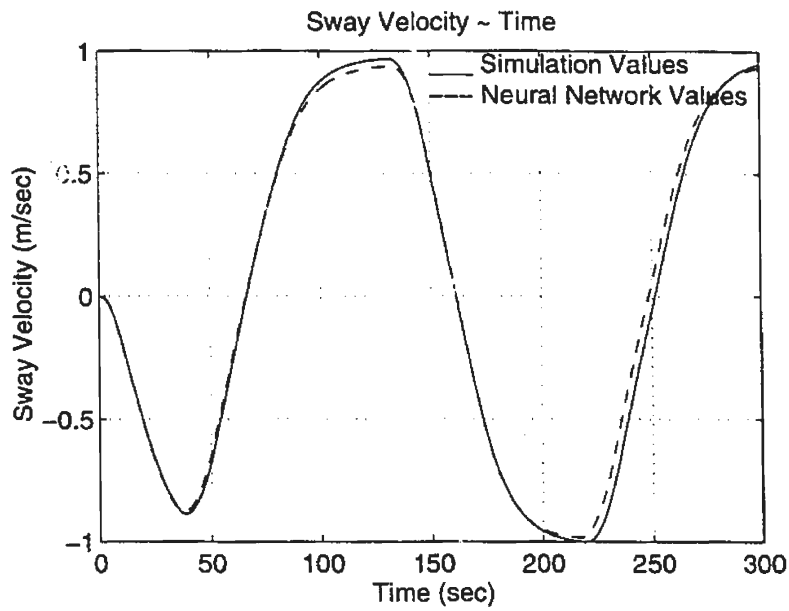


Figure 5.4: Predicted Sway Velocity of 20-20 deg Zigzag Manoeuvre

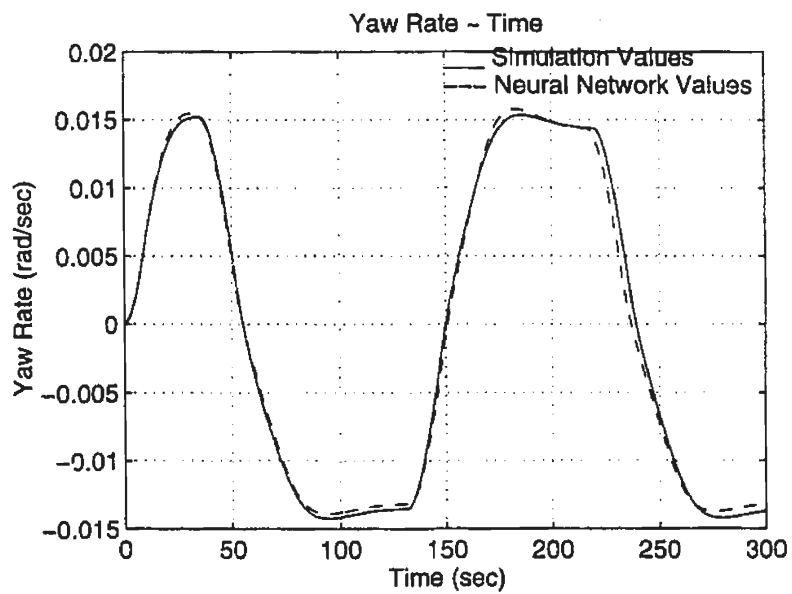


Figure 5.5: Predicted Yaw Rate of 20-20 deg Zigzag Manoeuvre

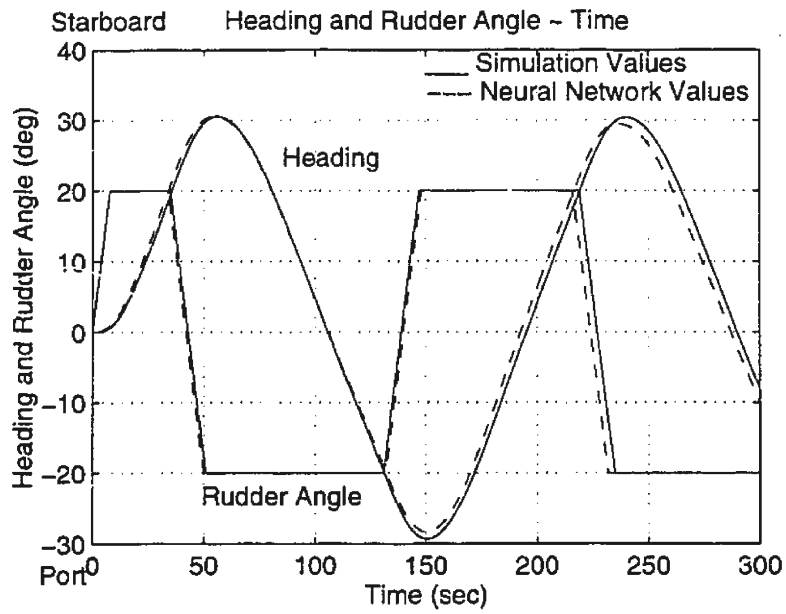


Figure 5.6: Predicted Heading Angle of 20-20 deg Zigzag Manoeuvre

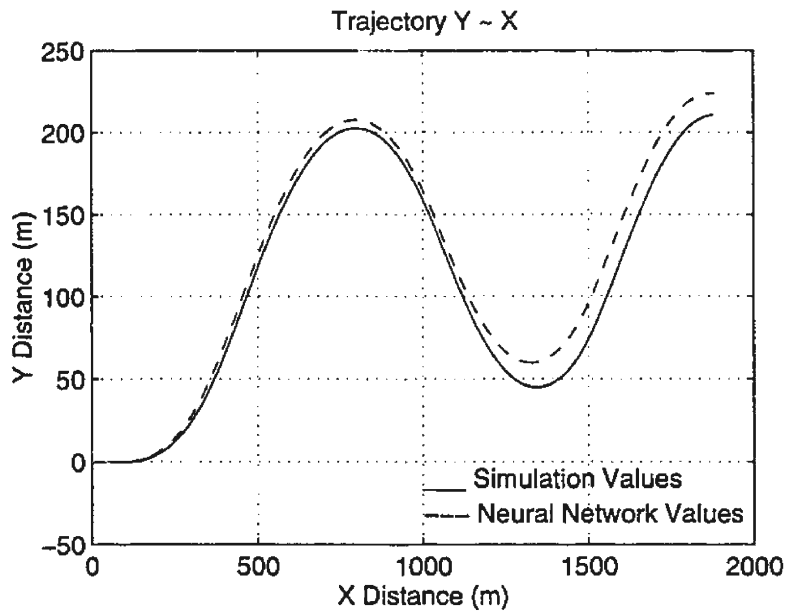


Figure 5.7: Predicted Trajectory of 20-20 deg Zigzag Manoeuvre

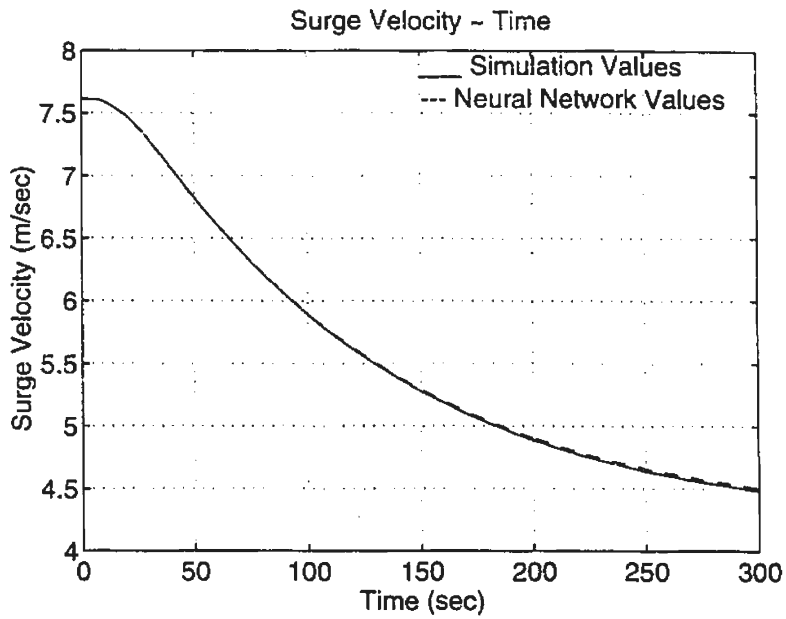


Figure 5.8: Predicted Surge Velocity of 25 deg Turning, Starboard

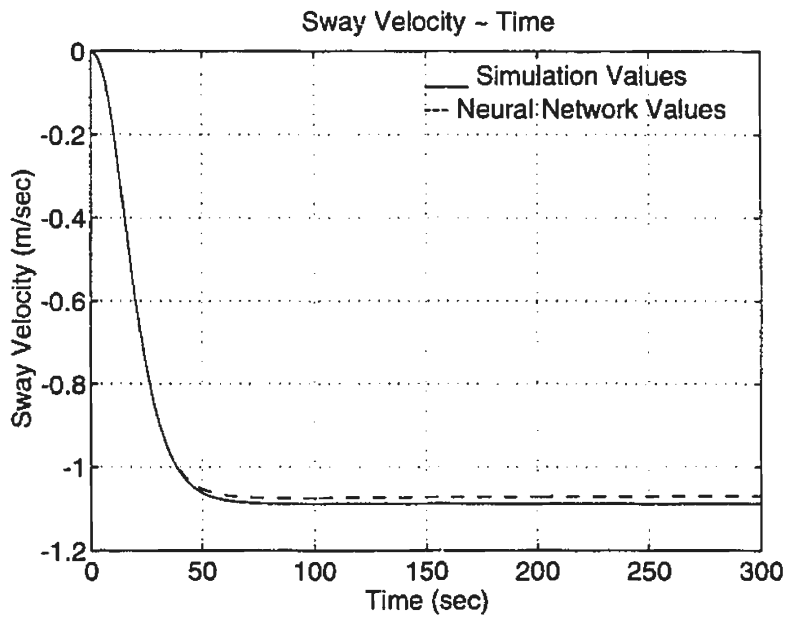


Figure 5.9: Predicted Sway Velocity of 25 deg Turning, Starboard

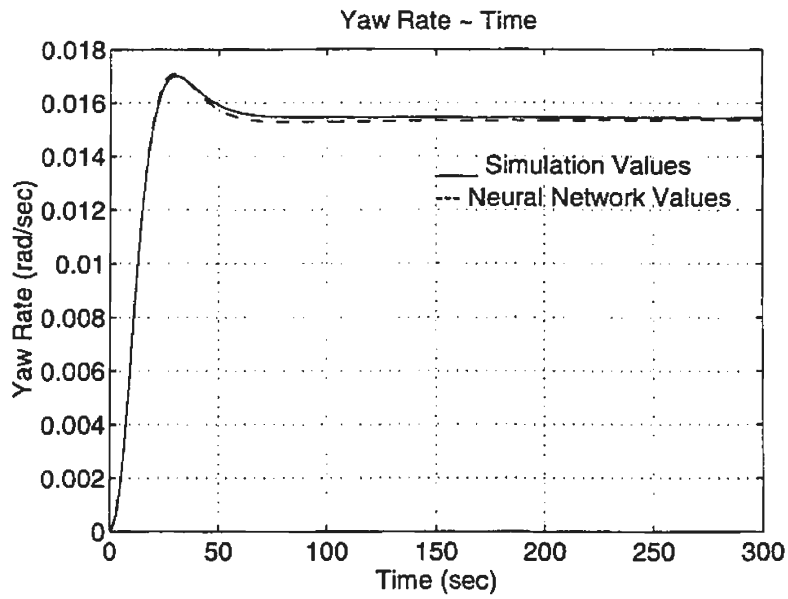


Figure 5.10: Predicted Yaw Rate of 25 deg Turning, Starboard

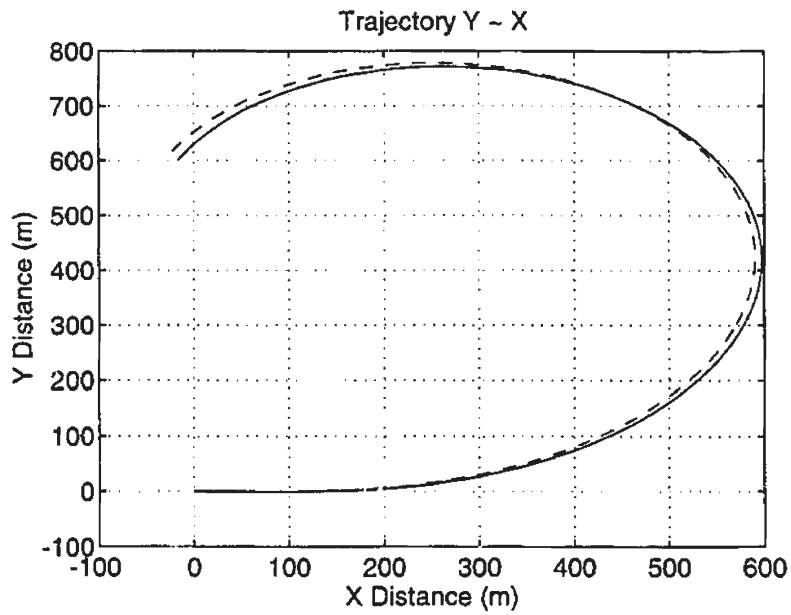


Figure 5.11: Predicted Trajectory of 25 deg Turing, Starboard

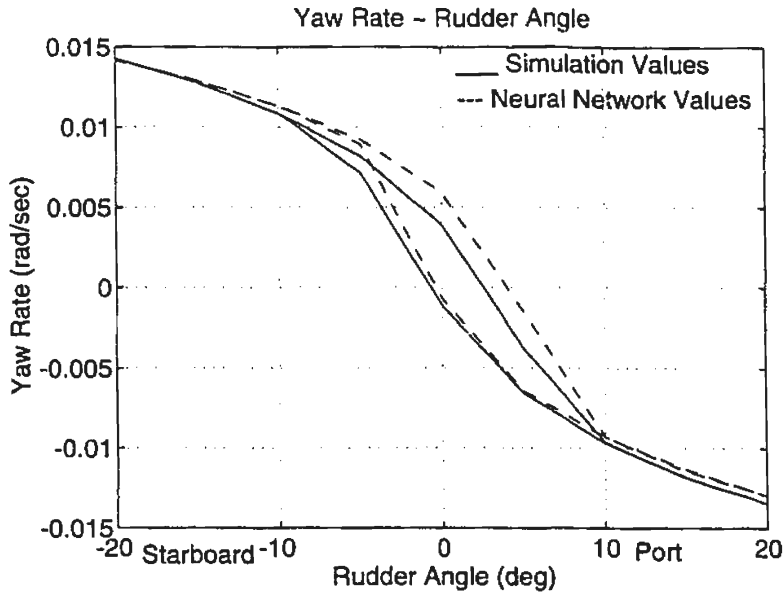


Figure 5.12: 20 deg Dieudonne Spiral Manoeuvre

5.3 Regression Analysis

In this section, we will show the results of a multi-regression analysis on the hydrodynamic forces using the software package MINITAB. The objective is to try to identify the individual hydrodynamic coefficients in the three lumped nonlinear functions, g_1 , g_2 and g_3 that are obtained from the neural network model. The coefficients are identified up to the third order and compared with the original ones used for simulations. We use 301 sets of data of u , v , r , δ and their corresponding lumped nonlinear functions, g_1 , g_2 and g_3 , that were calculated by neural network in the prediction of a 35-35 degree zigzag manoeuvre. Figures 5.13 and 5.14 show the data used in the regression analysis.

We set δu , δu^2 , δu^3 , v^2 , r^2 , δ_R^2 , $v^2\delta u$, $r^2\delta u$, $\delta_R^2\delta u$, vr , $v\delta_R$, $r\delta_R$, $vr\delta u$, $v\delta_R\delta u$,

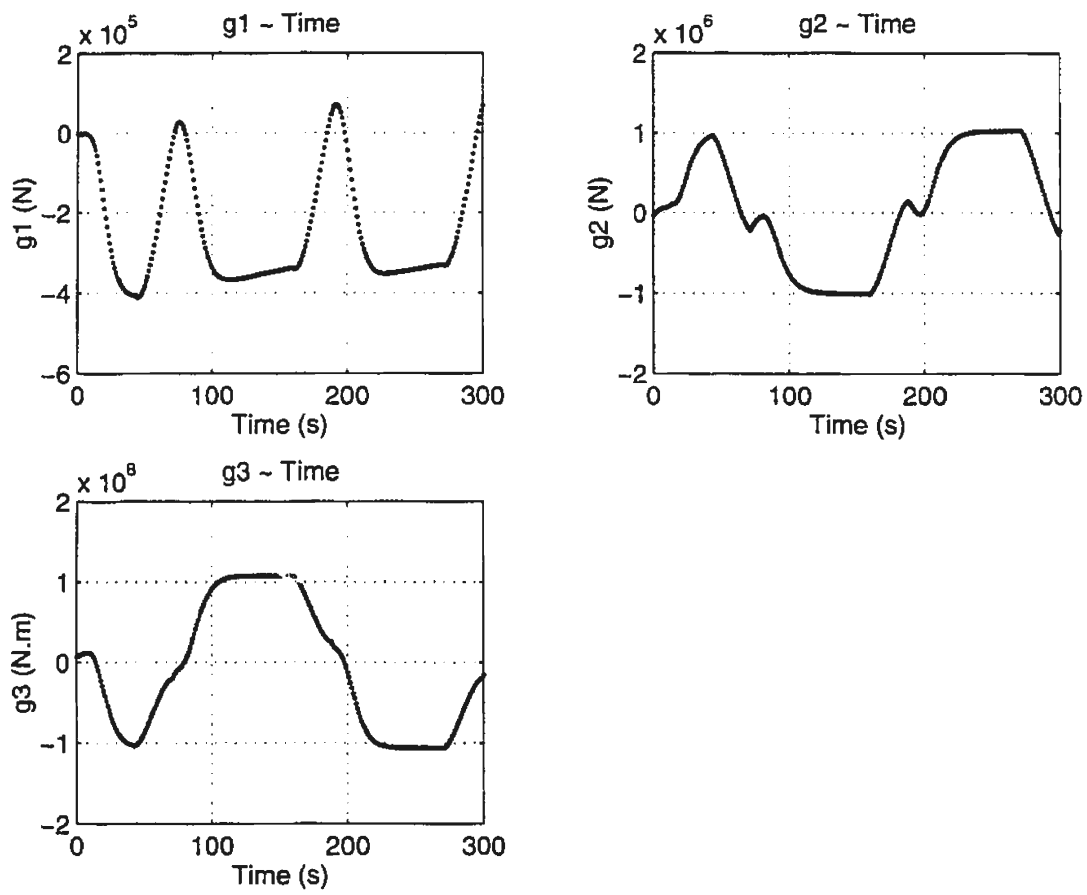


Figure 5.13: Lumped Nonlinear Functions g_1 to g_3 in 35 deg Zigzag Prediction

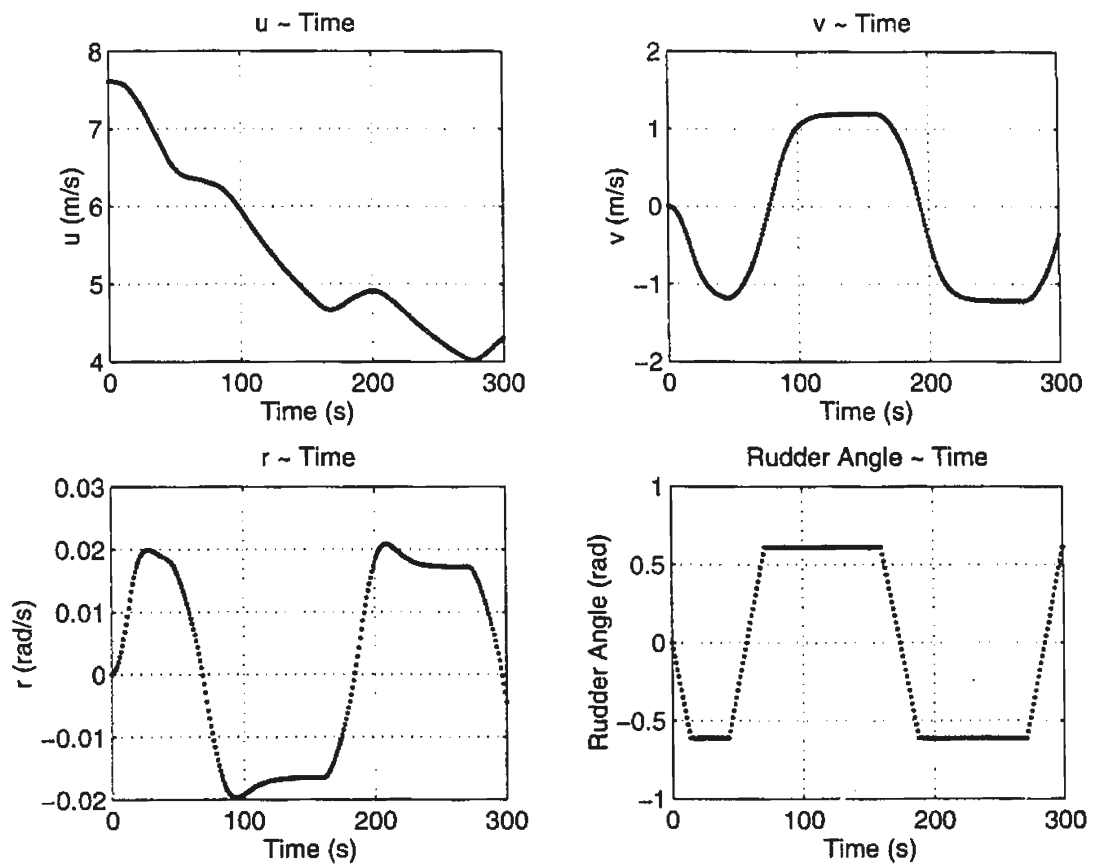


Figure 5.14: Velocities and Rudder Angles in 35-35 deg Zigzag Prediction

$r\delta_R\delta u$, as the multivariables of the lumped nonlinear function g_1 , set $v, v^3, vr^2, v\delta_R^2, v\delta u, r, r^3, rv^2, r\delta_R^2, r\delta u, r(\delta u)^2, \delta_R, \delta_R^3, \delta_Rv^2, \delta_Rr^2, \delta_R\delta u, \delta_R(\delta u)^2, vr\delta_R, \delta u, (\delta u)^2$ as the multivariables of the lumped nonlinear function g_2 , and set $v, v^3, vr^2, v\delta_R^2, v\delta u, r, r^3, rv^2, r\delta_R^2, r\delta u, r(\delta u)^2, \delta_R, \delta_R^3, \delta_Rv^2, \delta_Rr^2, \delta_R\delta u, \delta_R(\delta u)^2, vr\delta_R, \delta u, (\delta u)^2$ as the multivariables of the lumped nonlinear function g_3 . δu is equal to $u - u_0$. The values of these individual variables are calculated based on the 301 sets of data of u, v, r and δ_R provided from the above neural network prediction.

Using the multiple regression approach in MINITAB gives the predictor coefficients for each variable. Then, we analyze the results of regression and remove the highly correlated variables, say, rru or δ_R^2u , to make sure that the statistic index p-value less than 0.05 and R-sq greater than 0.95. The p-value in this section is the probability of getting the regression mapping model. When the p-value is small, the probability of obtaining the result purely by chance is small and the null hypothesis can be rejected. But how small does it have to be? The answer is set by convention as something smaller than 0.05. Monk (1991) stated that according to experience, 0.05 is small enough to prevent us from building theories on chance results but not so strict that experiments become extremely expensive to run because very large quantities of data have to be collected in order to rule out the possibility of a chance result. As to the R-sq, it is used to compare the deviance of the regression equation with the deviance from the mean. The higher the R-sq is the stronger the relationship between the variables.

The unusual observations in data should also be removed. The unusual obser-

vations in data are the data which deviate far from the regression mapping model. The removal of these points helps to find the regression predictors more accurately. Re-do the regression until the above statistical requirements are satisfied and no unusual observation points appear. The final regression equations are obtained as follows

$$\begin{aligned}
g_1 = & -1364.9 + 782\delta u + \frac{1}{2} * 18048.2\delta u^2 + \frac{1}{6} * 2574\delta u^3 \\
& + \frac{1}{2} * (-226472)v^2 + \frac{1}{2} * 17236738r^2 + \frac{1}{2} * (-18208)\delta_R^2 \\
& + \frac{1}{2} * 2862.2\delta_R^2\delta u + 16698306vr + 90865v\delta_R
\end{aligned} \tag{5.1}$$

$$\begin{aligned}
g_2 = & -30334 + 181042v + \frac{1}{6} * (-2549592)v^3 + \frac{1}{2} * (-1851248)v\delta_R^2 \\
& + (-59167)v\delta u + \frac{1}{2} * (-140688832)r\delta_R^2 + (-1419969)r\delta u \\
& + (-270453)\delta_R + \frac{1}{6} * (-5290458)\delta_R^3 + \frac{1}{2} * 762876\delta_R v^2
\end{aligned} \tag{5.2}$$

$$\begin{aligned}
g_3 = & 4127219 + 16850178v + \frac{1}{6} * 20248674v^3 \\
& + \frac{1}{2} * (-17542416)v\delta_R^2 + (-1391213568)r + \frac{1}{2} * (-4781049344)rv^2 \\
& + (-102215384)r\delta u + (-50902672)\delta_R + \frac{1}{6} * 177863376\delta_R^3 \\
& + \frac{1}{2} * 58221352 * \delta_R v^2 + (-1203891)\delta_R\delta u
\end{aligned} \tag{5.3}$$

The nonlinear hydrodynamic coefficients can be directly obtained from regression equations 5.1 to 5.3. The linear hydrodynamic coefficients can be solved by adding the Clarke's estimated linear coefficients to the ones from the regression

equations 5.1 to 5.3. Tables 5.1 to 5.3 give the details. In each of the three tables, the second column includes the hydrodynamic coefficients from the regression equations 5.1 to 5.3. The third column gives the nondimensional forms of the coefficients in the second column. The nondimensionization is based on L, B, T and u_0 system. The fourth column gives the linear coefficients estimated by Clarke's formula in Clarke et al. (1982). The fifth column gives the final estimated coefficients by adding Clarke's linear coefficients to the regression linear ones. The sixth column provides the original hydrodynamic coefficients for comparison with the final regression coefficients. The results in these three tables suggest that most of the coefficients have a good agreement with the original coefficients except some coupled acceleration coefficients such as $Y_{\dot{r}}$, $N_{\dot{v}}$. However, the errors do not affect the accuracy in the prediction of ship manoeuvres.

The regression coefficients shown in the fifth column have been used to simulate a 15-15 zigzag manoeuvre. The results in Figures 5.15 to 5.19 fit well with the simulation using the original hydrodynamic coefficients. Because the regression coefficients are obtained through two approximation processes, neural network approximation and regression approximation, it is reasonable that the results of 15-15 degree zigzag manoeuvre are not as perfect as those integrated directly based on the neural network model. The regression method presented here checked again the validity of the neural network model in training three lumped nonlinear functions. The results of checking are satisfactory and the good agreement in the 15-15 degree manoeuvre prediction indicates the good generalization of the network model once more.

Table 5.1: Regression and Original Coefficients (SURGE)

Coef.	Regres. V.	Nondim. V.	Clarke V.	Estimated V.	Original V.
$\Delta - X_{\dot{u}}$			0.17993	0.17993	0.177
X_u	782	0.000165623	-0.0253	-0.02513	-0.0253
X_{uu}	18048.2	0.029104573		0.029105	0.01896
X_{uuu}	2574	0.03160448		0.031604	-0.01302
X_{vv}	-226472	-0.365209325		-0.36521	-0.378
$X_{\delta\delta}$	-18208	-0.0005065	-0.04008	-0.04059	-0.04
X_{vuu}	0	0		0	0
X_{rru}	0	0		0	0
$X_{\delta\delta u}$	2862.2	0.0006062		0.000606	0
$X_{vr} + \Delta$	16698306	0.176691147		0.176691	0.168
$X_{v\delta}$	90865	0.019244698		0.019245	0.0196
$X_{r\delta}$	0	0		0	0
X_{vru}	0	0		0	0
$X_{v\delta u}$	0	0		0	0
$X_{r\delta u}$	0	0		0	0
X^0	-1364.9	-0.000037966		-3.8E-5	0

Table 5.2: Regression and Original Coefficients (SWAY)

Coef.	Regres. V.	Nondim. V.	Clarke V.	Estimated V.	Original V.
$\Delta - Y_{\bar{v}}$			0.364741	0.364741	0.327
$Y_{\bar{r}}$			-0.01209	-0.01209	-0.0007704
$Y_{\bar{v}}$	181042	0.0383	-0.27543	-0.23709	-0.244
Y_{vvv}	-2549592	-31.304		-31.304	-10.212
Y_{vrr}	0	0		0	0
$Y_{v\delta\delta}$	-1851248	-0.098020989		-0.09802	-0.0016
Y_{vu}	-59167	-0.00954		-0.00954	0
Y_{vuu}	0	0		0	0
$Y_{\bar{r}} - \Delta$	0	0	-0.1043	-0.1043	-0.105
Y_{rrr}	0	0		0	0
Y_{rvv}	0	0		0	6.46
$Y_{r\delta\delta}$	-140688832	-0.1955		-0.19552	0
Y_{ru}	-1419969	-0.015025233		-0.01503	0
Y_{ruu}	0	0		0	0
Y_{δ}	-270453	-0.007523	0.06	0.052477	0.0586
$Y_{\delta\delta\delta}$	-5290458	-0.1471617		-0.14716	-0.0585
$Y_{\delta vv}$	762876	1.2302		1.2302	-0.5
$Y_{\delta rr}$	0	0		0	0
$Y_{\delta u}$	0	0		0	0
$Y_{\delta uu}$	0	0		0	0
$Y_{vr\delta}$	0	0		0	0
Y^0	-30334	-0.000843783		-0.00084	-0.0008
Y_u^0	0	0		0	0
Y_{uu}^0	0	0		0	0

Table 5.3: Regression and Original Coefficients (YAW)

Coef.	Regres. V.	Nondim. V.	Clarke V.	Estimated V.	Original V.
$N_{\dot{v}}$			-0.00796	-0.00796	0.00221
$I_z - N_{\dot{r}}$			0.024085	0.024085	0.0175
N_v	16850178	0.023417147	-0.10538	-0.08196	-0.0555
N_{vvv}	20248674	1.631		1.631368	2.07
N_{vrr}	0	0		0	0
$N_{v\delta\delta}$	-17542416	-0.024379169		-0.02438	0.00528
N_{vu}	0	0		0	0
N_{vuu}	0	0		0	0
N_r	-1391213568	-0.0126864	-0.04602	-0.05871	-0.03747
N_{rrr}	0	0		0	0
N_{rvv}	-4781049344	-2.52751		-2.52751	-2.316
$N_{r\delta\delta}$	0	0		0	0
N_{ru}	-102215384	-0.00709698		-0.0071	0
N_{ruu}	0	0		0	0
N_{δ}	-50902672	-0.00929088	-0.03	-0.03929	-0.0293
$N_{\delta\delta\delta}$	177863376	0.032464		0.032464	0.02892
$N_{\delta vv}$	58221352	0.6160602341		0.616062	0.2064
$N_{\delta rr}$	0	0		0	0
$N_{\delta u}$	-1203891	-0.001673079		-0.00167	0
$N_{\delta uu}$	0	0		0	0
$N_{vr\delta}$	0	0		0	0
N^0	4127219	0.00075331		0.000753	0.00059
N_u^0	0	0		0	0
N_{uu}^0	0	0		0	0

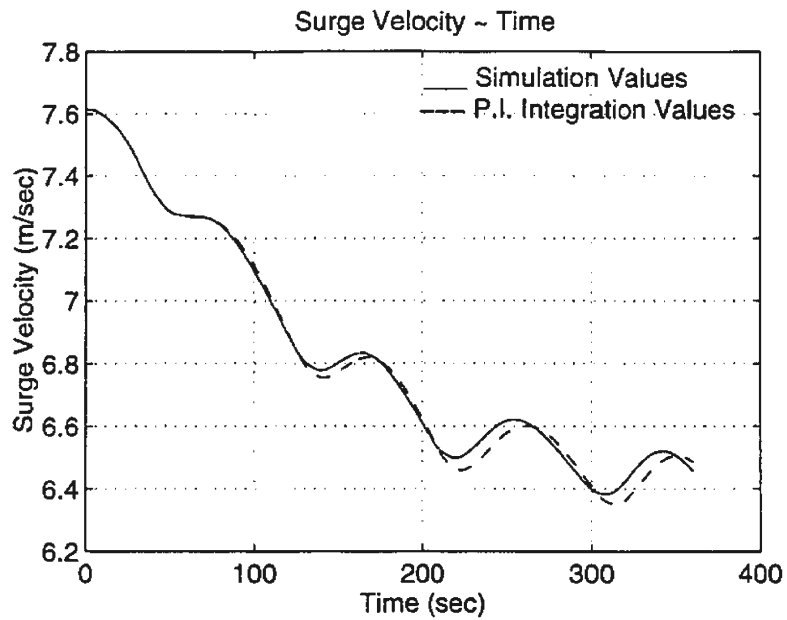


Figure 5.15: Predicted Surge Velocity of 15-15 deg Zigzag Manoeuvre

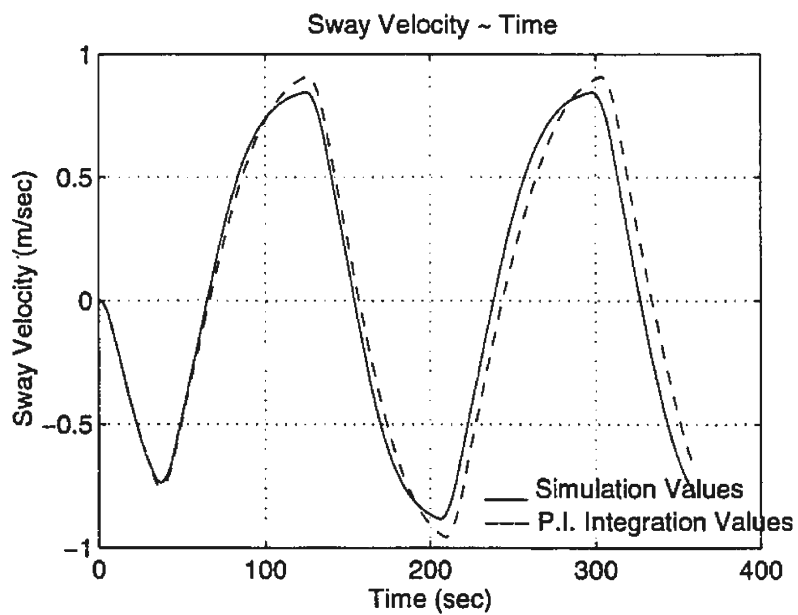


Figure 5.16: Predicted Sway Velocity of 15-15 deg Zigzag Manoeuvre

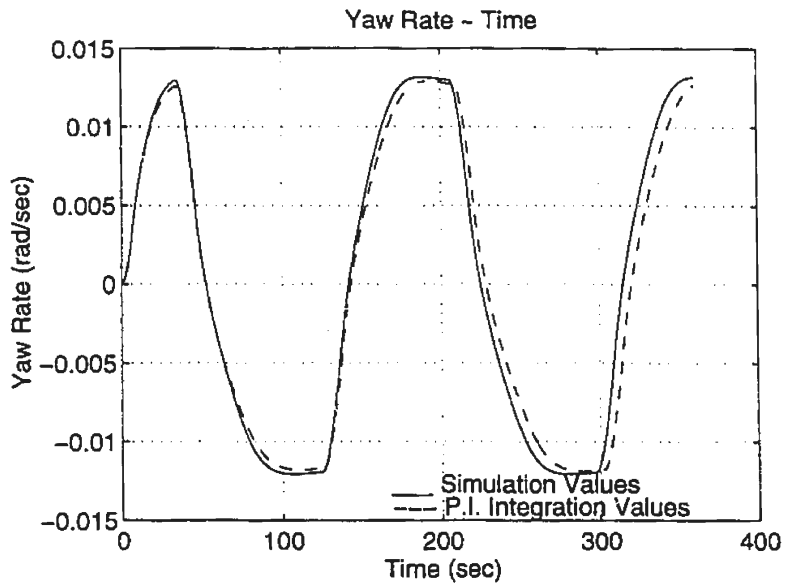


Figure 5.17: Predicted Yaw Rate of 15-15 deg Zigzag Manoeuvre

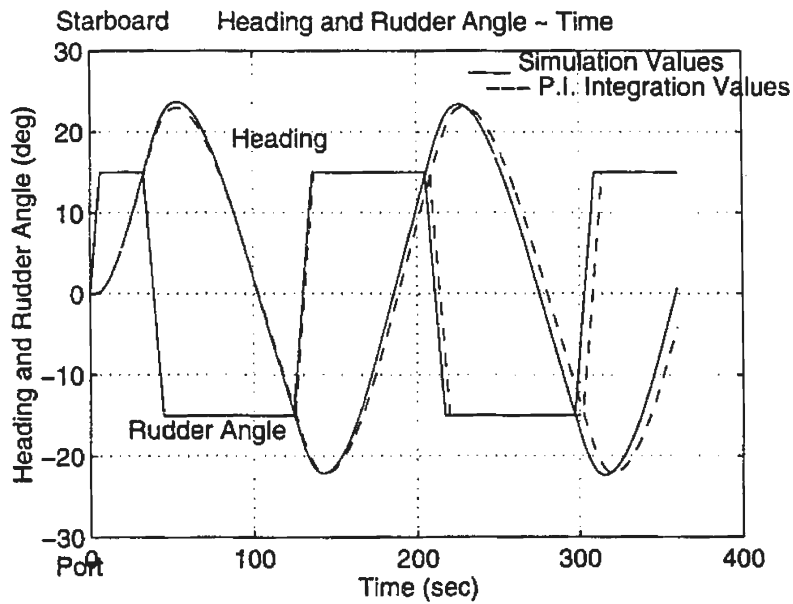


Figure 5.18: Predicted Heading Angle of 15-15 deg Zigzag Manoeuvre

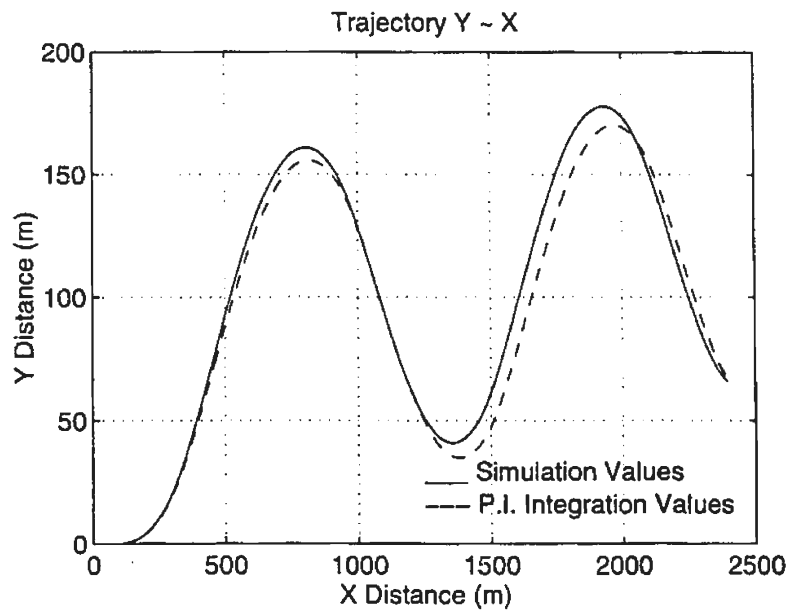


Figure 5.19: Predicted Trajectory of 15-15 deg Zigzag Manoeuvre

Chapter 6

Ship Turning Manoeuvre Prediction

6.1 Mathematical Formulation

In this chapter, we will introduce an approach to predict ship turning manoeuvres. In this thesis, we will follow the analysis developed by Clarke (1971). He stated that when a ship has a yaw rate, r , in a ship turning manoeuvre, it will have a corresponding side-slip velocity, v , and the relationship between r and v is almost linear. Figure 6.1 shows the relationships in a 30° , a 20° and a 10° turning manoeuvre simulations.

Thus, v can be expressed in terms of a high order polynomial in r , as follows

$$\begin{aligned} v &= v(r) \\ &= a_0 + a_1r + a_2r^2 + a_3r^3 + \dots \end{aligned} \tag{6.1}$$

If we try to map the relationship between v and r in equation 6.1, the neural network model can be suggested as a good approach. Since the coefficients in equation 6.1 are dependent on the rudder angle used in the turning manoeuvres, we will

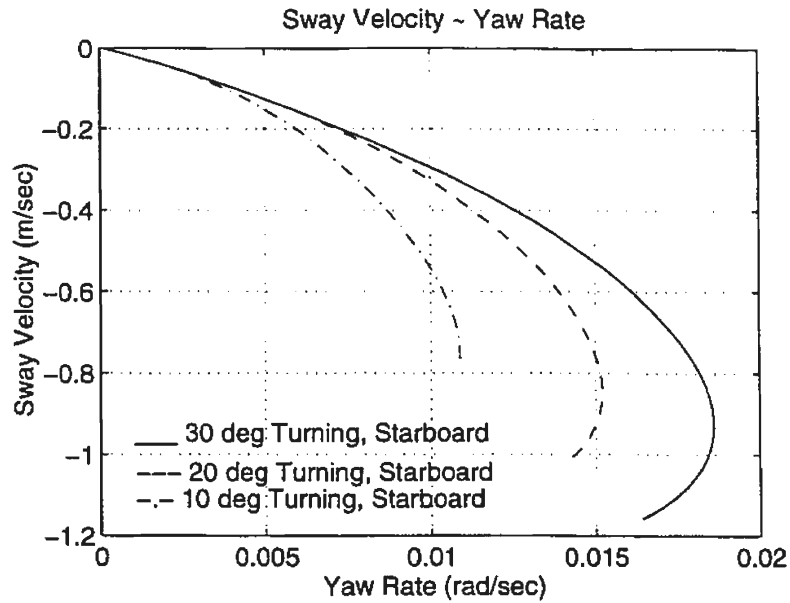


Figure 6.1: Relationships between v and r in Turning Manoeuvres

need a different set of neural network weights to map v and r for each rudder angle. The data of v and r for training neural networks can be obtained from simulations, ship model tests or full scale ship trials. In this thesis, we will use data of v and r from a 10° , a 20° and a 30° turning manoeuvre simulations which were used in chapter 3 to train three different neural network models.

After the mapping of equation 6.1 is done, the sway motion equation 3.4 can be replaced by

$$\begin{aligned}
 \dot{v} &= \frac{d(v(r))}{dt} \\
 &= \frac{d'(v(r))}{dr} \dot{r}
 \end{aligned} \tag{6.2}$$

Substituting equation 6.2 into the yaw motion equation 3.5 gives

$$\dot{r} = \frac{f_3(u, v, r, \delta_R)}{I_z - N_{\dot{r}} - N_{\dot{v}} \frac{d(v(r))}{dr}} \quad (6.3)$$

where the yaw moment, $f_3(u, v, r, \delta_R)$, is given in equation 3.8 and $\frac{d(v(r))}{dr}$ can be obtained by differentiating the neural network model with respect to r . The ship particulars and surge and yaw hydrodynamic coefficients used here are the same as those given in chapter 3. Together with the surge acceleration equation 3.9, equations 6.2 and 6.3 will enable us to get instantaneous surge velocities, sway velocities and yaw rates through a fourth order Runge-Kutta integration with time. Based on equations 3.12 to 3.14, trajectories can be obtained by integrating the velocities once more.

6.2 Mapping $v = v(r)$ using Neural Networks

Three different neural networks are trained for a 10° , a 20° and a 30° turning manoeuvres. In each of the networks, the input and output nodes are r and v , respectively. The training data of v and r come from simulations of a 10° , a 20° and a 30° turning manoeuvres (starboard), shown in Figure 6.1. The number of middle layer nodes is set to 5. The steepest descent search (see chapter 2) is adopted to adjust the input weights, W_{ij} , and the output weights, B_{ik} in an iterative fashion, starting from a random distribution of weights. Since the input data, r , are positive and the data of output target, v , are negative in the turning to starboard, we set the initial output weights, B_{ik} , negative. If the input, r , is positive and the values of the squashing function 2.2 are positive, the initial output weights, B_{ik} should be negative to guarantee the output with a negative value.

During the training process, we use a back propagation algorithm to calculate the derivatives of the sum-of-squared-error with respect to each weight as shown in equations 2.11 and 2.12. The training rate in these equations is set in the range from 10^{-3} to 10^{-1} to change the sensitivity of the weights. But, the rate cannot be increased without limitation, otherwise, the search cannot converge to the minimal point. Fifteen thousand iterations are required to train each of the three neural networks. Table 6.1 shows the sum-of-squared-error, E, after 15,000 iterations. Table 6.2 gives the trained weights for the 10° , the 20° and the 30° turning manoeuvres.

Table 6.1: Sum of Squared Error in Training

	10° Turning	20° Turning	30° Turning
Error	1.778437e-8	3.168374e-8	1.638284e-7

6.3 Results and Discussion

We have trained data for three rudder angles, 10 degrees, 20 degrees and 30 degrees. Figures 6.2 to 6.16 show the results of sway velocity, yaw rate, turning trajectories, sway acceleration and yaw acceleration in 10° , 20° and 30° turning manoeuvres, respectively. In these figures, the set of r's and v's fit well with the simulation values in the transient period of the circular motions. As the v and r gradually become constant, there exist a slight error compared with the simulation values. The code of prediction sets a separation time point after which r and v are kept constant. However, it is difficult to figure out the exact point where the yaw rate becomes constant. One can only estimate the approximate point at which r and v

Table 6.2: Trained Weights

Notation	10° Turning	20° Turning	30° Turning
$W_{1,1}$	-1.906287e-02	1.978335e-02	5.776109e-02
$W_{1,2}$	1.843463e+00	4.399924e-01	2.766127e-01
$W_{2,1}$	-2.470639e-02	-3.093730e+00	-4.756842e+00
$W_{2,2}$	-3.105290e-03	-6.400691e-02	-8.601323e-02
$W_{3,1}$	-3.202809e-01	7.327562e-02	9.395256e-02
$W_{3,2}$	-1.748573e+00	-2.120439e-01	-2.111839e-01
$W_{4,1}$	1.298166e+02	9.839515e+00	9.838378e+00
$W_{4,2}$	-2.677744e+01	7.365877e+00	7.451086e+00
$W_{5,1}$	1.105923e+01	8.051810e+00	9.432881e+00
$W_{5,2}$	1.990898e+01	7.150448e-01	6.660824e+00
$B_{1,1}$	-1.658517e+01	-2.982559e+00	-3.795949e+00
$B_{2,1}$	-4.133165e-01	1.544899e+00	7.996171e-01
$B_{3,1}$	-1.456758e+01	6.082410e+00	6.027607e+00
$B_{4,1}$	6.416173e+00	9.207373e+00	9.205272e+00
$B_{5,1}$	-1.276617e+00	8.060044e+00	8.167284e+00
$B_{6,1}$	0.000000e+00	0.000000e+00	0.000000e+00

approach constant values.

If the surge velocity loss is insignificant and the effect of the surge velocity on the sway and yaw motion is trivial, one can ignore the surge acceleration equation 3.9 and consider u as a constant during turning manoeuvres. In this method, the sway acceleration equation 6.2 is obtained using a neural network model and the yaw acceleration equation 6.3 is simplified by substituting equation 6.2 into equation 3.5. These manipulations will give a single yaw motion equation 6.3 in which only the hydrodynamic coefficients related to yaw motion are required. This can greatly simplify the work of prediction in ship turning manoeuvres. But, for the turning manoeuvres at different rudder angles, different neural networks are needed to map the different relationships between v and r . So, this method of prediction is less powerful than the one presented in chapters 4 and 5.

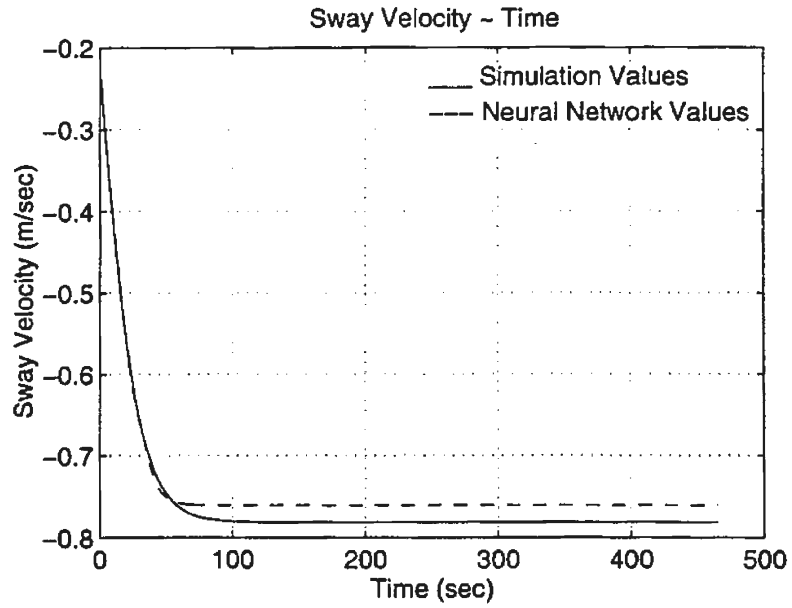


Figure 6.2: Sway Velocities in 10 degree Turning, Starboard

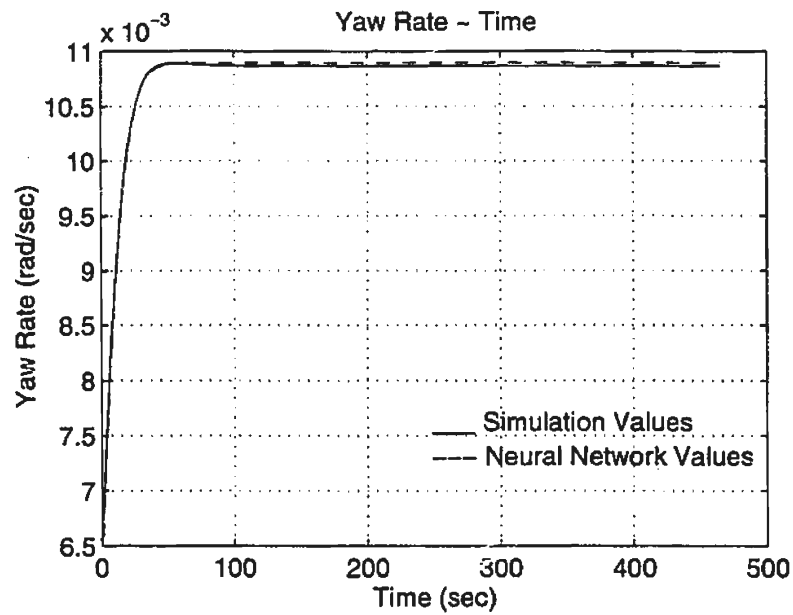


Figure 6.3: Yaw Rates in 10 degree Turning, Starboard

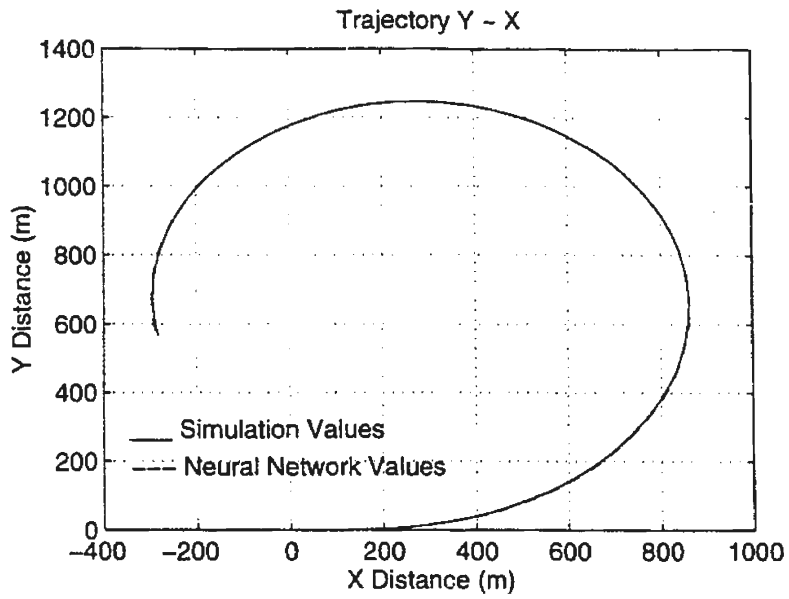


Figure 6.4: Trajectory in 10 degree Turning, Starboard

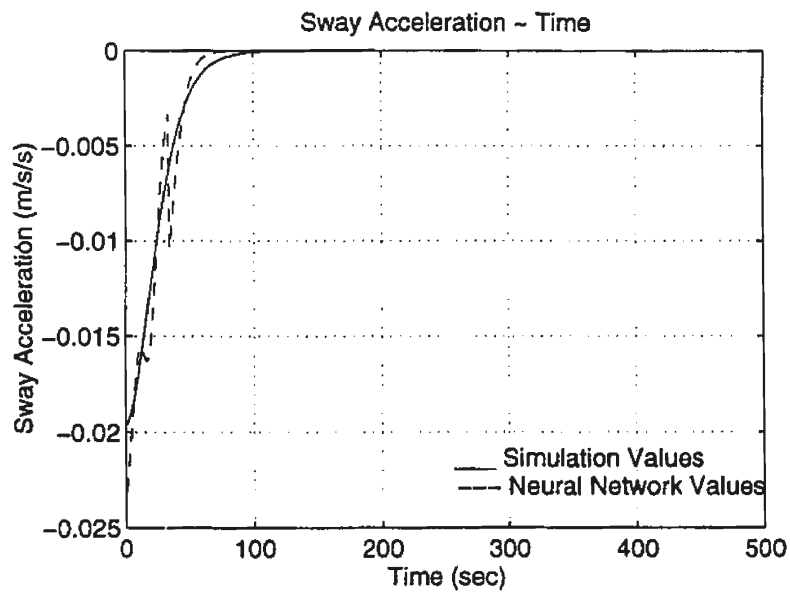


Figure 6.5: Sway Accelerations in 10 degree Turning, Starboard

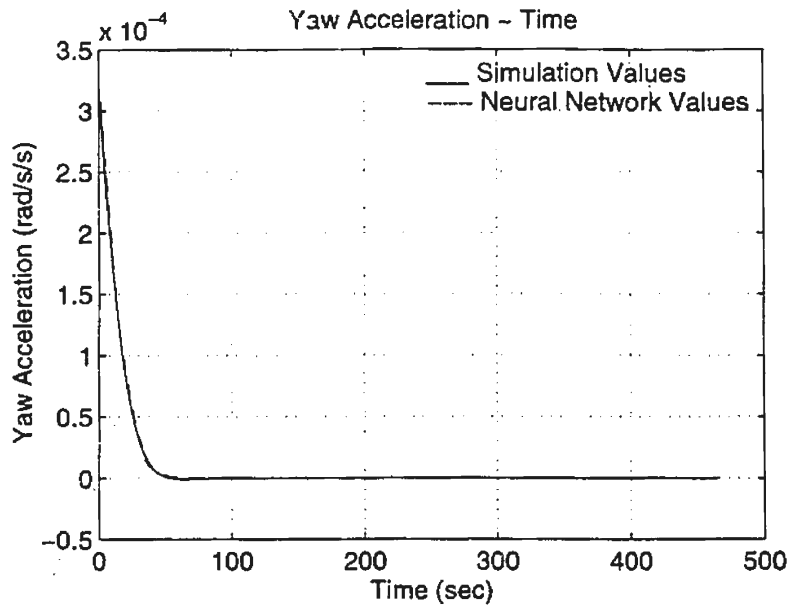


Figure 6.6: Yaw Accelerations in 10 degree Turning, Starboard

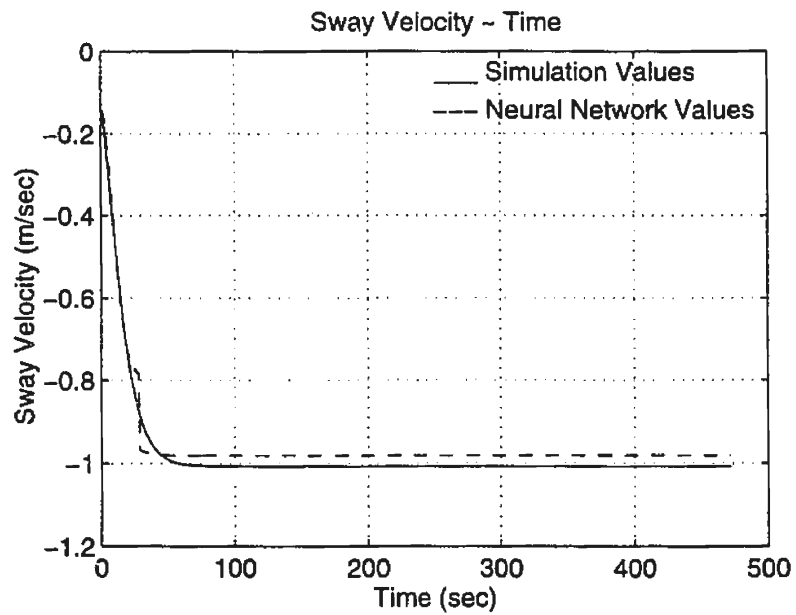


Figure 6.7: Sway Velocities in 20 degree Turning, Starboard

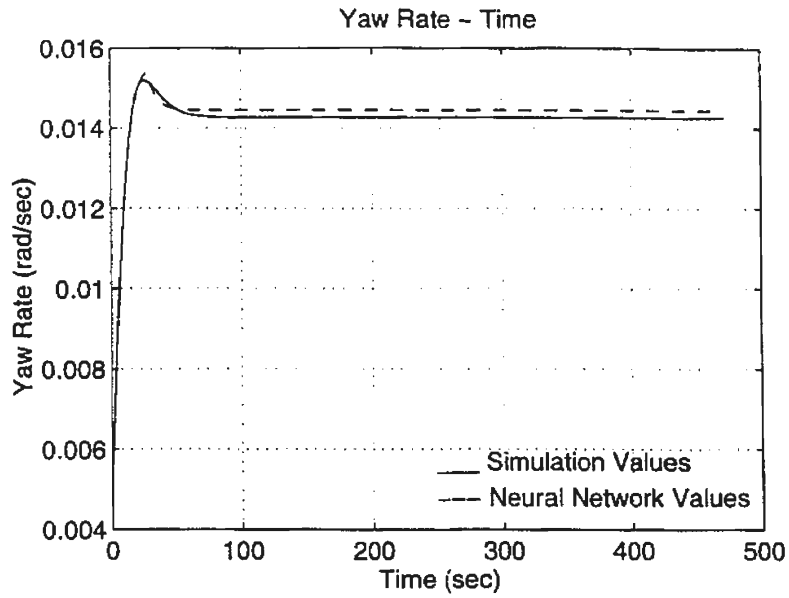


Figure 6.8: Yaw Rates in 20 degree Turning, Starboard

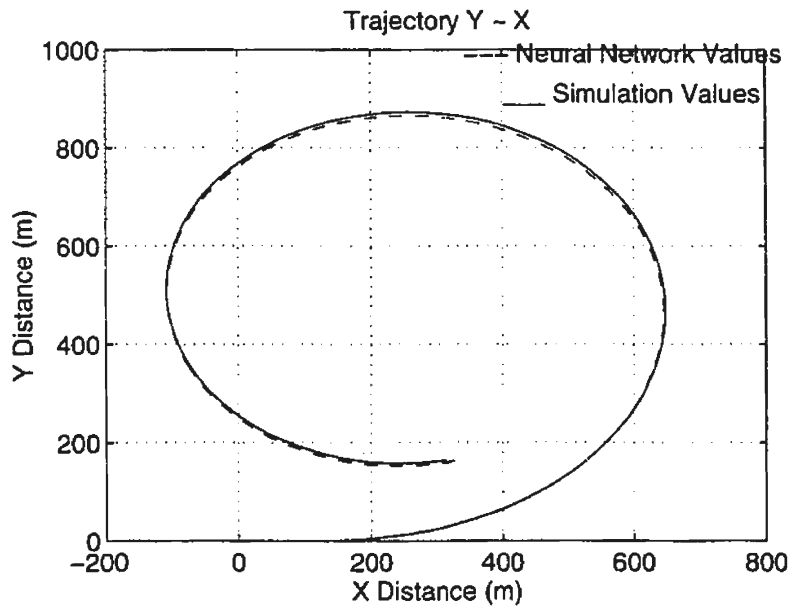


Figure 6.9: Trajectory in 20 degree Turning, Starboard

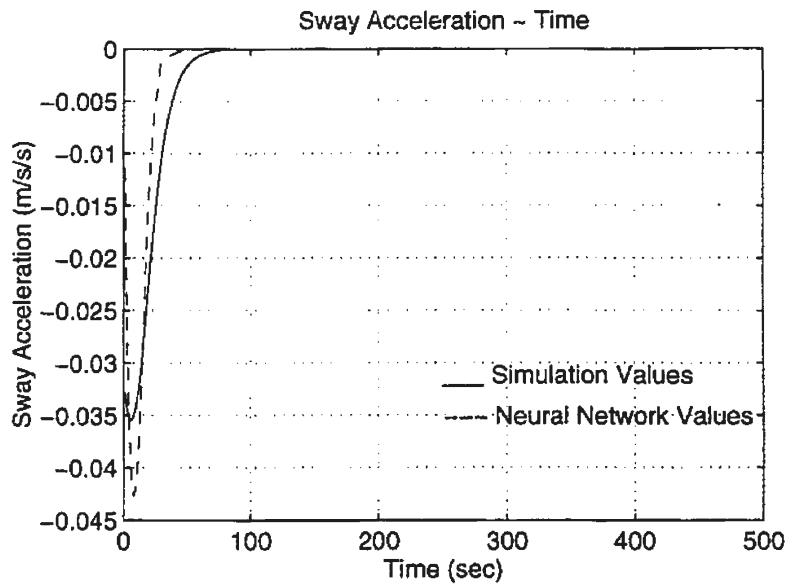


Figure 6.10: Sway Accelerations in 20 degree Turning, Starboard

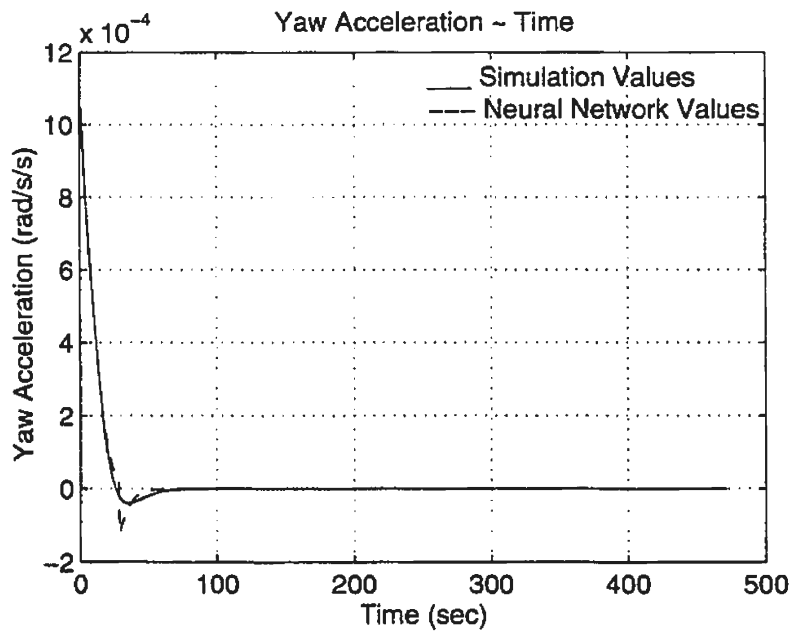


Figure 6.11: Yaw Accelerations in 20 degree Turning, Starboard

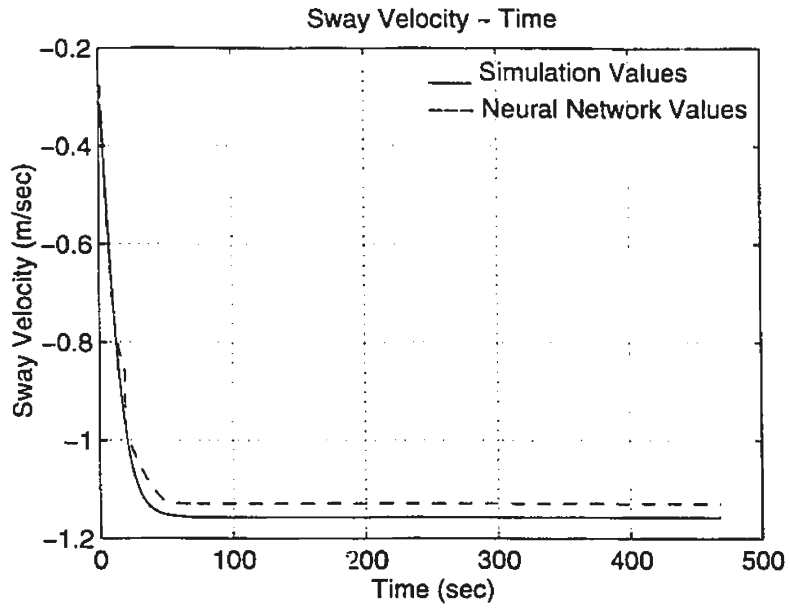


Figure 6.12: Sway Velocities in 30 degree Turning, Starboard

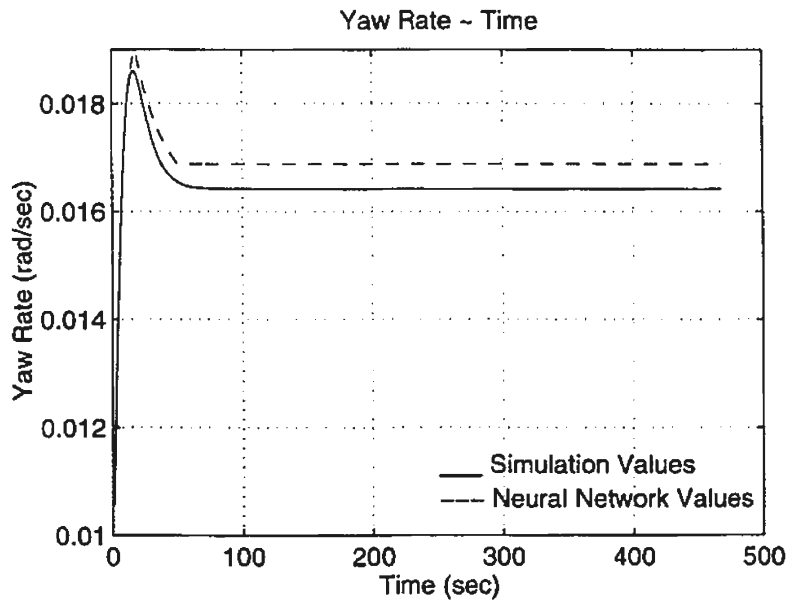


Figure 6.13: Yaw Rates in 30 degree Turning, Starboard

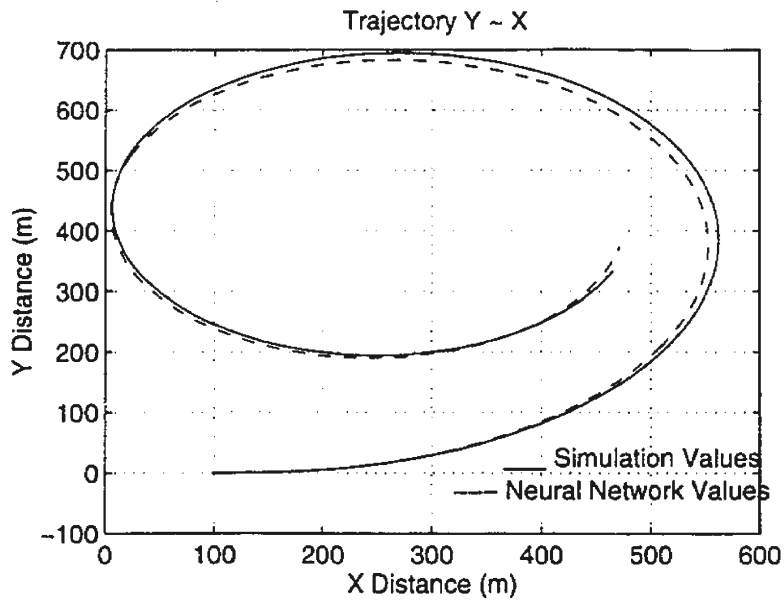


Figure 6.14: Trajectory in 30 degree Turning, Starboard

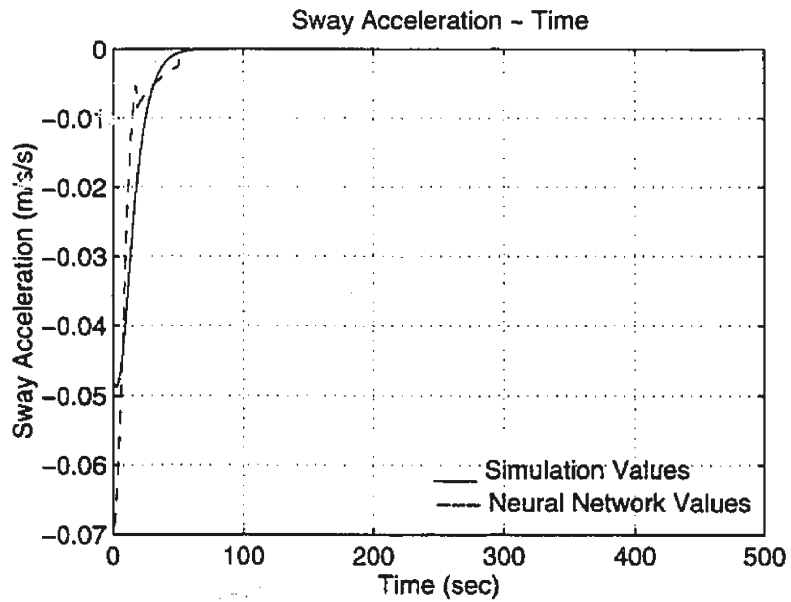


Figure 6.15: Sway Accelerations in 30 degree Turning, Starboard

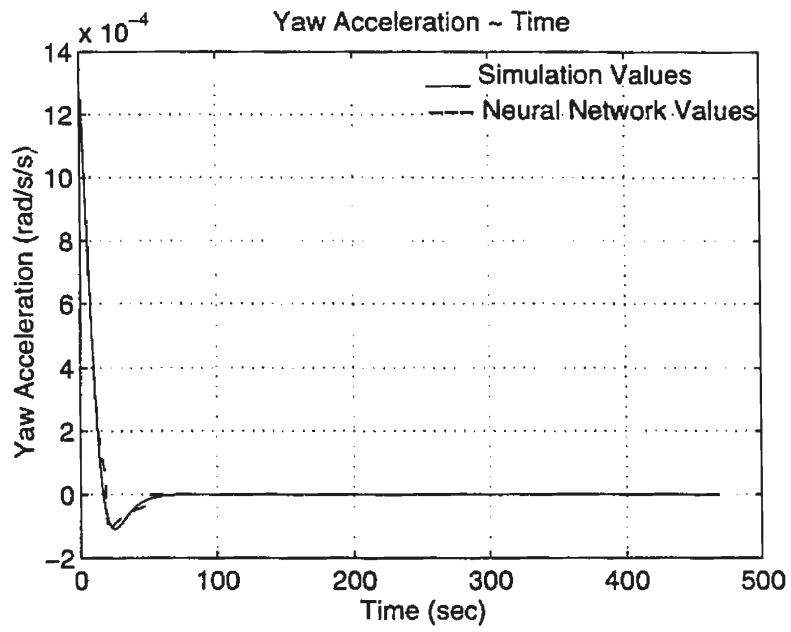


Figure 6.16: Yaw Accelerations in 30 degree Turning, Starboard

Chapter 7

Study of Sway and Yaw Motions in Random Waves

In this chapter, the main objective is to show that the random decrement concept can be extended to coupled sway-yaw motions and this can be the basis for another parametric identification technique. The simplest systems, the linear systems and the nonlinear systems of the sway-yaw motions are studied in this chapter. For each of the systems, we give the random responses, the free motion responses of sway and yaw velocities and their corresponding autocorrelation functions for comparison.

7.1 Exciting Wave Forces

7.1.1 Random Waves

The random wave excitation is simulated by the superposition of a number of sinusoidal waves obtained from the ITTC spectrum. The ITTC wave spectrum formula (two parameters) is appropriate to model open ocean wave conditions and is given as follows:

$$S(\omega) = \frac{A}{\omega^5} e^{(-B/\omega^4)} \quad (7.1)$$

in which

$$A = 173 \frac{H_{1/3}^2}{T_1^4}, \quad B = \frac{691}{T_1^4} \quad (7.2)$$

where S is the spectral density and ω is the wave frequency. The two parameters, $H_{1/3}$ and T_1 , are the significant wave height and the period corresponding to the average wave frequency. In this thesis, we take $H_{1/3} = 5$ m and $T_1 = 10$ sec. Figure 7.1 shows this spectrum.

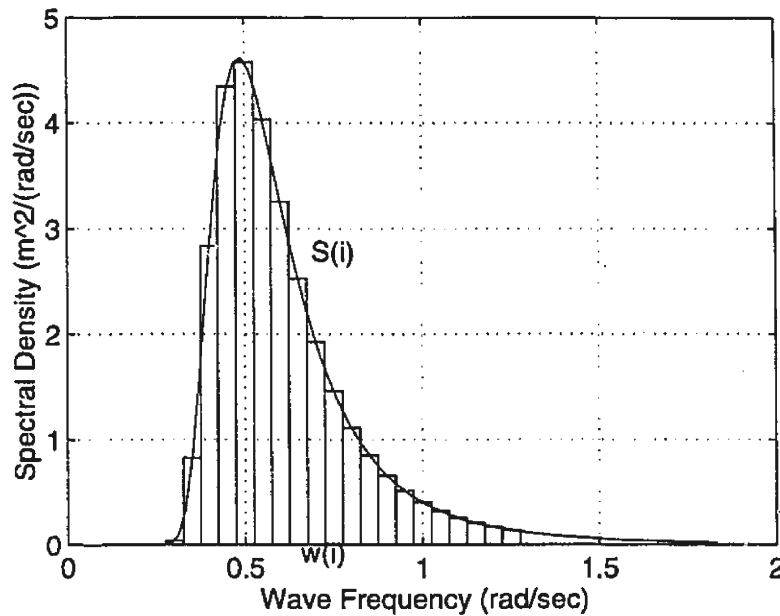


Figure 7.1: ITTC Spectrum

It is assumed that a random wave having an ITTC spectrum is composed of a large number of sinusoidal components. The frequency ω_i and the random phase angle θ_i of each of the sinusoidal components are expressed as follows:

$$\omega_i = \omega_b + \frac{i}{n-1}(\omega_f - \omega_b) \quad i = 0, 1, \dots, n-1 \quad (7.3)$$

$$\theta_i = 2\pi\gamma \quad 0 \leq \gamma \leq 1 \quad (7.4)$$

ω_i varies between frequency limits ω_b and ω_f in the frequency band of the ITTC spectrum. γ is an uniform random number chosen such that the phase angle varies between 0 and 2π .

The amplitude of the i th component of the wave is calculated using

$$A_i = \sqrt{2S_i d\omega} \quad (7.5)$$

where S_i is the spectrum density corresponding to ω_i and

$$d\omega = \frac{\omega_f - \omega_b}{n-1} \quad (7.6)$$

In this thesis, a random wave is constructed using twenty regular wave components with frequencies between $\omega_b = 0.3$ rad/sec and $\omega_f = 1.25$ rad/sec.

7.1.2 Wave Exciting Forces and Moments

The exciting forces and moments in random waves can be calculated by superposition of the exciting forces and moments produced by the individual regular waves which constitute a random wave. The exciting force and moment of one sinusoidal wave may be calculated by integrating the pressure distribution in the wave over the wetted surface of the hull. Only the pressure distribution in the incident wave is considered and the effect of the presence of the ship hull on the pressure distribution

is neglected. The resulting force is called the Froude-Krylov exciting force. This approximation can be considered accurate only if the wave length of the incident wave is large enough. The average wave length in this thesis can be estimated using the dispersion relationship in deep water as

$$\omega^2 = gk \quad (7.7)$$

we can get

$$\left(\frac{2\pi}{T_1}\right)^2 = g\frac{2\pi}{\lambda} \quad (7.8)$$

then the average wavelength of the random wave is

$$\lambda = \frac{gT_1^2}{2\pi} = \frac{9.8 * 10^2}{2\pi} = 156(m) \quad (7.9)$$

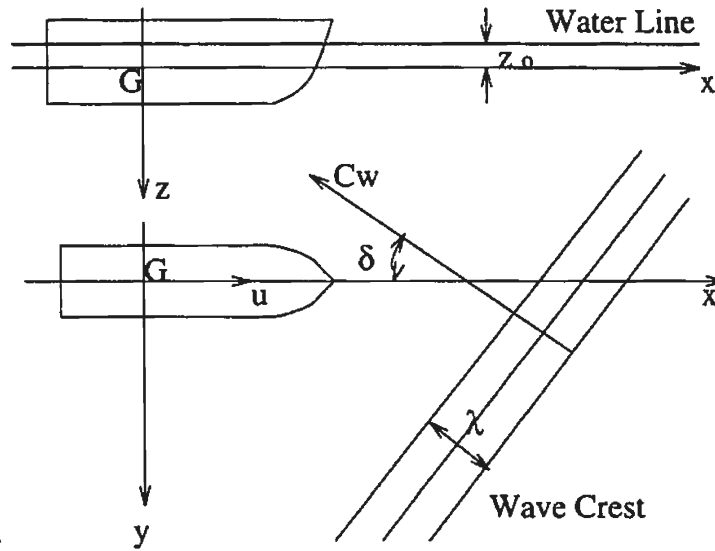


Figure 7.2: Coordinate Axes

The pressure distribution in the wave can be expressed in the hull coordinate system in Figure 7.2 as follows (Haddara, 1970):

$$p(x, y, z, t) = \rho g(z - z_0) - \rho g A_i e^{-k_i(z-z_0)} \sin(k_1 x - k_2 y + \omega t + \theta_i) \quad (7.10)$$

where

$$k_i = \omega_i^2 / g \quad (7.11)$$

$$k_1 = k_i \cos \delta \quad (7.12)$$

$$k_2 = k_i \sin \delta \quad (7.13)$$

$$\omega = \omega_i + k_i u \cos \delta \quad (7.14)$$

δ is the angle between the ship heading and the wave propagation direction. k_i , ω_i , A_i and θ_i are wave number, wave frequency, wave amplitude and wave phase angle, respectively. z_0 is the vertical distance from the waterline to the position of the center of gravity of the ship. ρ is the water density. u is the surge velocity of ship.

The sway exciting force, Y_f , and yaw exciting moment, N_f , calculated according to the Froude-Krylov hypothesis are given as

$$Y_f = \int \int_s -p(x, y, z, t) dx dz \quad (7.15)$$

$$N_f = \int \int_s p(x, y, z, t) (y dy dz - x dx dz) \quad (7.16)$$

If the ship is cut along the ship length into m sections, along the ship draft into n slices and along the beam into l segments. The exciting force and moment can be calculated in this way

$$Y_f = \sum_{k=1}^n \sum_{i=1}^m -p(x_{ik}, y_{ik}, z_{ik}, t) D x D z \quad (7.17)$$

$$\begin{aligned} N_f &= \sum_{k=1}^n \sum_{j=1}^l p(x_{jk}, y_{jk}, z_{jk}, t) y_{jk} D y D z \\ &+ \sum_{k=1}^n \sum_{i=1}^m [-p(x_{ik}, y_{ik}, z_{ik}, t)] x_{ik} D x D z \end{aligned} \quad (7.18)$$

Tables 7.1 and 7.2 give the offsets for calculation of the ship geometry. The wave exciting force of sway and the wave exciting moment of yaw for $A_i=0.503\text{m}$, $\omega_i=0.65\text{ rad/sec}$ and $\delta=45\text{ degrees}$ are shown in Figures 7.3 and 7.4. The amplitudes of exciting forces of sway and moments of yaw with different wave propagation directions from 0 to 180 degrees are given in Figures 7.5 and 7.6.

Table 7.1: Table of Offsets (Half-breadths, m)

Station	Half Breadth	bottom tangent	4-ft WL 1.219m	8-ft WL 2.438m	16-ft WL 4.877
0, FP	0		0.759	0.581	0.108
0.5	0.394		1.308	1.432	1.270
1	0.483		1.968	2.438	2.730
1.5	0.571		2.978	3.848	4.626
2	0.660		4.324	5.534	6.575
3	0.660	0.860	7.509	8.909	10.173
4	0.660	3.832	10.293	11.208	11.830
5	0.660	9.144	11.417	11.916	12.039
6	0.660	6.268	10.344	11.338	11.983
7	0.660	2.324	6.833	8.490	10.627
8	0.660	0.679	3.314	4.423	6.788
8.5	0.660	0.660	2.207	2.896	4.518
9	0.660		1.445	1.778	2.508
9.5	0.432		0.549	0.568	0.600
10; AP					
10-ft aft					

Table 7.2: Table of Offsets Continued (Half-breadths, m)

Station	24-ft WL 7.315m	27-ft WL 8.230m	32-ft WL 9.754m	40-ft WL 12.192m	Main Deck
0, FP			0.133	0.879	2.337
0.5	1.172	1.245	1.613	2.775	4.483
1	2.962	3.140	3.610	4.823	6.518
1.5	5.102	5.359	5.886	6.988	8.404
2	7.315	7.597	8.093	8.979	9.966
3	10.792	10.956	11.195	11.484	11.716
4	11.986	12.007	12.033	12.039	12.039
5	12.039	12.039	12.039	12.039	12.039
6	12.039	12.039	12.039	12.039	12.039
7	11.703	11.899	12.033	12.039	12.039
8	9.458	10.271	11.246	11.932	12.039
8.5	7.306	8.417	9.976	11.389	11.890
9	4.677	5.962	7.973	10.252	11.370
9.5	1.533	3.057	5.410	8.236	10.001
10, AP			2.130	4.861	6.826
10-ft aft				2.658	4.553

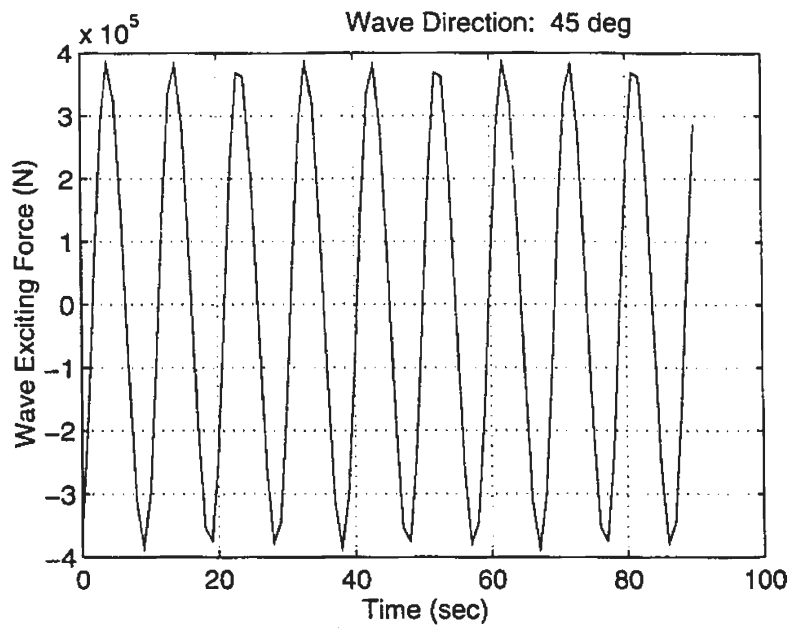


Figure 7.3: Wave Exciting Force of Sway

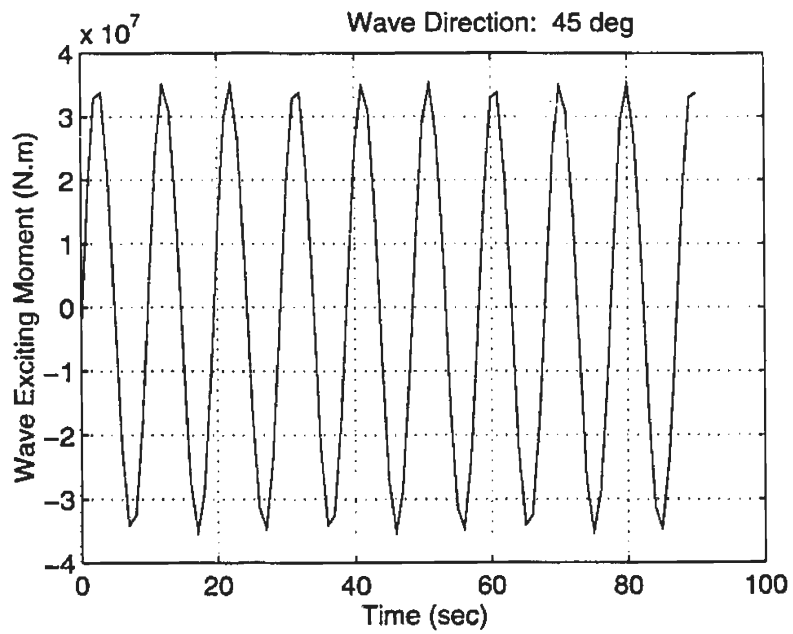


Figure 7.4: Wave Exciting Moment of Yaw

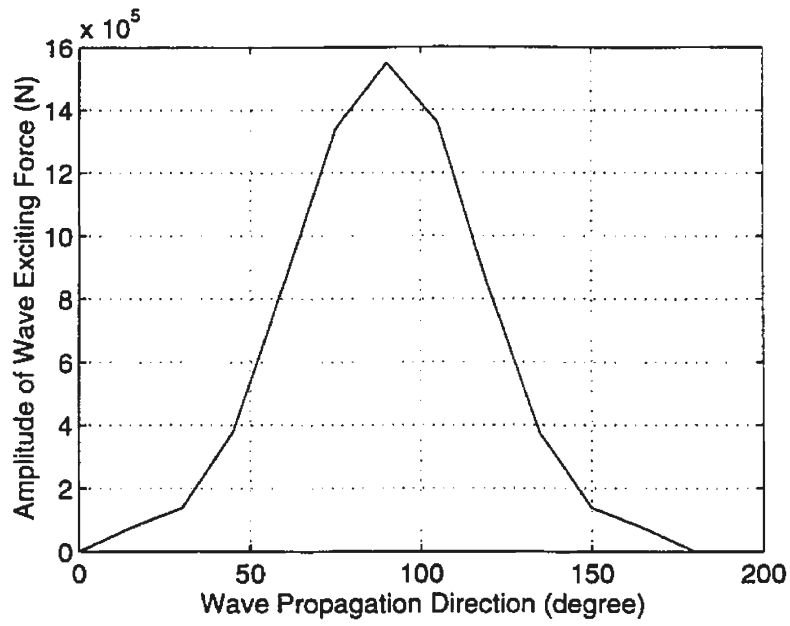


Figure 7.5: Amplitude of Wave Exciting Forces of Sway

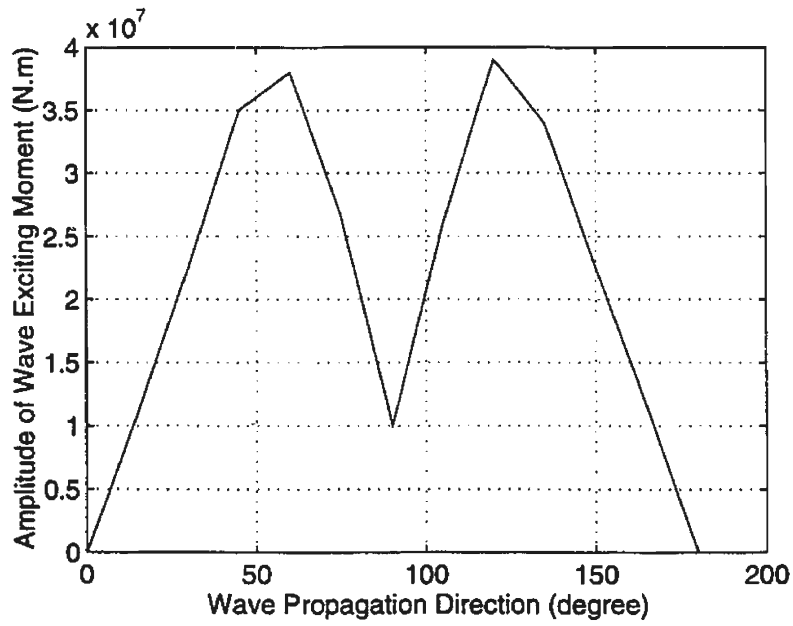


Figure 7.6: Amplitude of Wave Exciting Moments of Yaw

7.2 Simplest Case of Sway-Yaw Motions

7.2.1 Analytic and Numerical Solutions

Consider a ship that has only linear uncoupled hydrodynamic coefficients. The sway and yaw motion equations in random waves can be expressed as follows

$$(\Delta - Y_{\dot{v}})\dot{v} = Y_v v + Y_{\delta}\delta_R + Y_f(t) \quad (7.19)$$

$$(I_z - N_{\dot{r}})\dot{r} = N_r r + N_{\delta}\delta_R + N_f(t) \quad (7.20)$$

To simplify these equations, we assume that the rudder angle is set to zero when the ship with initial v_0 and r_0 is disturbed by the wave exciting forces. Thus, equations 7.19 and 7.20 become

$$\begin{aligned} \dot{v} &= \frac{Y_v}{\Delta - Y_{\dot{v}}}v + \frac{Y_f(t)}{\Delta - Y_{\dot{v}}} \\ &= a_{11}v + \frac{Y_f(t)}{\Delta - Y_{\dot{v}}} \end{aligned} \quad (7.21)$$

$$\begin{aligned} \dot{r} &= \frac{N_r}{I_z - N_{\dot{r}}}r + \frac{N_f(t)}{I_z - N_{\dot{r}}} \\ &= a_{22}r + \frac{N_f(t)}{I_z - N_{\dot{r}}} \end{aligned} \quad (7.22)$$

The solution of each of the above two equations is a combination of a homogeneous solution and a particular solution as follows

$$v(t) = v_0 e^{a_{11}t} + Y_f^*(t) \quad (7.23)$$

$$r(t) = r_0 e^{a_{22}t} + N_f^*(t) \quad (7.24)$$

If we take the logarithm of equations 7.23 and 7.24 with the wave excitation terms set to zero, one gets

$$\ln(v(t)) = \ln(v_0) + a_{11}t \quad (7.25)$$

$$\ln(r(t)) = \ln(r_0) + a_{22}t \quad (7.26)$$

The numerical solutions of equations 7.21 and 7.22 with the initial $v_0 = 1$ m/sec and $r_0 = -0.02$ rad/sec are shown in Figures 7.7 and 7.8. The solutions without wave excitation in these figures are the exact the homogeneous solutions in equations 7.21 and 7.22.

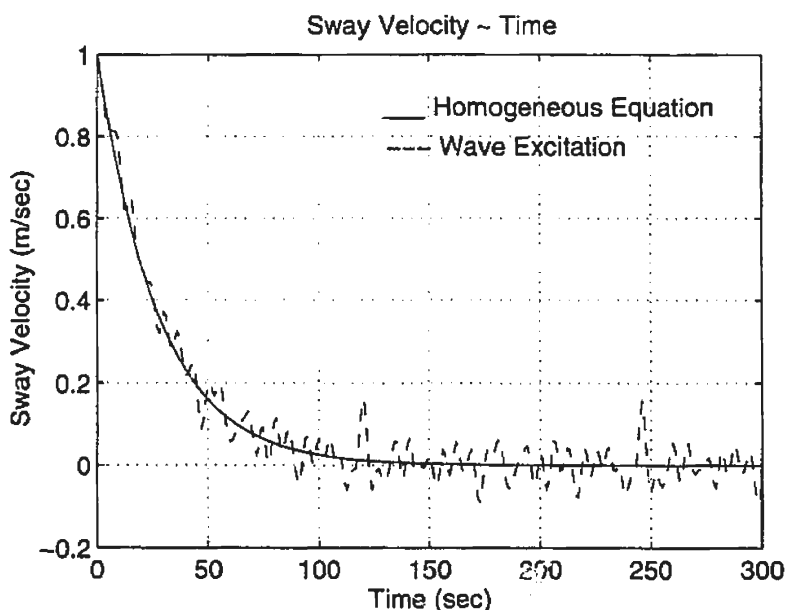


Figure 7.7: Responses of Sway Velocity in Simplest System

7.2.2 Autocorrelation Functions

The autocorrelation function $R_\phi(\tau)$ for random data $\phi(t)$ describes the general dependence of the values of the data at one time, on the values at a later time. An estimate for the autocorrelation between the values of $\phi(t)$ at time, t , and time, $(t + \tau)$ may be obtained by taking the product of the two values and averaging them over the observation time, T^* . Mathematically, the autocorrelation function

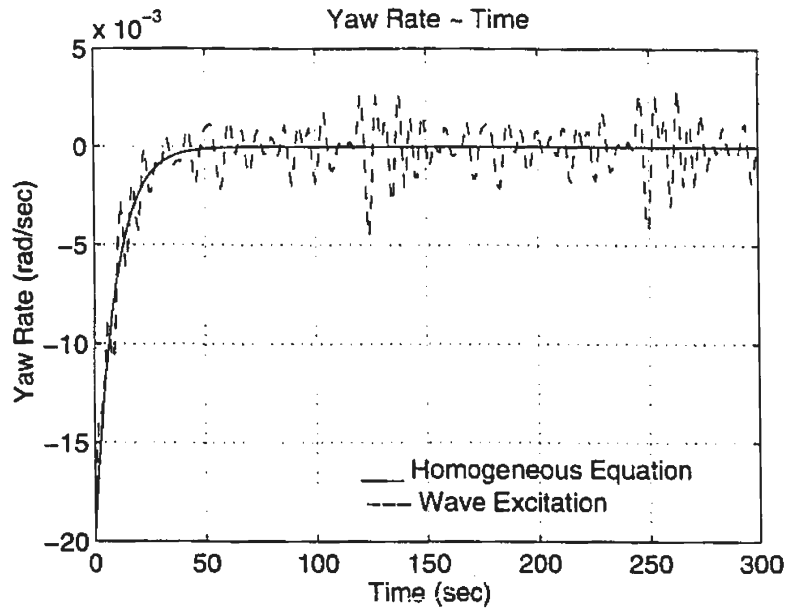


Figure 7.8: Responses of Yaw Rate in Simplest System

is represented by

$$R_{\phi}(\tau) = E[\phi(t)\phi(t + \tau)] = \lim_{T \rightarrow \infty} \frac{1}{T} \int_0^T \phi(t)\phi(t + \tau) dt \quad (7.27)$$

For discrete data, the autocorrelation function can be calculated using the formula

$$R_{\phi}(k) = \frac{1}{n} \sum_{t=1}^{n-k} \phi(t)\phi(t + k) \quad (7.28)$$

where $k = 0, 1, \dots, K$ and $1 \leq K < n$.

In Figures 7.9 and 7.10, the autocorrelation functions of the responses of $v(t)$ and $r(t)$ are calculated using a program based on equation 7.28. For comparison, we generate the curves of autocorrelation functions for the responses with the wave excitation term set to zero. We find that these curves of the autocorrelation fit well with those of excitation responses. It indicates that the process of autocorrelation

can eliminate the effect of a zero mean random process of waves.

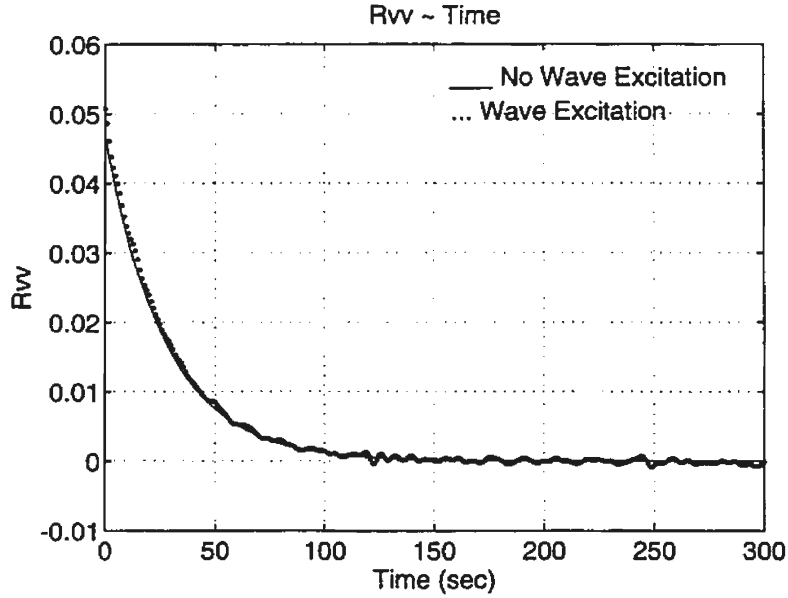


Figure 7.9: Autocorr. Functions of $v(t)$ in Simplest System

The analytic autocorrelation functions of equations 7.23 and 7.24 with the excitation terms set to zero can be developed as follows

$$\begin{aligned}
 R_{vv}(\tau) &= \lim_{T^* \rightarrow \infty} \frac{1}{T^*} \int_0^{T^*} v(t)v(t+\tau)dt \\
 &= \lim_{T^* \rightarrow \infty} \frac{1}{T^*} \int_0^{T^*} v_0 e^{a_{11}t} v_0 e^{a_{11}(t+\tau)} dt \\
 &= \lim_{T^* \rightarrow \infty} \frac{v_0^2}{2a_{11}T^*} e^{a_{11}\tau} (e^{2a_{11}T^*} - 1) \\
 &= -\frac{v_0^2}{2a_{11}T^*} e^{a_{11}\tau} \tag{7.29}
 \end{aligned}$$

where $\lim_{T^* \rightarrow \infty} e^{2a_{11}T^*} = 0$ because $a_{11} < 0$. T^* is the observation time. In a similar way, we can get the autocorrelation function for yaw rate, r , as follows

$$R_{rr}(\tau) = -\frac{r_0^2}{2a_{22}T^*} e^{a_{22}\tau} \tag{7.30}$$

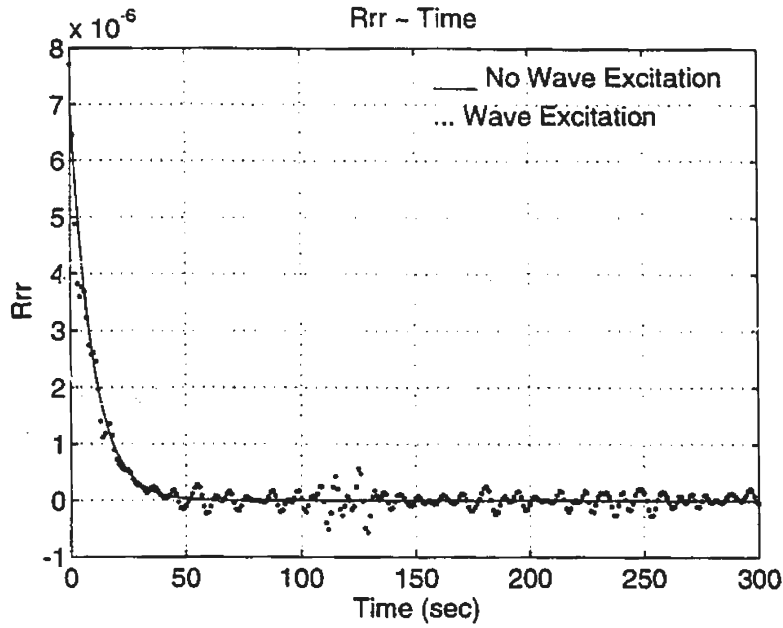


Figure 7.10: Autocorr. Functions of $r(t)$ in Simplest System

where $a_{22} < 0$. Both the autocorrelation functions of wave and no wave excitation should have the same forms as shown in equations 7.29 and 7.30. When we take the logarithm of the hand side of equations 7.29 and 7.30, the logarithm of R_{vv} and R_{rr} can be obtained as follows

$$\ln(R_{vv}(\tau)) = \ln\left(-\frac{v_0^2}{2a_{11}T^*}\right) + a_{11}\tau \quad (7.31)$$

$$\ln(R_{rr}(\tau)) = \ln\left(-\frac{r_0^2}{2a_{22}T^*}\right) + a_{22}\tau \quad (7.32)$$

It is easy to find that the slope of line in equation 7.31 is the same as the one in equation 7.25. So is the case for equations 7.32 and 7.26. Figure 7.11 shows the curves of $\ln(v(t))$, $\ln(r(t))$, $\ln(R_{vv})$ and $\ln(R_{rr})$. In Figure 7.11, the points of $\ln(v(t))$ and $\ln(r(t))$ are scattered away from the straight line after a certain time period because the values of R_{vv} and R_{rr} vibrate at the zero point with time as

shown in Figures 7.9 and 7.10 and the logarithm program forces the negative values to become positive.

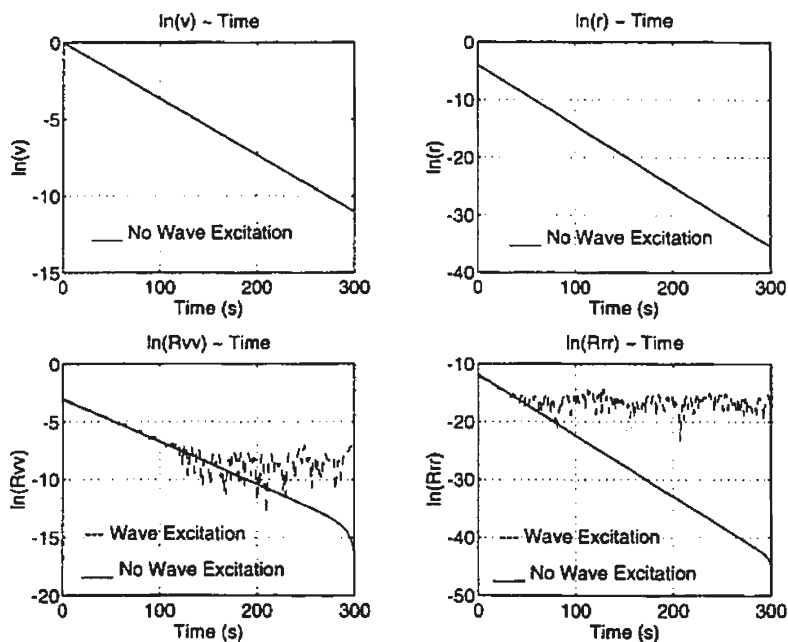


Figure 7.11: Logarithm of the Functions in Simplest System

7.3 The Linear System

The linear system for describing sway and yaw motions in random waves can be expressed in the following form:

$$(\Delta - Y_{\dot{v}})\dot{v} - Y_{\dot{r}}\dot{r} = Y_v v + Y_r r + Y_{\delta}\delta_R + Y_f(t) \quad (7.33)$$

$$-N_{\dot{v}}\dot{v} + (I_z - N_{\dot{r}})\dot{r} = N_v v + N_r r + N_{\delta}\delta_R + N_f(t) \quad (7.34)$$

To simplify the problem, we set the rudder angle to zero. The motion of the ship in random waves will be the motion with an initial sway velocity and yaw rate

and the rudder angle set to zero. The linear system then can be described by

$$\begin{aligned}
 \dot{v} &= \frac{[(I_z - N_{\dot{r}})Y_v + Y_{\dot{r}}N_v]v}{(\Delta - Y_{\dot{v}})(I_z - N_{\dot{r}}) - N_{\dot{v}}Y_{\dot{r}}} \\
 &+ \frac{[(I_z - N_{\dot{r}})Y_r + Y_{\dot{r}}N_r]r}{(\Delta - Y_{\dot{v}})(I_z - N_{\dot{r}}) - N_{\dot{v}}Y_{\dot{r}}} \\
 &+ \frac{(I_z - N_{\dot{r}})Y_f(t) + Y_{\dot{r}}N_f(t)}{(\Delta - Y_{\dot{v}})(I_z - N_{\dot{r}}) - N_{\dot{v}}Y_{\dot{r}}} \\
 &= a_{11}v + a_{12}r + Y_f^*(t)
 \end{aligned} \tag{7.35}$$

$$\begin{aligned}
 \dot{r} &= \frac{[N_{\dot{v}}Y_v + (\Delta - Y_{\dot{v}})N_v]v}{(\Delta - Y_{\dot{v}})(I_z - N_{\dot{r}}) - N_{\dot{v}}Y_{\dot{r}}} \\
 &+ \frac{[N_{\dot{v}}Y_r + (\Delta - Y_{\dot{v}})N_r]r}{(\Delta - Y_{\dot{v}})(I_z - N_{\dot{r}}) - N_{\dot{v}}Y_{\dot{r}}} \\
 &+ \frac{N_{\dot{v}}Y_f(t) + (\Delta - Y_{\dot{v}})N_f(t)}{(\Delta - Y_{\dot{v}})(I_z - N_{\dot{r}}) - N_{\dot{v}}Y_{\dot{r}}} \\
 &= a_{21}v + a_{22}r + N_f^*(t)
 \end{aligned} \tag{7.36}$$

The numerical solution of equations 7.35 and 7.36 with the initial $v_0 = 1$ m/sec, $\dot{v}_0 = 0$, $r_0 = -0.02$ rad/sec and $\dot{r}_0 = 0$ is shown in Figures 7.12 and 7.13. For comparison, the solution of equations 7.35 and 7.36 without wave excitations is also calculated.

In equations 7.35 and 7.36 with the excitation term set to zero, the characteristic roots, λ_1 and λ_2 of this linear system satisfy the following characteristic function:

$$\lambda^2 - (a_{11} + a_{22})\lambda + a_{11}a_{22} - a_{12}a_{21} = 0 \tag{7.37}$$

The solution of the two roots is as follows

$$\lambda_{1,2} = \frac{a_{11} + a_{22}}{2} \pm \frac{\sqrt{(a_{11} - a_{22})^2 + 4a_{12}a_{21}}}{2} \tag{7.38}$$

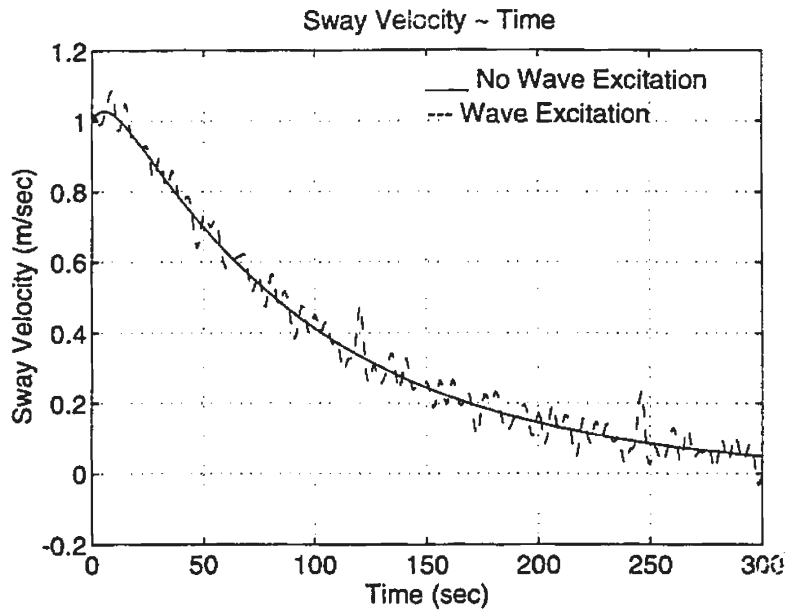


Figure 7.12: Responses of Sway Velocity in Linear System

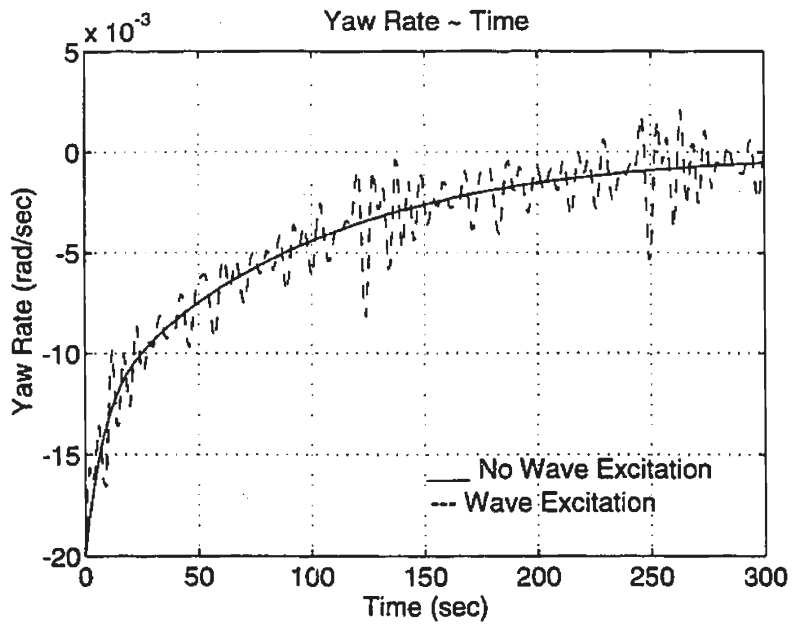


Figure 7.13: Responses of Yaw Rate in Linear System

For the ship particulars and coefficients used in chapter 2, we get $\lambda_1 < \lambda_2 < 0$. So, the analytical solution for equations 7.35 and 7.36 without wave excitation will be in form of

$$v = c_1 e^{\lambda_1 t} + c_2 e^{\lambda_2 t} \quad (7.39)$$

$$r = d_1 e^{\lambda_1 t} + d_2 e^{\lambda_2 t} \quad (7.40)$$

where according to the initial conditions, the constants can be obtained as follows

$$c_1 = \frac{v_0 \lambda_2}{\lambda_2 - \lambda_1} \quad (7.41)$$

$$c_2 = \frac{-v_0 \lambda_1}{\lambda_2 - \lambda_1} \quad (7.42)$$

$$d_1 = \frac{r_0 \lambda_2}{\lambda_2 - \lambda_1} \quad (7.43)$$

$$d_2 = \frac{-r_0 \lambda_1}{\lambda_2 - \lambda_1} \quad (7.44)$$

When we calculate the autocorrelation functions of $v(t)$ and $r(t)$ in this linear system, the random wave excitation can be deleted by the autocorrelation functions shown in Figures 7.14 and 7.15.

The autocorrelation function of equation 7.39 can be developed in the following form:

$$\begin{aligned} R_{vv}(\tau) &= \lim_{T^* \rightarrow \infty} \frac{1}{T^*} \int_0^{T^*} (c_1 e^{\lambda_1 t} + c_2 e^{\lambda_2 t})(c_1 e^{\lambda_1(t+\tau)} + c_2 e^{\lambda_2(t+\tau)}) dt \\ &= \frac{1}{T^*} \left[(-1) \left(\frac{c_1}{2\lambda_1} + \frac{c_2}{\lambda_1 + \lambda_2} \right) c_1 e^{\lambda_1 \tau} \right. \\ &\quad \left. + (-1) \left(\frac{c_2}{2\lambda_2} + \frac{c_1}{\lambda_1 + \lambda_2} \right) c_2 e^{\lambda_2 \tau} \right] \\ &= k_1 c_1 e^{\lambda_1 \tau} + k_2 c_2 e^{\lambda_2 \tau} \end{aligned} \quad (7.45)$$

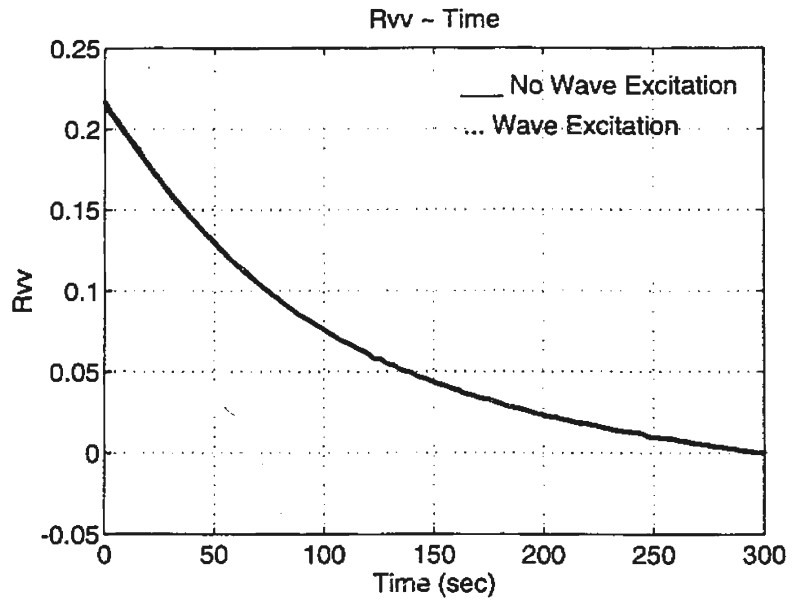


Figure 7.14: Autocorr. Functions of $v(t)$ in Linear System

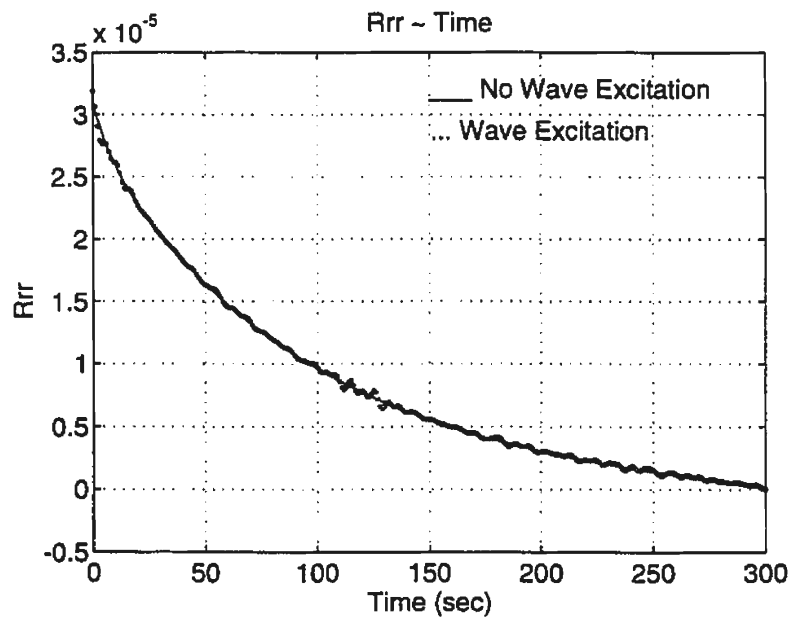


Figure 7.15: Autocorr. Functions of $r(t)$ in Linear System

where the constants k_1 and k_2 are combinations of c_1 and c_2 .

In a similar form, R_{rr} is obtained as follows

$$R_{rr}(\tau) = l_1 d_1 e^{\lambda_1 \tau} + l_2 d_2 e^{\lambda_2 \tau} \quad (7.46)$$

where the constants l_1 and l_2 are combinations of d_1 and d_2 . In this linear system, the autocorrelation functions of $v(t)$ and $r(t)$ are one of the general solutions of equations 7.39 and 7.40. Through the process of autocorrelation, we can eliminate the effect of random excitation and find one solution of the motion equations in the linear system.

7.4 The Nonlinear System

In the nonlinear system, the sway and yaw motion equations in random waves can be obtained as follows:

$$(\Delta - Y_{\dot{v}})\dot{v} - Y_{\dot{r}}\dot{r} = f_2(u, v, r, \delta_R) + Y_f(t) \quad (7.47)$$

$$-N_{\dot{v}}\dot{v} + (I_z - N_{\dot{r}})\dot{r} = f_3(u, v, r, \delta_R) + N_f(t) \quad (7.48)$$

where $f_2(u, v, r, \delta_R)$ and $f_3(u, v, r, \delta_R)$ are hydrodynamic force and moment given in equations 3.7 and 3.8. The initial conditions for the numerical solution is $v_0 = 1\text{m/sec}$, $\dot{v}_0 = 0$, $r_0 = -0.02\text{ rad/sec}$ and $\dot{r}_0 = 0$. The numerical solutions of equations 7.47 and 7.48 are shown in Figures 7.16 and 7.17. The solutions for no wave excitation are also given for comparison.

The autocorrelation functions for $v(t)$ and $r(t)$ with wave excitation and without wave excitation are given in Figures 7.18 and 7.19. The curves of the autocorrelation

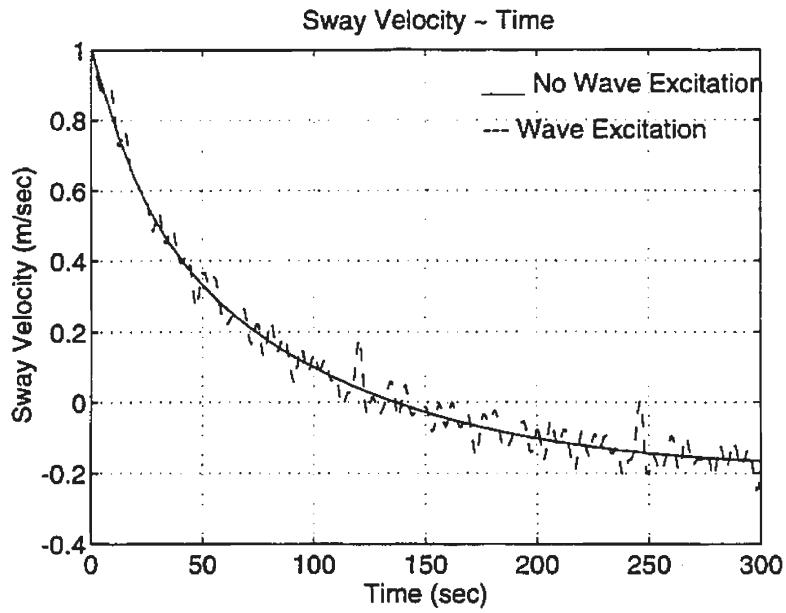


Figure 7.16: Responses of Sway Velocity in Nonlinear System

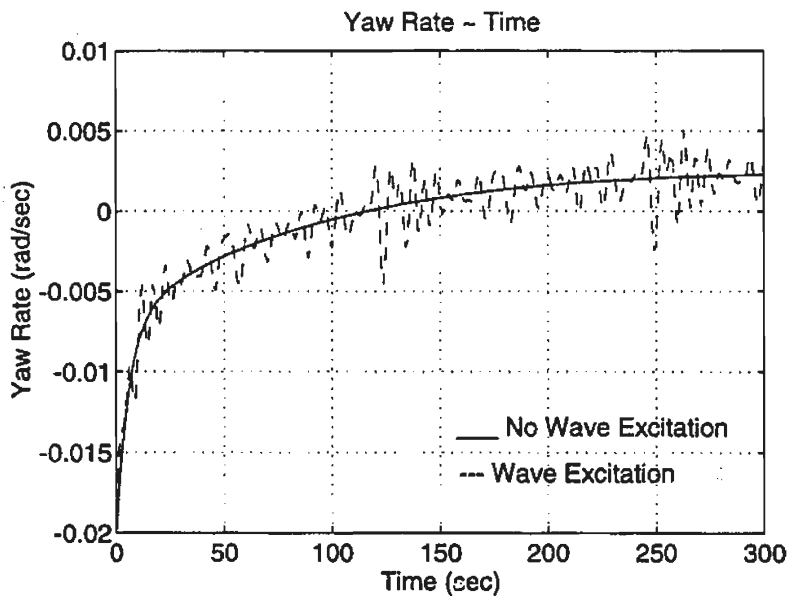


Figure 7.17: Responses of Yaw Rate in Nonlinear System

function with wave excitation have a good agreement with those without wave excitation.

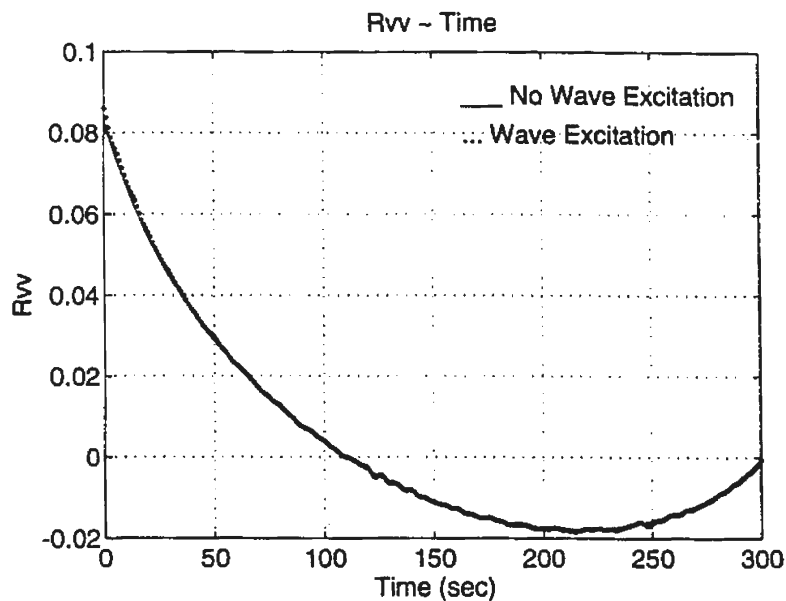


Figure 7.18: Autocorr. Functions of $v(t)$ in Nonlinear System.

7.5 Discussion

In case of the simplest sway-yaw motion system, it is easy to find the parameters, a_{11} and a_{22} , by taking logarithm of the autocorrelation functions of sway and yaw velocities in random waves. The slopes of the logarithm functions are exactly the values of a_{11} and a_{22} .

For the nonlinear system, the autocorrelation for the nonlinear sway and yaw motions excited by random waves are similar to the free sway and yaw motions. The autocorrelation functions may help us to identify the parameters in the nonlinear

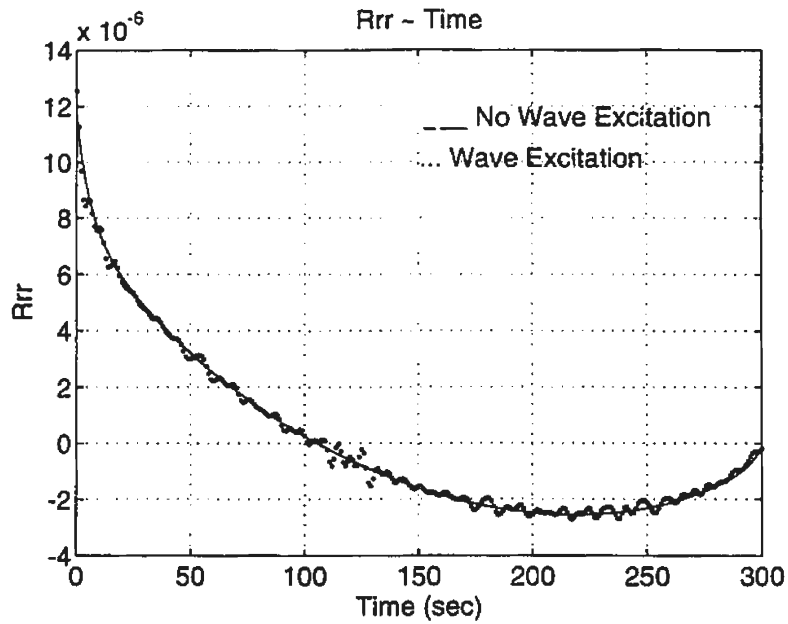


Figure 7.19: Autocorr. Functions of $r(t)$ in Nonlinear System

equations of the sway and yaw motions. However, the theory to prove the validity of the above statement for the nonlinear system is not available now. This can be a logical extension for this work.

Chapter 8

Conclusions

In this work, we have presented three methods for the parametric identification of the manoeuvring motions of ships. The results of the method developed in chapter 4 show that using one set of data from a zigzag manoeuvre, we are able to formulate a model which can represent the manoeuvrability of the ship under different conditions, with sufficient accuracy. This method can then be used to formulate manoeuvring models for different ships using their full scale trial data. From the theoretical basis of the proposed method and the results it has produced so far, this new method has some advantages over other existing parametric identification methods for ship manoeuvrability prediction. These advantages are:

1. Elimination of scale effects. The inputs for this neural network model are data of surge, sway, yaw velocities and rudder angles from the full scale ship trials during standard ship manoeuvres. No model tests or considerations of viscous scale effects are required.

2. The cost is minimized. If the input data to the identification model is directly

obtained from the measuring instruments that usually exist on board the ship, the cost of trial is limited.

3. The accuracy of the identification process can be easily checked, because actual ship responses are measured for the validation of the identification model.

4. The new method can effectively avoid the cancellation effects of hydrodynamic coefficients by only applying linear and nonlinear components in the expansion of hydrodynamic forces.

5. Unlike other identification techniques developed for this problem, only one set of measured data of reasonable length is sufficient to formulate the model using this method. This will greatly save ship trial resources and increase the efficiency of the parametric identification work.

The work in chapter 6 provides an attempt to predict ship turning manoeuvres. The approach in chapter 6 can reduce the required motion equations to one, i.e., the yaw equation. But, for different rudder angle turning manoeuvres, different mappings of sway and yaw velocities are needed. Thus, this approach is less robust than the method developed in chapter 4.

In chapter 7, we have presented a study of the sway and yaw motions in random waves. Using a simple analysis, we have shown that the concept of a random decrement can be extended to the coupled sway-yaw motion in random waves. The

results are preliminary and the analysis needs to be extended and validated. This is the subject of future work.

References

- Abkowitz, M. A. (1980). " *Measurement of Hydrodynamic Characteristics from Ship Manoeuvring Trials by System Identification,*" Transactions of the Society of Naval Architects and Marine Engineers, Vol. 88, pp. 283-318.
- Abkowitz, M. A. and Liu, G. (1988). " *Measurement of Ship Resistance, Powering and Manoeuvring Coefficients from Simple Trials During a Regular Voyage,*" Transactions of the Society of Naval Architects and Marine Engineers, Vol. 96, pp. 97-128.
- Clarke, D. (1971). " *A New Nonlinear Equation for Ship Manoeuvring,*" International Shipbuilding Process, Vol. 18, No. 201, pp. 181-197.
- Clarke, D., Gedling, P. and Hine, G. (1982). " *The Application of Manoeuvring Criteria in Hull Design Using Linear Theory,*" Transactions of The Royal Institution of Naval Architects, Vol. 125, pp. 45-68.
- Crane, C. L., Eda, H. and Landsburg, A. (1989). " *Principles of Naval Architecture,*" The Society of Naval Architects and Marine Engineers, N.J., Vol. 3, pp. 191-429.
- Cybenko, G. (1989). " *Approximation by Superpositions of a Sigmoidal Function,*" Mathematics of Control, Signals, and Systems, Vol. 2, No. 4, pp. 303-314.

- Dieudonne, J. (1953).** "Collect French Papers on Stability of Route of Ships at Sea, 1949-1950," DTRC Translation 246.
- Eda, H., Seibold F. and DeBord, F. W. (1982).** "Manoeuvring Performance of Ships in Critical Channels," SNAME Transactions, Vol. 90, pp. 195-228.
- Gertler, M. (1959).** "The DTMB Planar Motion Mechanism System," Symposium of Towing Tank Facilities, Zagreb, Yugoslavia.
- Gill, M. A. (1975).** "The Identification of Manoeuvring Equations from Ship Trials Results," Transactions of The Royal Institute of Naval Architects, Vol. 117, pp. 145-157.
- Haddara, M. (1970).** "On the Stability of Ship Motion in Regular Oblique Waves," College of Engineering, University of California, Report No. NA 70-2.
- Haddara, M. and Sabin, G. (1995).** "Parametric Identification of Hydrodynamic Characteristics from Ship Manoeuvring Trials Using Neural Networks," the 24th American Towing Tank Conference, Texas A&M University, U.S.A..
- Hinchey, M. (1994).** "A Neural Network Fit to Icebreaker Resistance Data," Off-shore Mechanics and Arctic Engineering, Vol. 116, pp. 252-254.
- Hornik, K., Stinchcombe, M. and White, H. (1989).** "Multilayer Feed Forward Networks and Universal Approximations," Neural Networks, Vol. 2, pp. 359-366.
- Hush, D. R. and Horne, B. (1993).** "Progress in Supervised Neural Networks," IEEE Signal Processing Magazine, pp. 8-39.

- IEEE Press, (1992a). "*Neural Networks: Theoretical Foundations and Analysis*".
- IEEE Press, (1992b). "*Artificial Neural Networks: Paradigms, Applications and Software Implementations*".
- Inoue, S., Hirano, M., Kijima, K. and Takashina, J. (1981a). "*Hydrodynamic Derivatives on Ship Manoeuvring*," International Shipbuilding Process, Rotterdam, Netherlands, Vol. 28, No. 321, pp. 112-125.
- Inoue, S., Hirano, M., Kijima, K. and Takashina, J. (1981b). "*A Practical Calculation Method of Ship Manoeuvring Motion*," International Shipbuilding Process, Rotterdam, Netherlands, Vol. 28, No. 325, pp. 207-222.
- Kijima, K., Tanaka, S., Furukawa, Y. and Hori, T. (1993). "*On a Prediction Method of Ship Manoeuvring Characteristics*," Proceeding of MARSIM '93, Vol. 1, pp. 285-294.
- Mikelis, N. E. and Price, W. G. (1980). "*Comparisons of Acceleration Coefficients and Correction Factors Associated Between Theory and Experiments*," Trans. RINA, Vol. 122, pp. 90-111.
- Monk, A. (1991). "*Exploring Statistics with MINITAB*," John Wiley & Sons Ltd, Rexdale, Ontario, Canada. pp. 181-211.
- Panama Canal Regulations (1977). "*Manoeuvring Characteristics. Data Required*," Code of Federal Regulations, 35 Panama Canal, Par.103, 41a.

- Remez, V. U. (1989).** " *Theoretical Determination of Ships Manoeuvrability Hydrodynamic Characteristics*", Proceeding of PRADS '89, Vol. 3, Paper No. 100.
- Trankle, T. L. (1989).** " *Identification of T.V. Kings Pointer Hydrodynamic Model Using Sea Trials Inertial Data*," Proceeding of the 22nd American Towing Tank Conference, St. John's, Newfoundland, Canada, pp. 508-514.
- Wu, X. and Liu, Z. (1990).** " *Calculation of Manoeuvring Hydrodynamic Force Including the Effects of Free Surface and Separated Vortex*," 19th ITTC Proceedings, Vol. 2.
- Yang, Y., Jiang, W. and Jia, C. (1992).** " *The Application of Data Base in Calculating Hydrodynamic Coefficients of Ship Manoeuvring Mathematical Model*," Proceedings of 6th Manoeuvrability Symposium in China.

Appendices

Appendix A

Results Using a Great Lake Bulk Carrier

In the appendix, results are given for the work in chapters 4 and 5 using another different ship, a 730-ft Great Lake Bulk Carrier. This ship's principal particulars and its hydrodynamic coefficients can be found in Eda et al. (1982).

A.1 Ship Principal Particulars and Hydrodynamic Coefficients

Table A.1: Ship Principal Particulars

Length	Beam	Draft	Block Coef.	Velocity	Rudder Rate
217.627 m	23.005 m	8.100 m	0.905	5.144 m/sec	2.5 deg/sec

Table A.2: Hydrodynamic Coefficients of 730-ft Great Lake Bulk Carrier

Coefficients (X-equation)	Values	Coefficients (Y-equation)	Values	Coefficients (N-equation)	Values
$\Delta - X_{\dot{u}}$	0.19505	$\Delta - Y_{\dot{v}}$	0.33234	$N_{\dot{v}}$	0
X_u	-0.02000	Y_r	0	$I_z - N_r$	0.02724
X_{uu}	0.01800	Y_v	-0.32535	N_v	-0.08732
X_{uuu}	-0	Y_{vvv}	-7.38289	N_{vvv}	-3.04665
X_{vv}	-0.26007	Y_{vrr}	-0.60718	N_{vrr}	0.07576
X_{rr}	0.01310	$Y_{v\delta\delta}$	0	$N_{v\delta\delta}$	0
$X_{\delta\delta}$	-0.09833	Y_{vu}	0	N_{vu}	0
X_{vvu}	0	Y_{vuu}	0	N_{vuu}	0
X_{rru}	0	$Y_r - \Delta$	-0.16200	N_r	-0.04433
$X_{\delta\delta u}$	0	Y_{rrr}	2.40185	N_{rrr}	-0.24180
$X_{vr} + \Delta$	0.299023	Y_{rvv}	0	N_{rvv}	-0.84361
$X_{v\delta}$	0	$Y_{r\delta\delta}$	0	$N_{r\delta\delta}$	0
$X_{r\delta}$	0	Y_{ru}	0	N_{ru}	0
X_{vru}	0	Y_{ruu}	0	N_{ruu}	0
$X_{v\delta u}$	0	Y_{δ}	0.08194	N_{δ}	-0.04675
$X_{r\delta u}$	0	$Y_{\delta\delta\delta}$	-0.25469	$N_{\delta\delta\delta}$	0.23857
X^0	0	$Y_{\delta vv}$	0	$N_{\delta vv}$	0
		$Y_{\delta rr}$	0	$N_{\delta rr}$	0
		$Y_{\delta u}$	0	$N_{\delta u}$	0
		$Y_{\delta uu}$	0	$N_{\delta uu}$	0
		$Y_{vr\delta}$	0	$N_{vr\delta}$	0
		Y^0	0	N^0	0
		Y_u^0	0	N_u^0	0
		Y_{uu}^0	0	N_{uu}^0	0

A.2 Neural Network Training Results

The neural network is trained using data from a 35-35 degree zigzag manoeuvre simulation. The inputs to the networks are surge, sway velocities, yaw rate and rudder angle. The output targets are lumped nonlinear functions, g_1 to g_3 . Three neural networks are used to map the three lumped nonlinear functions. Details are in chapter 4.

Table A.3: Estimated Nondimensional Linear Coefficients of Surge

	$\Delta - X_{\dot{u}}$	X_u	$X_{\delta\delta}$
Clarke Values	0.20089	-0.02000	-0.09720
Original Val.	0.19505	-0.02000	-0.09833

Table A.4: Estimated Nondimensional Linear Coefficients of Sway

	$\Delta - Y_{\dot{v}}$	$Y_{\dot{r}}$	Y_v	$Y_r - \Delta$	Y_{δ}
Clarke Values	0.34968	-0.00516	-0.23715	-0.13349	0.08100
Original Val.	0.33234	0.00000	-0.32535	-0.16200	0.08194

Table A.5: Estimated Nondimensional Linear Coefficients of Yaw

	$N_{\dot{v}}$	$I_z - N_{\dot{r}}$	N_v	N_r	N_{δ}
Clarke Values	0.00002	0.02577	-0.06891	-0.03526	-0.04050
Original Val.	0.00000	0.02724	-0.08732	-0.04433	-0.04675

Table A.6: Trained Weights

Notation	Weights of g_1	Weights of g_2	Weights of g_3
$W_{1,1}$	5.895030e-01	-1.644226e-02	-4.978991e-01
$W_{1,2}$	-5.101392e-01	-7.713196e-02	-2.853818e-01
$W_{1,3}$	-4.659019e-01	1.928862e-01	5.776727e-03
$W_{1,4}$	-4.460121e-02	-1.619135e-01	3.656041e-02
$W_{1,5}$	-4.867011e-02	-4.117465e-01	-1.245193e-02
$W_{2,1}$	-2.046416e-01	-1.677549e-01	-5.201320e-01
$W_{2,2}$	2.385297e-01	-1.597654e-01	1.717111e-01
$W_{2,3}$	2.272791e-01	1.184133e-01	3.020742e-01
$W_{2,4}$	2.810622e-01	2.055512e-01	1.657087e-01
$W_{2,5}$	-2.168948e-01	7.063461e-02	4.414481e-02
$W_{3,1}$	-6.145441e-02	-6.958561e-02	-4.223113e-02
$W_{3,2}$	-6.821217e-02	-5.005843e-02	2.536432e-01
$W_{3,3}$	4.816088e-01	7.552275e+00	-1.080965e+00
$W_{3,4}$	-4.123380e-01	-5.573477e+00	4.341185e-01
$W_{3,5}$	2.271601e+00	7.338701e+00	2.734414e+00
$W_{4,1}$	4.649881e-01	7.052553e+00	9.620253e-01
$W_{4,2}$	1.569679e+00	-4.823933e+00	-1.254879e+00
$W_{4,3}$	3.362712e-01	-2.522815e+00	9.223097e-01
$W_{4,4}$	1.151579e-01	6.926483e-01	3.038447e-01
$W_{4,5}$	4.851341e-01	1.962100e+00	-2.477811e+00
$W_{5,1}$	3.962634e-01	8.427783e-01	-6.726365e-01
$W_{5,2}$	-8.201121e-03	-5.228190e+00	6.987717e-01
$W_{5,3}$	1.236354e+00	-1.233700e+00	5.641754e-01
$W_{5,4}$	5.895262e-01	1.560384e+00	6.774639e-01
$W_{5,5}$	1.041159e+00	6.161842e-01	2.903182e-01
$W_{6,1}$	6.128371e-01	-2.470856e+00	6.764593e-01
$W_{6,2}$	5.301277e-01	3.890111e+00	1.833881e-01
$W_{6,3}$	7.278556e-01	-7.132983e-01	-4.262110e-01
$W_{6,4}$	7.153789e-01	3.512534e+00	7.672549e-01
$W_{6,5}$	7.600573e-01	-9.446703e+00	8.054027e-01
$W_{7,1}$	2.109046e-01	1.439624e-01	2.462407e-01
$W_{7,2}$	4.104700e-02	-4.667036e+00	-2.101112e+00
$W_{7,3}$	3.354941e-01	-2.145962e+00	-4.853948e-02

Table A.7: Trained Weights (continued)

Notation	Weights of g_1	Weights of g_2	Weights of g_3
$W_{7,4}$	2.651775e-01	-1.449891e+00	3.016999e-01
$W_{7,5}$	3.458968e-01	3.680478e+00	4.902010e-01
$W_{8,1}$	5.677670e-02	5.543678e+00	5.072873e-01
$W_{8,2}$	-1.026354e-01	-7.485739e+00	-1.156052e+00
$W_{8,3}$	-3.303378e-01	-3.831410e-01	-8.224130e-01
$W_{8,4}$	4.583949e-01	1.054555e+00	-9.894984e-02
$W_{8,5}$	5.035724e-01	2.210118e-01	1.149003e+00
$W_{9,1}$	1.750813e-01	-1.362159e+00	-2.129860e+00
$W_{9,2}$	2.231805e-01	1.490996e+00	-3.719720e+00
$W_{9,3}$	-5.124242e-01	-5.247389e+00	-3.029870e+00
$W_{9,4}$	8.924522e-01	9.821609e-01	2.242333e-01
$W_{9,5}$	4.135829e-01	-7.330523e-02	2.356684e+00
$W_{10,1}$	1.056319e+00	1.431287e+00	-4.757902e-01
$W_{10,2}$	3.427937e-01	-5.987463e+00	-1.234124e+00
$W_{10,3}$	1.016600e+00	3.011864e-01	-2.540875e-02
$W_{10,4}$	3.613229e-01	-1.559887e-01	1.424949e+00
$W_{10,5}$	-5.335799e-01	-2.786591e+00	-2.503572e+00
$W_{11,1}$	8.915049e-01	-1.135106e+00	1.248511e+00
$W_{11,2}$	8.189336e-01	-2.802571e+00	-4.441569e+00
$W_{11,3}$	1.075846e+00	3.700991e-01	-1.289067e-01
$W_{11,4}$	6.594945e-01	-2.973912e+00	-1.118210e+00
$W_{11,5}$	1.657708e-01	6.759818e+00	1.911629e+00
$B_{1,1}$	2.881164e-01	-5.625140e-01	2.609107e+00
$B_{2,1}$	-1.772791e-01	-4.733456e+00	-2.907100e+00
$B_{3,1}$	-2.705117e-01	-2.057686e+00	1.344162e+00
$B_{4,1}$	1.721803e-01	2.303149e+00	-1.477014e+00
$B_{5,1}$	2.651809e-01	-3.330589e+00	-1.622480e+00
$B_{6,1}$	6.119982e-01	7.620719e-01	8.719896e-01
$B_{7,1}$	-3.971309e-01	-5.380048e+00	6.877767e-01
$B_{8,1}$	1.201942e-01	-1.733426e+00	6.242699e-01
$B_{9,1}$	7.603484e-01	-6.288702e-01	1.144689e+00
$B_{10,1}$	-2.353278e-01	2.390890e+00	2.699315e-02
$B_{11,1}$	4.143471e-01	-2.118129e+00	2.667664e+00
$B_{12,1}$	2.748926e-01	-7.088545e+00	-5.379578e-01

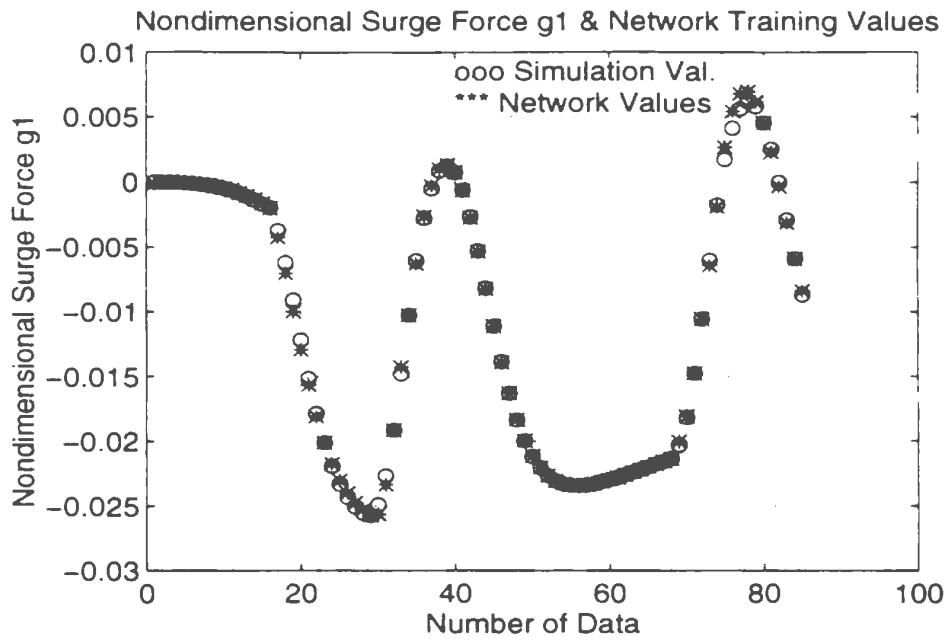


Figure A.1: Trained Network Force g_1 and Simulation Values

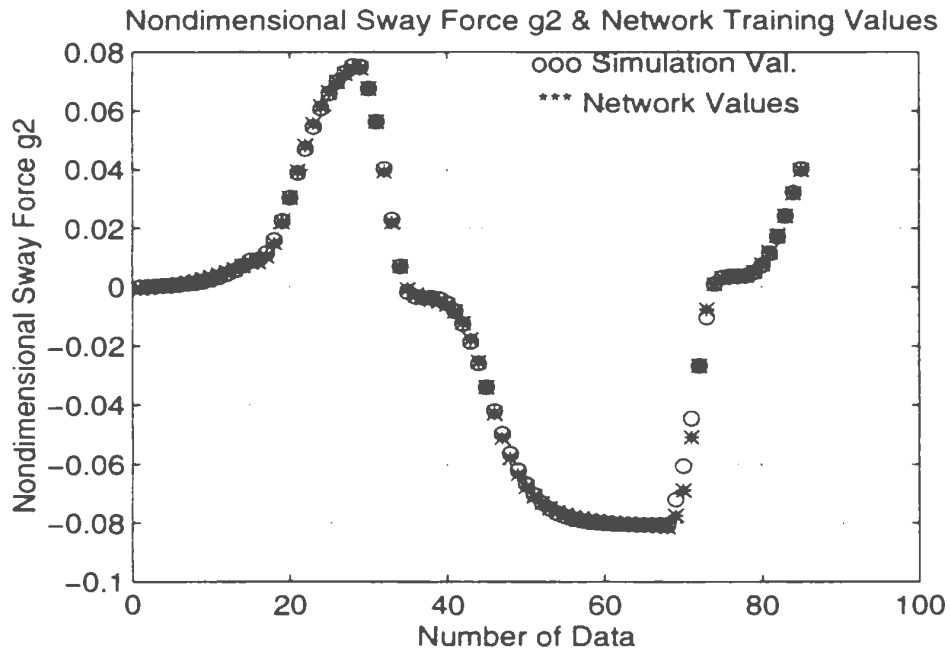


Figure A.2: Trained Network Force g_2 and Simulation Values

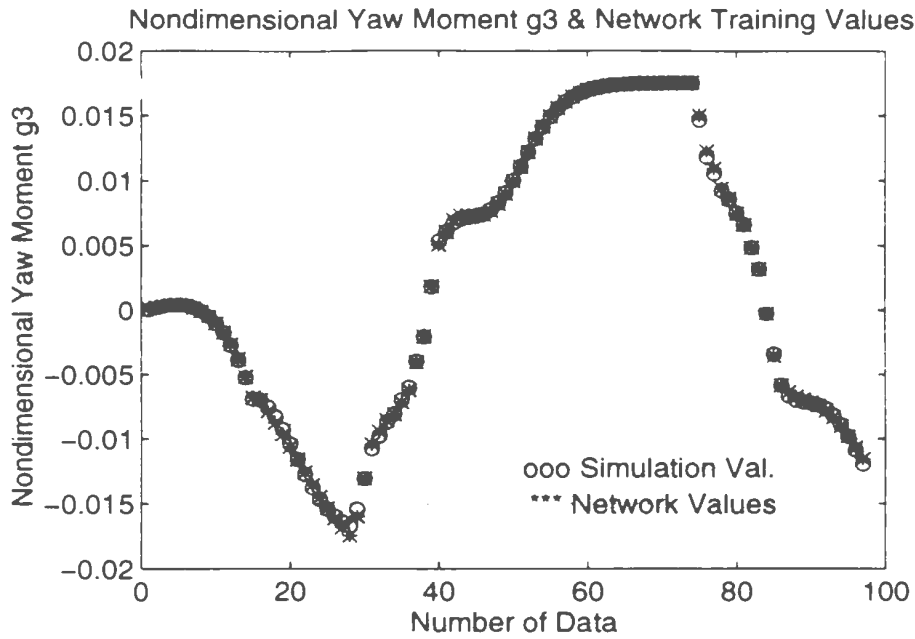


Figure A.3: Trained Network Moment g_3 and Simulation Values

A.3 Prediction of Ship Manoeuvres (1)

In this section, the results of the prediction of the 35-35 degree zigzag manoeuvre are given. This can check how well the trained neural network results fit with the expected simulation values.

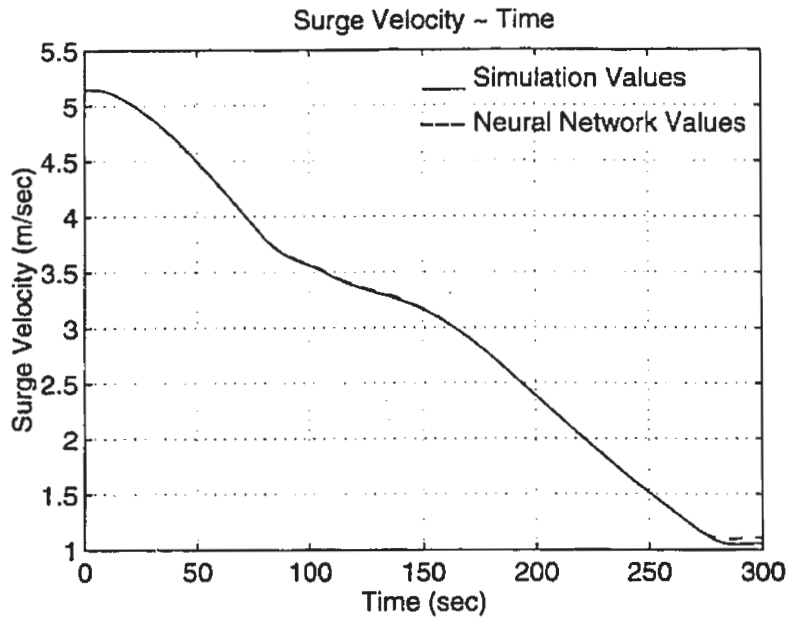


Figure A.4: Predicted Surge Velocity of 35-35 deg Zigzag Manoeuvre

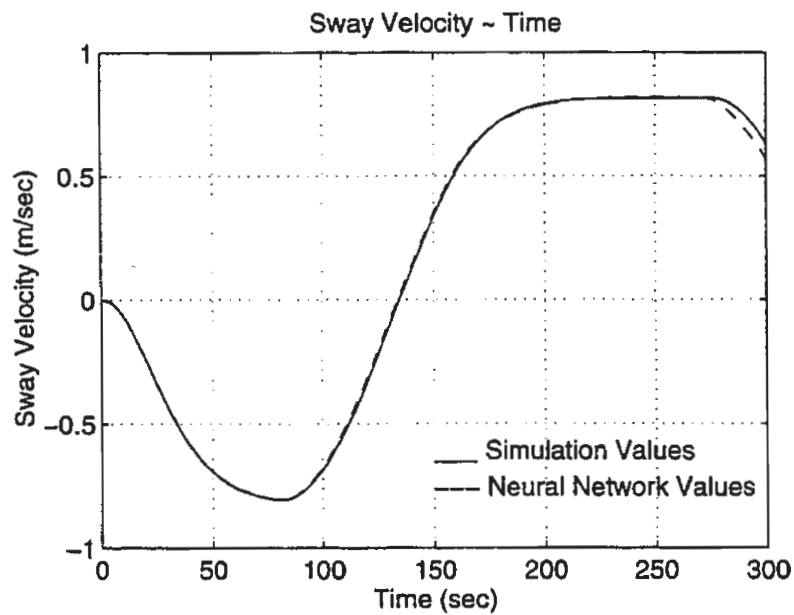


Figure A.5: Predicted Sway Velocity of 35-35 deg Zigzag Manoeuvre

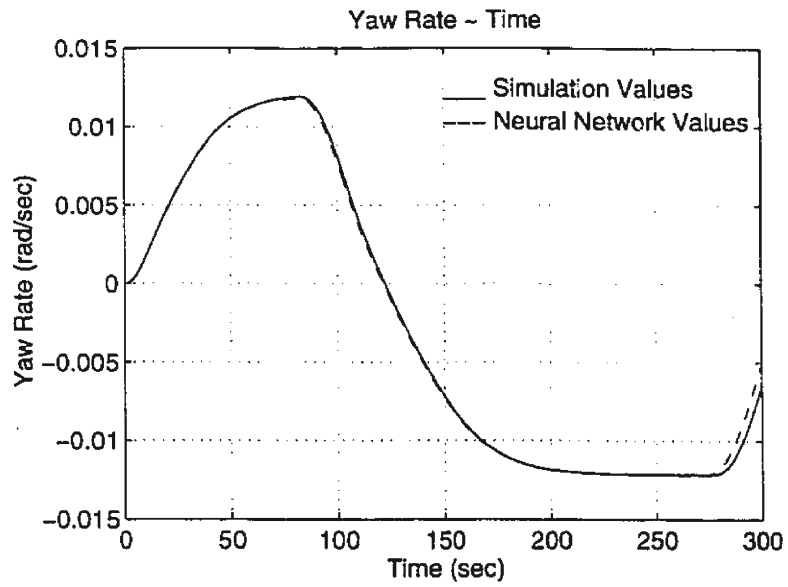


Figure A.6: Predicted Yaw Rate of 35-35 deg Zigzag Manoeuvre

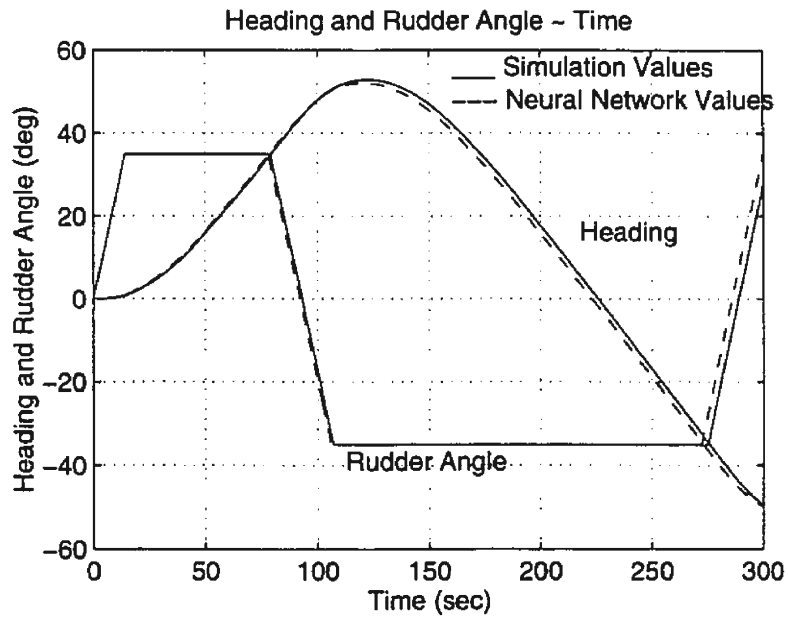


Figure A.7: Predicted Heading Angle of 35-35 deg Zigzag Manoeuvre

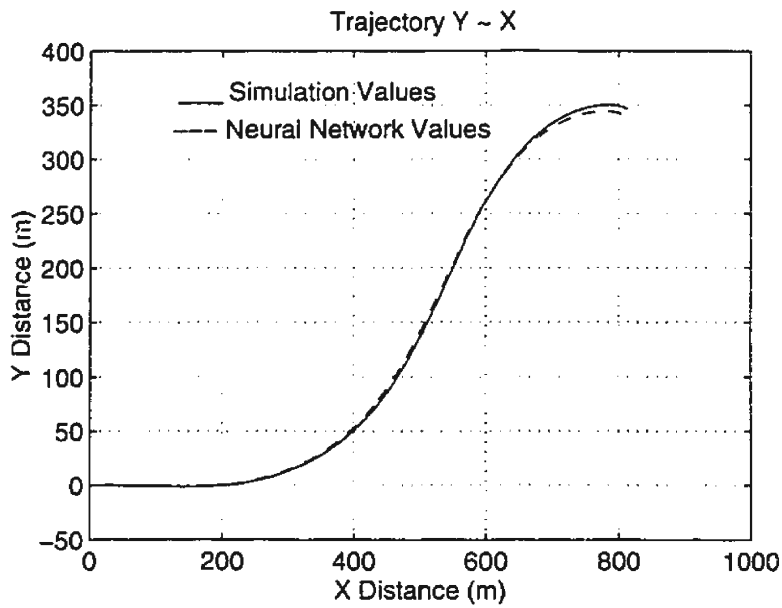


Figure A.8: Predicted Trajectory of 35-35 deg Zigzag Manoeuvre

A.4 Prediction of Ship Manoeuvres (2)

In this section, a 20-20 degree zigzag manoeuvre and a 25 degree turning manoeuvre are predicted to check the generalization of the neural network model trained from a 35-35 degree zigzag manoeuvre.

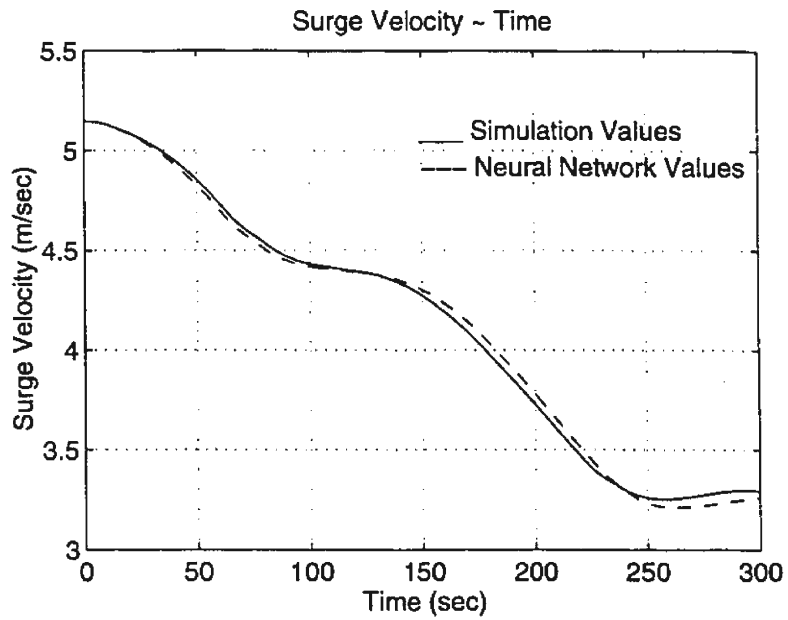


Figure A.9: Predicted Surge Velocity of 20-20 deg Zigzag Manoeuvre

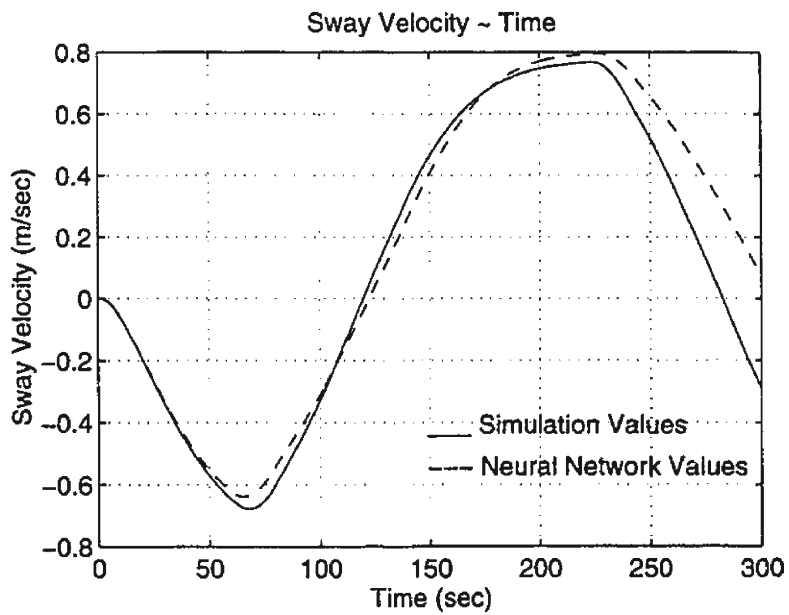


Figure A.10: Predicted Sway Velocity of 20-20 deg Zigzag Manoeuvre

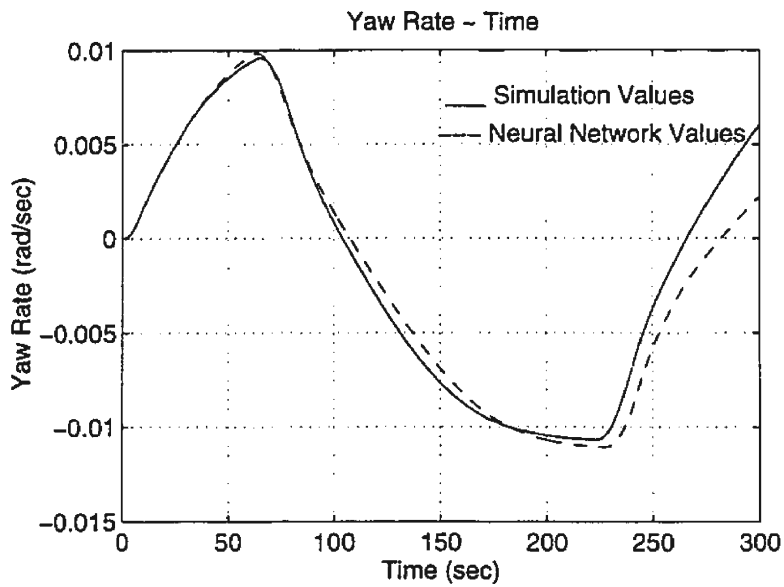


Figure A.11: Predicted Yaw Rate of 20-20 deg Zigzag Manoeuvre

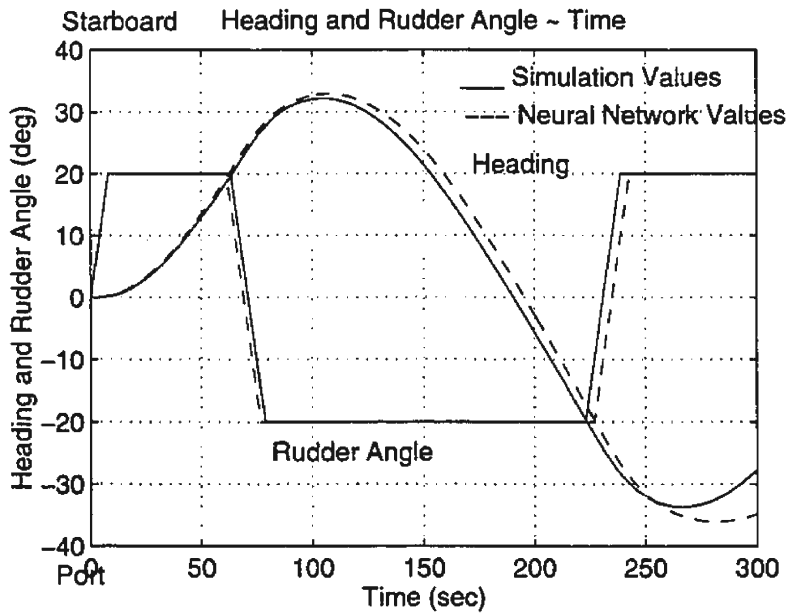


Figure A.12: Predicted Heading Angle of 20-20 deg Zigzag Manoeuvre

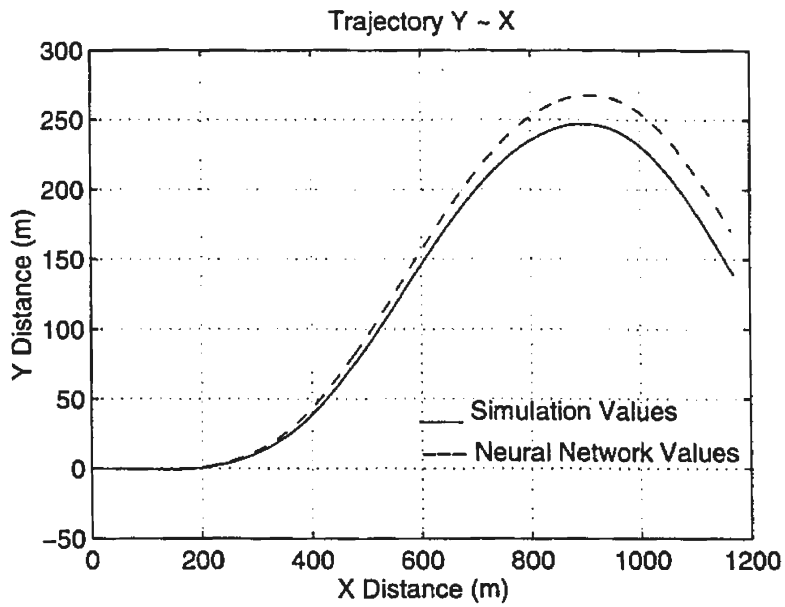


Figure A.13: Predicted Trajectory of 20-20 deg Zigzag Manoeuvre

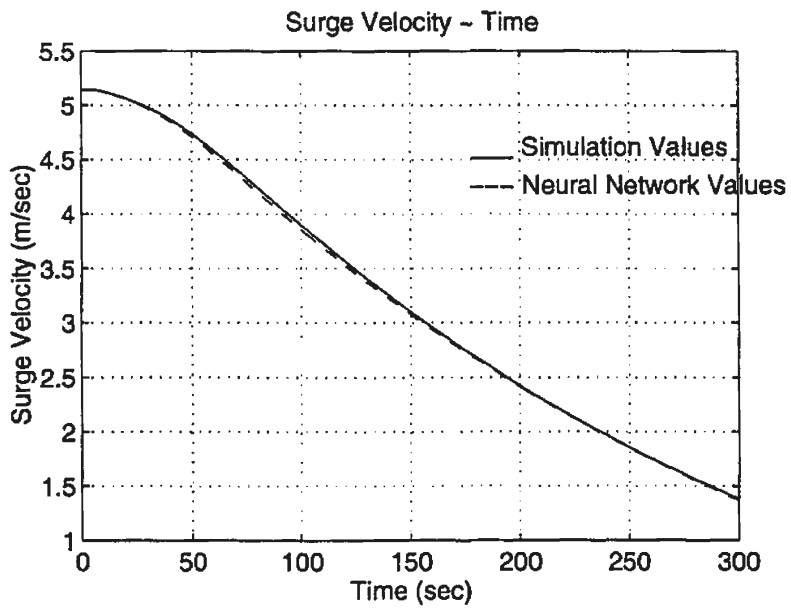


Figure A.14: Predicted Surge Velocity of 25 deg Turning, Starboard

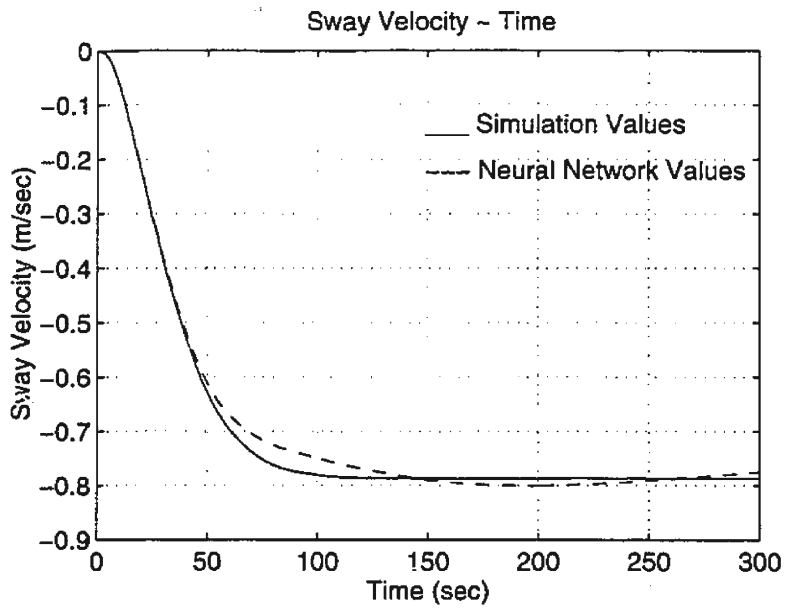


Figure A.15: Predicted Sway Velocity of 25 deg Turning, Starboard

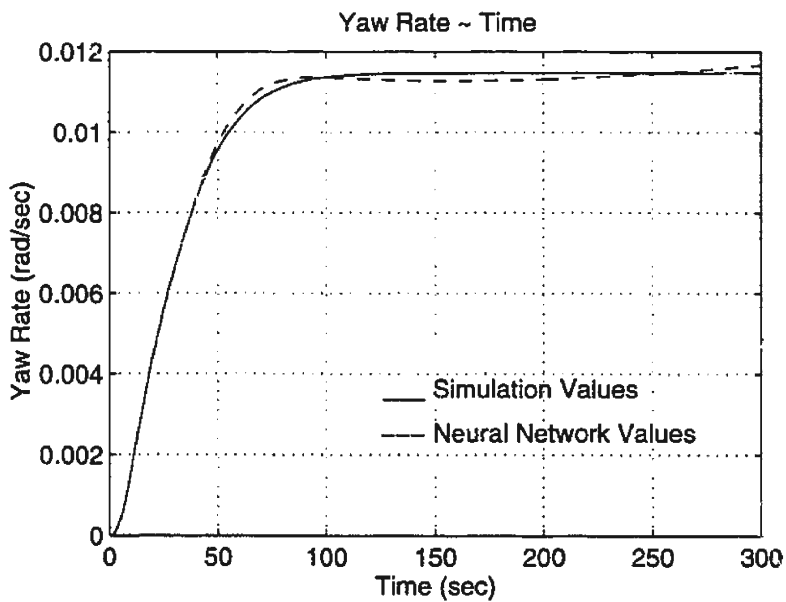


Figure A.16: Predicted Yaw Rate of 25 deg Turning, Starboard

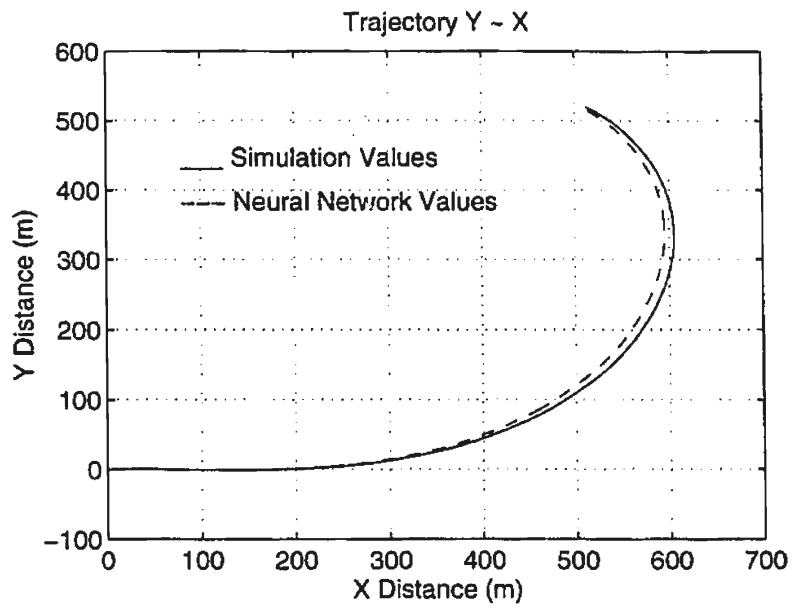


Figure A.17: Predicted Trajectory of 25 deg Turing, Starboard

Appendix B

Neural Network Training Code

```
cccccccccccccccccccccccccccccccccccccccccccccccccccccccccccc
c      Code of Neural Network                                c
c      for Training Sway Force                              c
c      (Similar to Codes for training                      c
c      Surge Force and yaw Moments                          c
cccccccccccccccccccccccccccccccccccccccccccccccccccccccccccc
c      input layer weights : wi
c      output layer weights : wo
c      net inputs : ri
c      net outputs : ro
c      target outputs : rt
c      middle outputs : rm/rms
c      errors : eo / ems
c      learning rate : rate
c      target data (f): ttd
c      net data(f): tnn
c      inputs of
c      surge speed: u
c      sway speed: v
c      yaw rate: r
c      rudder angle: del
c      middle layer neurons : net
c      number of training loops : kit
c      number of data points : kot
c      number of inputs : kin
c      number of outputs : kon
c
c      implicit real*8(a-z)
c      integer i,j,net,met,kin,kon,kot,mot,iseed,it,iot
c      dimension wi(99,11),wo(99,11),tnn(222),ttd(222)
c      dimension vdot(222),rdot(222)
c      dimension u(222),v(222),r(222),del(222)
```

```

dimension ri(11),ro(11),rt(11),rm(99)
dimension rms(99),rmsd(99)
dimension eo(11),ems(99)
common/two/yvdot,yrdot,yv,yr,yb
c
c Read Principal Dimensions of a Ship
open(1,file='init.d',status='unknown')
read(1,*) len,bre,dra,cb,rho,u0
close(1)
open(1,file='dat.d',status='unknown')
read(1,*) rate,scale,sin,sout
read(1,*) net,kin,kon
read(1,*) kit,kot,mot
kin=kin+1
close(1)
open(2,file='series.o',status='unknown')
do 100 i=1,kot
100 read(2,*) du,u(i),v(i),r(i)
continue
close(2)
open(3,file='accele.o',status='unknown')
do 103 i=1,kot
103 read(3,*) du, del(i),du1,vdot(i),rdot(i)
del(i)=del(i)*3.1415927d0/180.d0
continue
close(3)

c Generate Linear Coef. from Clarke's Formulas
call coe(len,bre,dra,cb,rho,u0)

C Generate Target Data
open(4,file='func2.o',status='unknown')
do 104 i=1,kot
ttd(i)=yvdot*vdot(i)-yrdot*rdot(i)
& -yv*v(i)-yr*r(i)-yb*del(i)
write(4,*) i, del(i), ttd(i)
ttd(i)=ttd(i)/(0.5d0*rho*len
&*dra*u0*u0)
104 continue
close(4)

c Using Nonlinear Velocities
do i=1,kot
u(i)=u(i)/u0
v(i)=v(i)/u0
r(i)=r(i)*len/u0
end do

c
c Initiate Weights
c Use Random Weights
if(mot.eq.1) then
iseed=123457

```

```

do 5 i=1,net
do 5 j=1,kin
gwi=ran(iseed)
wi(i,j)=gwi*sin
5 continue
met=net+1
do 10 i=1,met
do 10 j=1,kon
gwo=ran(iseed)
wo(i,j)=gwo*sout
10 continue
else
c Use Old Weights
open(2,file='weights2.d',status='unknown')
met=net+1
do 25 j=1,met
read(2,*) wo(j,1)
25 continue
do 50 j=1,net
do 50 i=1,kin
read(2,*) wi(j,i)
50 continue
close(2)
end if

c Loop of kit Trainings
it=1
iot=1
do 1, while (it.lt.kit)
c
c Loop of kot data
do 2, while (iot.lt.kot)
ri(1)=u(iot)
ri(2)=v(iot)
ri(3)=r(iot)
ri(4)=del(iot)
ri(5)=1.d0
rt(1)=ttd(iot)
do 33 i=1,net
rm(i)=0.0d0
do 22 j=1,kin
rm(i)=rm(i)+wi(i,j)*ri(j)
22 continue

if (rm(i).ge.25.d0) then
rms(i)=1.0d0
else if (rm(i).lt.(-25.d0)) then
rms(i)=0.0d0
else

```

```

rms(i)=1.0d0/(1.0d0+dexp(-rm(i)))
end if

rmsd(i)=rms(i)*(1.0d0-rms(i))
33 continue
rms(met)=1.0d0
do 66 i=1,kon
ro(i)=0.0d0
do 44 j=1,met
ro(i)=ro(i)+wo(j,i)*rms(j)
44 continue
66 continue
c Error
do 77 j=1,net
ems(j)=0.0d0
77 continue
do 99 i=1,kon
eo(i)=rt(i)-ro(i)
eo(i)=eo(i)*scale
do 88 j=1,net
ems(j)=ems(j)+eo(i)*wo(j,i)
88 continue
99 continue
c Update Weights
car=0.0d0
do 242 i=1,kon
do 121 j=1,met
cor=dabs(eo(i)*rms(j))
if(cor.ge.car) car=cor
121 continue
242 continue
do 222 i=1,kon
do 111 j=1,met
cor=eo(i)*rms(j)
wo(j,i)=wo(j,i)+rate*sout*cor/car
111 continue
222 continue
car=0.0d0
do 484 i=1,kin
do 363 j=1,net
cor=dabs(ems(j)*rmsd(j)*ri(i))
if(cor.ge.car) car=cor
363 continue
484 continue
do 444 i=1,kin
do 333 j=1,net
cor=ems(j)*rmsd(j)*ri(i)
wi(j,i)=wi(j,i)+rate*sin*cor/car
333 continue
444 continue

```

```

        iot=iot+1
    2  continue
c
        it=it+1
    1  continue
c
    End of Training
C
c
    Output of Net
    iot=1
    do 555, while (iot.lt.kot)
    ri(1)=u(iot)
    ri(2)=v(iot)
    ri(3)=r(iot)
    ri(4)=del(iot)
    ri(5)=1.d0
    do 303 i=1,net

    rm(i)=0.0d0
    do 202 j=1,kin
    rm(i)=rm(i)+wi(i,j)*ri(j)
202  continue

    if (rm(i).ge.25.d0) then
    rms(i)=1.0d0
    else if (rm(i).lt.(-25.d0)) then
    rms(i)=0.0d0
    else
    rms(i)=1.0d0/(1.0d0+dexp(-rm(i)))
    end if

303  continue
    rms(met)=1.0d0
    do 606 i=1,kon
    ro(i)=0.0d0
    do 404 j=1,met
    ro(i)=ro(i)+wo(j,i)*rms(j)
404  continue
606  continue
    tnn(iot)=ro(1)
    iot=iot+1
555  continue
c
c
    Data of Net and Target
    open(4,file='dat2.o',status='unknown')
    do 777 i=1,kot
    write(4,*) ttd(i),tnn(i)
777  continue
    close(4)
c
    Output Weights
    open(3,file='weights2.d',status='unknown')
    do 888 j=1,met
    write(3,*) wo(j,1)
888  continue

```

```

do 999 j=1,net
do 999 i=1,kin
write(3,*) wi(j,i)
999 continue
close(3)
c End of Main Program

c Sub-program of Clarke's Formulas for Linear Coef
subroutine coe(len,bre,dra,cb,rho,u0)
implicit real*8 (a-z)
common/two/yvdot,yrdot,yv,yr,yb
pi = 3.1415927d0
disp=rho*len*bre*dra*cb
yvdotd=-pi*(dra/len)*(dra/len)*(1.0d0
& +0.16d0*cb*bre/dra-5.1d0*(bre/len)*(bre/len))
& *len/dra
yvdot=yvdotd*0.5d0*rho*len*len*dra
yvdot=disp - yvdot

yrdotd=-pi*(dra/len)*(dra/len)
& *(0.67d0*bre/len-0.0033d0*(bre/dra)*(bre/dra))
& *len/dra
yrdot=yrdotd*0.5d0*rho*len*len*len*dra

yvd=-pi*(dra/len)*(dra/len)
& *(1.0d0+0.40d0*cb*bre/dra)*len/dra
yv=yvd*0.5d0*rho*len*dra*u0

yrd=-pi*(dra/len)*(dra/len)
& *(-0.5d0+2.2d0*bre/len-0.08d0*bre/dra)
& *len/dra
yr=yrd*0.5d0*rho*len*len*dra*u0
yr=yr-disp*u0

ybd=0.02d0*dra/len*3*len/dra
yb=ybd*0.5d0*rho*len*dra*u0*u0
return
end

dat.d
*****
1.0E-6 1.0 1.0 1.0 rate, scale, sin, sout
11 4 1 net, kin, kon
6000000 85 0 kit, kot, mot

init.d
*****
Lenghth, Beam, Draft, Cb, Water Density, U0
152.4 21.763 8.138 0.6 1000.0 7.614

```



